



QA: QA

ANL-NBS-HS-000054 REV 00

July 2006

Data Analysis for Infiltration Modeling: Bedrock Saturated Hydraulic Conductivity Calculation

Prepared for:

U.S. Department of Energy
Office of Civilian Radioactive Waste Management
Office of Repository Development
1551 Hillshire Drive
Las Vegas, Nevada 89134-6321

Prepared by:

Bechtel SAIC Company, LLC
1180 Town Center Drive
Las Vegas, Nevada 89144

Under Contract Number
DE-AC28-01RW12101

DISCLAIMER

This report was prepared as an account of work sponsored by an agency of the United States Government. Neither the United States Government nor any agency thereof, nor any of their employees, nor any of their contractors, subcontractors or their employees, makes any warranty, express or implied, or assumes any legal liability or responsibility for the accuracy, completeness, or any third party's use or the results of such use of any information, apparatus, product, or process disclosed, or represents that its use would not infringe privately owned rights. Reference herein to any specific commercial product, process, or service by trade name, trademark, manufacturer, or otherwise, does not necessarily constitute or imply its endorsement, recommendation, or favoring by the United States Government or any agency thereof or its contractors or subcontractors. The views and opinions of authors expressed herein do not necessarily state or reflect those of the United States Government or any agency thereof.

QA: QA

**Data Analysis for Infiltration Modeling: Bedrock Saturated
Hydraulic Conductivity Calculation**

ANL-NBS-HS-000054 REV 00

July 2006

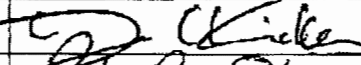
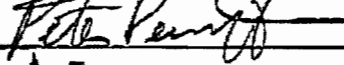
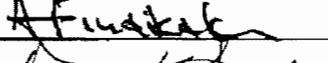
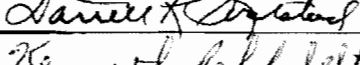
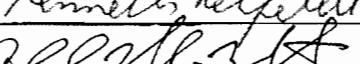
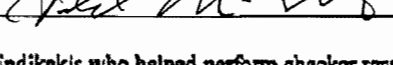
BSC

Scientific Analysis Signature Page/ Change History

Page iii

1. Total Pages: 150

Complete only applicable items.

2. Scientific Analysis Title			
Data Analysis for Infiltration Modeling: Bedrock Saturated Hydraulic Conductivity Calculation			
3. DI (including Rev. No.)			
ANL-NBS-HS-000054 REV 00			
	Printed Name	Signature	Date
4. Originator	Dwayne C. Kicker		7/6/06
Originator	Peter Persoff		7/6/06
5. Checker	James T. Kam <i>for</i>		7.6.06
6. QER	Darrell K. Svalstad		7/6/06
7. Responsible Manager/ Lead	Kenneth Rehfeldt		7/7/06
8. Responsible Manager	Gerald H. Nieder-Westermann		07/07/06
9. Remarks			
This document was developed through the contribution of Angelos N. Findikakis who helped perform checker responsibilities on the overall document. In addition, contributions were made by Timothy J. Vogt and Alexander J. Sanchez who helped perform checker responsibilities for Section 6.2.			
Change History			
10. Revision No.	11. Description of Change		
00	Initial Issue		

INTENTIONALLY LEFT BLANK

CONTENTS

	Page
ACRONYMS.....	ix
1. PURPOSE.....	1-1
2. QUALITY ASSURANCE.....	2-1
3. USE OF SOFTWARE	3-1
4. INPUTS.....	4-1
4.1 DIRECT INPUTS.....	4-1
4.2 CRITERIA.....	4-1
4.3 CODES, STANDARDS, AND REGULATIONS.....	4-1
5. ASSUMPTIONS.....	5-1
5.1 FRACTURE CHARACTERISTICS	5-1
5.1.1 Assumption 1: Fracture Characteristics for the Tptpv3 Vitric Subzone.....	5-1
5.1.2 Assumption 2: Fracture Characteristics for Zeolitic Rock	5-1
5.1.3 Assumption 3: Fracture Characteristics for the Tcpuc Zone	5-2
5.1.4 Assumption 4: Fracture Characteristics for the Tcpm Zone.....	5-3
5.1.5 Assumption 5: Fracture Characteristics for the Tcpuv Vitric Zone.....	5-3
5.1.6 Assumption 6: Fracture Characteristics for the Tcbuc, Tcbm, and Tcbic Zones.....	5-4
5.1.7 Assumption 7: Fracture-Volume-Fraction Distribution.....	5-4
5.1.8 Assumption 8: Fracture Proportion.....	5-5
5.1.9 Assumption 9: Fracture Infill.....	5-5
5.2 SATURATED HYDRAULIC CONDUCTIVITIES OF ROCK MATRIX AND FRACTURE-FILLING CALICHE	5-6
5.2.1 Assumption 10: Representativeness of Boreholes Samples	5-6
5.2.2 Assumption 11: Lognormal Spatial Distributions	5-6
5.2.3 Assumption 12: Similarity of the Tiva Canyon and Topopah Spring Formations.....	5-7
5.2.4 Assumption 13: Relationship of Porosity and Saturated Hydraulic Conductivity.....	5-7
5.2.5 Assumption 14: Standard Deviation	5-8
5.2.6 Assumption 15: Similarity of Identifying Properties.....	5-8
5.2.7 Assumption 16: Use of Log-Uniform Uncertainty Distributions	5-8
6. SCIENTIFIC ANALYSIS DISCUSSION.....	6-1
6.1 INTRODUCTION	6-1
6.2 ASSESSMENT OF BEDROCK GEOLOGY	6-5
6.2.1 Regional Geology	6-5
6.2.2 Development of Bedrock Hydrogeologic Units for Infiltration Modeling.....	6-6

CONTENTS (CONTINUED)

	Page
6.3 CALCULATION OF FRACTURE VOLUME FRACTION	6-28
6.4 CALCULATION OF BEDROCK SATURATED HYDRAULIC CONDUCTIVITY	6-35
6.4.1 Input Data.....	6-36
6.4.2 Assignment of Samples to Lithologic Units	6-38
6.4.3 Analysis of K_{sat} Data.....	6-38
6.4.4 Analysis of Sparse Matrix K_{sat} Data	6-39
6.4.5 K_{sat} of the Bulk Bedrock Material.....	6-46
6.5 UNCERTAINTIES AND LIMITATIONS	6-62
6.5.1 Conceptual Uncertainty	6-62
6.5.2 Data Uncertainty	6-63
7. CONCLUSIONS.....	7-1
8. INPUTS AND REFERENCES	8-1
8.1 DOCUMENTS CITED.....	8-1
8.2 CODES, STANDARDS, REGULATIONS, AND PROCEDURES.....	8-6
8.3 SOURCE DATA, LISTED BY DATA TRACKING NUMBER	8-7
8.4 OUTPUT DATA, LISTED BY DATA TRACKING NUMBER	8-10
8.5 SOFTWARE CODES.....	8-10
APPENDIX A – CORRELATION OF GEOLOGIC MAP UNITS AND INFILTRATION HYDROGEOLOGIC UNITS	A-1
APPENDIX B – PROPAGATION OF VARIABILITY OR UNCERTAINTY FOR MEASURANDS WITH LOGNORMAL DISTRIBUTIONS.....	B-1
APPENDIX C – MEAN OF AND STANDARD DEVIATION OF LOG-UNIFORM DISTRIBUTIONS	C-1

FIGURES

	Page
6-1. Simplified Lithostratigraphic Column of Timber Mountain Group and Paintbrush Group at Yucca Mountain.....	6-6
6-2. Bedrock Geology Coverage Supplied by Source Files for the Infiltration Model Area	6-7
6-3. Revised Bedrock Geologic Map of the Central Block Area.....	6-9
6-4. Geology Coverage: Scotbons.....	6-10
6-5. Digital Geologic Map	6-11
6-6. Distribution of Infiltration Hydrogeologic Units across the Infiltration Model Area	6-26
6-7. Density Versus Depth in Borehole for Samples in Tptrn	6-43
6-8. Ranking of Porosity and K_{sat} for Tptpln Samples	6-44
6-9. Method of Estimating Geometric Mean K_{sat} from One K_{sat} Measurement and Several Porosity Measurements	6-45
6-10. Method of Estimating Geometric Mean K_{sat} from Two K_{sat} Measurements and Several Porosity Measurements	6-45
6-11. Distribution of Saturated Hydraulic Conductivity over the Infiltration Model Area Based on the Consideration of Filled Fractures	6-50
6-12. Variation of Bulk Saturated Hydraulic Conductivity, K_{sat} , as a Function of Various Partially Filled Fracture Networks, with Comparison to the Alcove 1 Infiltration Test	6-57

TABLES

	Page
1-1. Hierarchy of Stratigraphic and Symbol Nomenclature at Yucca Mountain	1-3
4-1. Direct Inputs.....	4-2
6-1. Indirect Inputs	6-3
6-2. Bedrock Mapping Units Used in the Source File	6-12
6-3a. Assignment of Infiltration Hydrogeologic Units	6-18
6-3b. Assignment of Infiltration Hydrogeologic Units to Geologic Framework Model Stratigraphic Units	6-25
6-3c. Percentage of Each Infiltration Hydrogeologic Unit Within the Total Model Area.....	6-27
6-4. Summary of Percent Fracture Results from Surface Mapping	6-29
6-5. Summary of Percent Fracture Results from Underground Mapping	6-31
6-6. Summary of Fracture-Volume-Fraction Results for Each Rock Type	6-33
6-7. Comparison of Fracture-Volume-Fraction Results to an Alternative FracMAN Approach.....	6-36
6-8. Matrix Saturated Hydraulic Conductivity for Each Rock Type, Fracture-Filling Caliche Saturated Hydraulic Conductivity, and Comparison with an Alternative Calculation	6-40
6-9. Bulk Bedrock K_{sat} Based on the Consideration of Filled Fractures.....	6-48
6-10a. Comparison of Bedrock K_{sat} with all Fractures Filled to K_{sat} with 100 μ m Unfilled Aperture in All Fractures	6-54
6-10b. Equivalent Fracture Apertures Calculated from Hydrologic Properties Analysis.....	6-59
6-11. Summary of Bulk Bedrock K_{sat}	6-61
6-12. Calculation of Combined Uncertainty of K_{bulk} for IHU 405	6-65
7-1. Mapping of Yucca Mountain Review Plan Acceptance Criteria and Bedrock Saturated Hydraulic Conductivity Calculation	7-4
A-1. Detailed Correlation of Geologic Map Units to Lithostratigraphic, Infiltration Hydrogeologic, and Unsaturated Zone Flow Model Units.....	A-5

ACRONYMS

ESF	Exploratory Studies Facility
IHU	infiltration hydrogeologic unit
UZ	unsaturated zone
UZTT	Unsaturated Zone Transport Test

INTENTIONALLY LEFT BLANK

1. PURPOSE

The purpose of this analysis is to provide a robust and defensible estimate of bedrock saturated hydraulic conductivity near the soil-bedrock interface for use in the development of a model of net infiltration at the Yucca Mountain site. As described in the Corrective Action Program under Condition Reports 6334 and 7627, the original infiltration estimates and associated bedrock saturated hydraulic conductivities (BSC 2004 [DIRS 170007]) have transparency and traceability issues and as such are noncompliant with qualification requirements. Therefore, this analysis is required because the original bedrock saturated hydraulic conductivities (BSC 2004 [DIRS 170007], Table B-3) could not be traced to qualified data sources.

This analysis includes an appropriate quantification of the uncertainty and variability in the calculation of bedrock saturated hydraulic conductivity. The output from this analysis provides a composite geologic map to correlate bedrock units, as well as bedrock saturated hydraulic conductivity data that are traceable and transparent to support the development of an infiltration model (BSC 2006 [DIRS 176107], Sections 1, 1.1.2, and 1.1.4).

To achieve the goals of this analysis, a hydrogeologic stratigraphic system has been developed consisting of infiltration hydrogeologic units (IHUs) that have differing hydrogeologic properties with special emphasis on saturated hydraulic conductivity. The IHUs are defined on the basis of lithostratigraphic contacts in boreholes (BSC 2004 [DIRS 170029]). Saturated hydraulic conductivity values are from measurements on the core from boreholes in GFM2000 and from various other sources, including boreholes in the Unsaturated Zone Transport Test (UZTT) at the Busted Butte test facility and surface-based samples (Section 6.4). The correlation of lithostratigraphic and IHUs enables the extrapolation of the IHUs to exposures at the ground surface where most of the correlated lithostratigraphic units have been documented in geologic maps (Day et al. 1998 [DIRS 101557]; Scott and Bonk 1984 [DIRS 104181]; Slate et al. 2000 [DIRS 150228], Open-File Report 99-554-A).

For map units that do not have any correlative IHU, proxy IHUs have been proposed that are based on similarities in lithostratigraphic characteristics. These correlations of IHUs to lithostratigraphic units to map units are the basis for the bedrock saturated hydraulic conductivity map (Section 6.2).

Data are reported herein as either saturated hydraulic conductivity K_{sat} (dimension L/T), $\log_{10} K_{sat}$, or $\ln K_{sat}$, and permeability (dimension L²) is only introduced when needed for comparison with data from other reports. Bedrock is defined as the uppermost consolidated rock immediately beneath the soil cover, if any. Bedrock lithology varies by location (Section 6.2).

For each bedrock geologic unit, the approach used to calculate the mean and the variance of the bedrock saturated hydraulic conductivity is as follows:

- The bedrock is modeled as consisting of matrix rock and fractures filled, at least at the soil-bedrock interface, with caliche (Section 5.1.9)
- Each of these materials is characterized by the geometric mean of K_{sat} and the standard deviation of $\log_{10} K_{sat}$ (Sections 6.4.3 and 6.4.4)

- The fraction of the soil-bedrock interface occupied by fractures, termed the fracture volume fraction, is characterized by a beta distribution (Section 6.3)
- The bedrock hydraulic conductivity is calculated by combining these data and by propagating the uncertainty (Section 6.4.5 and Appendix B).

The mean and the variance of K_{sat} of each IHU calculated in this manner applies to the bedrock area of the respective IHU, as shown in Section 6.4.5.1. Therefore, the variance describes the spatial variability of K_{sat} for each IHU based on the consideration of filled fractures.

This analysis refers to the K_{sat} of the matrix rock material, the K_{sat} of the fracture infilling material, and the K_{sat} of the bedrock. The K_{sat} of the bedrock is calculated as the arithmetic mean of the matrix saturated hydraulic conductivity and the filled-fracture saturated hydraulic conductivity, each weighted by its respective volume fraction. When referring to the K_{sat} of the bedrock, the terms “bulk bedrock K_{sat} ,” “bedrock K_{sat} ,” “bulk K_{sat} ,” and “ K_{bulk} ” are used interchangeably, depending upon context.

Field observations show that, in general, at least some proportion of the fractures is not completely filled (Section 6.4.5.4). Comparison of the infiltration rate measured in the Alcove 1 infiltration test, with the mean bulk bedrock K_{sat} for IHU number 404 (Section 6.5.4.3), also suggests that the fractures at that location are not completely filled. Therefore, the bulk bedrock saturated hydraulic conductivity calculated for filled fractures is regarded as a lower bound of bulk bedrock saturated hydraulic conductivity. The upper bound of bulk bedrock K_{sat} has been calculated based on the consideration of an additional 200 μm hydraulic aperture with all fractures (Section 6.4.5.4).

The recommended values for bulk bedrock saturated hydraulic conductivity are provided in Section 6.4.5.5, including the means and standard deviations of their uncertainty distributions, which are log-uniformly distributed between the upper and lower bounds.

This analysis has been developed in accordance with *Technical Work Plan for: Infiltration Model Assessment, Revision, and Analyses of Downstream Impacts* (BSC 2006 [DIRS 176107]). The technical work plan (BSC 2006 [DIRS 176107], Sections 1.1.2 and 1.1.3) limits the scope of this calculation to the development of a defensible bedrock saturated hydraulic conductivity data set for use in an infiltration model. A calculation standard not identified in the technical work plan (BSC 2006 [DIRS 176107], Section 3.1) has been applied to this calculation (Section 4.3).

Bedrock saturated hydraulic conductivity is variable among geologic units. The lithostratigraphic framework for rocks at Yucca Mountain is described in several reports (BSC 2004 [DIRS 170029]; Buesch et al. 1996 [DIRS 100106]; Buesch and Spengler 1999 [DIRS 107905]).

The hierarchy of stratigraphic and symbol nomenclature is listed in Table 1-1, with a complete listing of lithostratigraphic units provided in Appendix A (Table A-1). The bedrock saturated hydraulic conductivity data set developed herein describes the spatial variability of the saturated hydraulic conductivity at the interface between the soil and bedrock and is only intended for use as input to an infiltration model.

Table 1-1. Hierarchy of Stratigraphic and Symbol Nomenclature at Yucca Mountain

Nomenclature	Stratigraphic and Symbol Hierarchy
Paintbrush Group	T Tertiary
Tiva Canyon Tuff (formation rank)	p Paintbrush Group
Yucca Mountain Tuff	t Topopah Spring Tuff
Pah Canyon Tuff	r crystal-rich member
Topopah Spring Tuff	v vitric
	l densely welded subzone
	v vitrophyre interval

Source: Buesch et al. 1996 [DIRS 100106], Table 1.

NOTE: Example: Tpcplnc2 – Tiva Canyon Tuff, crystal-poor member, lower nonlithophysal (zone), columnar (subzone), clay-altered pumice (interval).

INTENTIONALLY LEFT BLANK

2. QUALITY ASSURANCE

Development of this analysis and supporting calculation activities have been determined subject to the Yucca Mountain Project quality assurance program, as indicated in the technical work plan (BSC 2006 [DIRS 176107], Section 8.1). Approved quality assurance procedures (BSC 2006 [DIRS 176107], Section 4.1) have been used to conduct and document the activities described in this analysis. The technical work plan also identifies the methods used to control the electronic management of data (BSC 2006 [DIRS 176107], Section 8.4). The calculations herein were conducted and documented following LP-SIII.9Q-BSC, *Scientific Analyses*.

This analysis examines the properties of natural barriers, meaning the bedrock layers above the repository, that are classified in *Q-List* (BSC 2005 [DIRS 175539]) as “Safety Category,” because they are important to waste isolation as defined in LS-PRO-0203, *Q-List and Classification of Structures, Systems, and Components*. This analysis contributes to the analysis and modeling data used to support postclosure performance assessment. The conclusions of this analysis do not affect the repository design or engineered features important to safety, as defined in LS-PRO-0203.

INTENTIONALLY LEFT BLANK

3. USE OF SOFTWARE

Controlled and baselined software used in the development of this analysis includes ARCINFO (ARCINFO V.7.2.1, STN: 10033-7.2.1-00 [DIRS 157019]), running on a Silicon Graphics Inc. machine with an IRIX 6.5 operating system.

ARCINFO was used to create the bedrock geologic file. ARCINFO was selected for use because it is the standard geographic information system used by the Yucca Mountain Project, is a widely accepted standard Geographic Information Systems protocol in the general scientific community, and has the required capabilities to read and transform the information on the digital source files into the file format required for use in an infiltration model (BSC 2006 [DIRS 176107], Section 1.1.4).

ARCINFO is appropriate for the applications used in this analysis and is consistent with its intended use in accordance with IT-PRO-0011, *Software Management*. This software is validated for the purpose of manipulating Geographic Information Systems data for use in Yucca Mountain Project reports in accordance with IT-PRO-0011. The software was used only within this range of validation.

EARTHVISION® (EARTHVISION V.5.1, STN: 10174-5.1-00 [DIRS 167994]), running on a Silicon Graphics Inc. machine with an IRIX 6.5 operating system, was used to extract information from DTN: MO0012MWDGFM02.002 [DIRS 153777].

EARTHVISION® is required for the use of files in DTN: MO0012MWDGFM02.002 [DIRS 153777] and is, therefore, the appropriate software for use in accordance with IT-PRO-0011. This software is validated for the purpose of manipulating Geographic Information Systems data for use in Yucca Mountain Project reports, as specified in software qualification documentation (CRWMS M&O 2000 [DIRS 153526]), in accordance with IT-PRO-0011. The software was used only within this range of validation.

FracMAN has been used elsewhere to develop stochastically defined fracture systems that are representative of the host rock mass. While results from other sources using FracMAN are cited in Sections 5.1 and 6.3, this software item was not used to develop data in this analysis.

Standard functions of Microsoft® Excel® 2000 9.0.6926 SP-3, a commercial off-the-shelf exempt software, in accordance with IT-PRO-0011, Section 1.4, were used in this analysis. This software was used to perform support calculation activities, to calculate fracture volume fraction, and to develop statistical descriptions of fracture infill and matrix saturated hydraulic conductivities. Additionally, Excel® was used to process and summarize saturated hydraulic conductivity data and to provide graphical presentation of the results.

Standard functions of Mathsoft® Mathcad® version 13.0 (509121419), a commercial off-the-shelf software, were also used in this analysis. This software item was used to perform support calculation activities. Mathcad® was used to calculate bulk bedrock saturated hydraulic conductivity for each IHU. Mathcad® was also used to calculate the spatial variability and uncertainty of the bulk bedrock saturated hydraulic conductivity data.

Section 6 documents the use of standard functions of commercial off-the-shelf software in sufficient detail to allow independent repetition of the software in accordance with LP-SIII.9Q-BSC, Attachment 2.

Specifically, Section 6 provides:

- The formula or algorithm used
- A listing of the inputs to the formula or algorithm
- A listing of the outputs from the formula or algorithm
- Narrative to describe the calculation(s).

Excel® and Mathcad® calculation files are provided in output DTN: MO0605SPAFABRP.004.

4. INPUTS

4.1 DIRECT INPUTS

This analysis uses available data from the Technical Data Management System for rock matrix saturated hydraulic conductivity from core specimens, fracture infill saturated hydraulic conductivity from core specimens, fracture characteristics from surface and underground mapping, and bedrock geologic mapping. Direct inputs and associated sources used in this analysis are listed in Table 4-1. These data are appropriate for this bedrock saturated hydraulic conductivity analysis.

4.2 CRITERIA

Activities described here are subject to regulatory review per the acceptance criteria in *Yucca Mountain Review Plan, Final Report*, NUREG-1804 (NRC 2003 [DIRS 163274], Section 2.2.1.3.5.3); acceptance criteria 2 and 3, related to infiltration data, are as follows:

- Acceptance Criterion 2: Data are sufficient for model justification:
 - The effects of fracture properties, fracture distributions, matrix properties, heterogeneities, time-varying boundary conditions, evapotranspiration, depth of soil cover, and surface-water runoff and runoff are considered, such that net infiltration is not underestimated.
- Acceptance Criterion 3: Data uncertainty is characterized and propagated through the model abstraction:
 - Models use parameter values, assumed ranges, probability distributions, and bounding assumptions that are technically defensible, reasonably account for uncertainties and variabilities, and do not result in an underrepresentation of the risk estimate.
 - The technical bases for the parameter values used in this abstraction are provided.
 - Possible statistical correlations are established between parameters in this abstraction. An adequate technical basis or bounding argument is provided for neglected correlations.

4.3 CODES, STANDARDS, AND REGULATIONS

Codes, standards, or regulations applicable to this work are defined in the technical work plan (BSC 2006 [DIRS 176107], Section 3). Additionally, ANSI/NCSL Z540-2-1997 [DIRS 157394], *American National Standard for Calibration — U.S. Guide to the Expression of Uncertainty in Measurement*, is the calculation standard that has been applied to the assessment of uncertainty in Appendix B.

Table 4-1. Direct Inputs

Input Data Description	Parameter	Location in This Analysis	Source
Bedrock geology	Geologic mapping	Section 6.2.2, Figures 6-2, 6-3, and 6-6, Table 6-2, Appendix A; Output DTN: MO0603SPAGRIDD.003	DTN: GS971208314221.003 [DIRS 107128], <i>cb6k.ps</i>
	Geologic mapping	Section 6.2, Table 6-2; Output DTN: MO0603SPAGRIDD.003	DTN: GS930283117461.001 [DIRS 107027], Records Package MOY-940125-02-18, ACC: HQS.19880517.1443
	Geologic mapping	Section 6.2.2, Figures 6-2, 6-4, and 6-6, Table 6-2, Appendix A; Output DTN: MO0603SPAGRIDD.003	DTN: MO0003COV00095.000 [DIRS 146848], <i>scotbons.e00</i>
	Geologic mapping	Section 6.2.2, Figures 6-2, 6-5, and 6-6, Table 6-2, Appendix A; Output DTN: MO0603SPAGRIDD.003	DTN: MO0603GSCGEOMP.000 [DIRS 176585], <i>ofr-99-0554-e00.tar</i>
	Rock units	Section 3; Section 6.2.2, Figure 6-6, Table 6-3b; Output DTN: MO0603SPAGRIDD.003	DTN: MO0012MWDGFM02.002 [DIRS 153777]
Surface fracture mapping at the drainage cut at the North Ramp Starter Tunnel	Fracture aperture (mm), infill thickness (mm), fracture length (ft)	Section 6.3, Table 6-4; Output DTN: MO0605SPAFABRP.004, <i>Fracture Volume Fraction for Each Rock Type v7.xls</i> , worksheet 'Surface Calculation'; Output DTN: MO0605SPABEDRK.005	DTN: GS980608314224.004 [DIRS 175707], Table S04374_001, <i>DRAINAGE.xls</i>
	Fracture map		DTN: GS940408314224.004 [DIRS 157228], <i>channel.PDF</i>
Surface fracture mapping at Antler Ridge, Pavement ARP-1	Fracture aperture (mm), fracture length (ft)		DTN: GS940308314222.001 [DIRS 175720], Table S96400_001
	Fracture map		DTN: GS940308314222.001 [DIRS 175720], Records Package MOY-010123-26-09, ACC: MOL.19950123.0094
Surface fracture mapping at Fran Ridge, Pavement P2001	Fracture aperture (mm), fracture length (ft)		DTN: GS950108314222.001 [DIRS 175708], Tables S96319_001 and S96319_002
	Map area (m ²)		DTN: GS950108314222.001 [DIRS 175708], Records Package MOY-950817-21-02, ACC: MOL.19960213.0253, p. 13
Surface fracture mapping data from NRG-1 Pavement	Fracture aperture (mm), fracture length (m)		DTN: GS060208314222.001 [DIRS 176825], Table S06034_001
	Fracture map		DTN: GS060208314222.001 [DIRS 176825]

Table 4-1. Direct Inputs (Continued)

Input Data Description	Parameter	Location in This Analysis	Source
Surface fracture mapping at the PTn section of Solitario Canyon, Pavements FS-1, FS-2, and FS-3	Fracture aperture (mm), fracture length (m)	Section 6.3, Table 6-4; Output DTN: MO0605SPAFABRP.004, <i>Fracture Volume Fraction for Each Rock Type v7.xls</i> , worksheet 'Surface Calculation'; Output DTN: MO0605SPABEDRK.005 (Continued)	DTN: GS950508314222.003 [DIRS 175723], Table S97370_001
	Fracture map		DTN: GS950508314222.003 [DIRS 175723], Records Package MOY-010110-14-01, ACC: MOL.19960129.0083, pp. 1, 34, and 67
Surface fracture mapping at UZ-7A Drill Pad	Fracture aperture (mm), fracture length (m)		DTN: GS960808314222.001 [DIRS 175721], Table S98071_001
	Fracture map		DTN: GS960808314222.001 [DIRS 175721], Records Package MOY-010119-16-07, ACC: MOL.19980305.0108, Figure 2
Underground fracture mapping in the North Ramp	Maximum fracture aperture (mm), maximum fracture infill thickness (mm), fracture length above traceline (m), fracture length below traceline (m)	Section 6.3, Table 6-5; Output DTN: MO0605SPAFABRP.004, <i>Fracture Volume Fraction for Each Rock Type v7.xls</i> , worksheet 'Underground Calculation 1'; Output DTN: MO0605SPABEDRK.005	DTN: GS971108314224.020 [DIRS 105561], Table S98062_001
		Section 6.3, Table 6-5; Output DTN: MO0605SPAFABRP.004, <i>Fracture Volume Fraction for Each Rock Type v7.xls</i> , worksheets 'Underground Calculation 1' and/or 'Underground Calculation 2'; Output DTN: MO0605SPABEDRK.005	DTN: GS971108314224.021 [DIRS 106007], Table S98076_001
			DTN: GS971108314224.022 [DIRS 106009], Table S98063_001
Underground fracture mapping in the South Ramp			DTN: GS971108314224.023 [DIRS 106010], Table S98064_001
		Section 6.3, Table 6-5; Output DTN: MO0605SPAFABRP.004, <i>Fracture Volume Fraction for Each Rock Type v7.xls</i> , worksheets 'Underground Calculation 2' and/or 'Underground Calculation 3'; Output DTN: MO0605SPABEDRK.005	DTN: GS970208314224.003 [DIRS 106048], Table S97164_001

Table 4-1. Direct Inputs (Continued)

Input Data Description	Parameter	Location in This Analysis	Source
Underground fracture mapping in the South Ramp (Continued)	Maximum fracture aperture (mm), maximum fracture infill thickness (mm), fracture length above traceline (m), fracture length below traceline (m) (Continued)	Section 6.3, Table 6-5; Output DTN: MO0605SPAFABRP.004, <i>Fracture Volume Fraction for Each Rock Type v7.xls</i> , worksheets 'Underground Calculation 2' and/or 'Underground Calculation 3'; Output DTN: MO0605SPABEDRK.005 (Continued)	DTN: GS970808314224.008 [DIRS 106049], Table S97510_001
			DTN: GS970808314224.010 [DIRS 106050], Table S97511_001
			DTN: GS970808314224.012 [DIRS 106057], Table S97512_001
Underground fracture mapping in the Cross Drift			DTN: GS990408314224.001 [DIRS 108396], Table S99426_001
			DTN: GS990408314224.002 [DIRS 105625], Table S99427_001
Underground fracture mapping at Busted Butte			DTN: GS990708314224.007 [DIRS 164604], Table S00076_001
Matrix hydrologic properties measured on core samples from several boreholes	Saturated hydraulic conductivity, depth and lithology of samples.	Sections 6.4.1 and 6.4.2; Output DTN: MO0605SPAFABRP.004, <i>Matrix and fracture-fill Ksat for each rock type.xls</i> , worksheet 'Original DTNs(1)'; Output DTN: MO0605SPABEDRK.005	DTN: MO0109HYMXP.001 [DIRS 155989], Table S01144_001
Matrix hydrologic properties measured on core samples from WT-24	Saturated hydraulic conductivity		DTN: GS980708312242.011 [DIRS 107150], Table S98249_006
	Porosity	Section 6.4.1; Output DTN: MO0605SPAFABRP.004, <i>Matrix and fracture-fill Ksat for each rock type.xls</i> , worksheet 'Original DTNs(1)'; Output DTN: MO0605SPABEDRK.005	DTN: GS980708312242.010 [DIRS 106752], Table S98248_006
Matrix hydrologic properties measured on core samples from SD-6			DTN: GS980808312242.014 [DIRS 106748], Table S98285_002
	Saturated hydraulic conductivity	Sections 6.4.1 and 6.4.2; Output DTN: MO0605SPAFABRP.004, <i>Matrix and fracture-fill Ksat for each rock type.xls</i> , worksheet 'Original DTNs(1)'; Output DTN: MO0605SPABEDRK.005	DTN: GS980908312242.038 [DIRS 107154], Table S98388_004

Table 4-1. Direct Inputs (Continued)

Input Data Description	Parameter	Location in This Analysis	Source
Matrix hydrologic properties measured on core samples from SD-7, SD-9, SD-12, UZ-14, and UZ-16	Saturated hydraulic conductivity (Continued)	Sections 6.4.1 and 6.4.2; Output DTN: MO0605SPAFABRP.004, <i>Matrix and fracture-fill Ksat for each rock type.xls</i> , worksheet 'Original DTNs(1)'; Output DTN: MO0605SPABEDRK.005 (Continued)	DTN: GS980908312242.041 [DIRS 107158], Table S98386_004
Matrix hydrologic properties measured on Exploratory Studies Facility cores		Section 6.4.1; Output DTN: MO0605SPAFABRP.004, <i>Matrix and fracture-fill Ksat for each rock type.xls</i> , worksheet 'Original DTNs(1)'; Output DTN: MO0605SPABEDRK.005	DTN: GS971008312231.006 [DIRS 107184], Table S98373_005
Matrix hydrologic properties measured on Busted Butte cores			DTN: GS990308312242.007 [DIRS 107185], Table S99180_003
			DTN: GS990708312242.008 [DIRS 109822], Tables S99391_001 and S99391_002
Depth to contacts with geologic units	Lithology of samples	Section 6.4.2; Output DTN: MO0605SPAFABRP.004, <i>Matrix and fracture-fill Ksat for each rock type.xls</i> , worksheet 'contacts00md.dat'; Output DTN: MO0605SPABEDRK.005	DTN: MO0012MWDGFM02.002 [DIRS 153777], <i>contacts00md.dat</i>
Hydrologic properties measured on fracture-filling caliche	Saturated hydraulic conductivity of fracture-filling caliche	Section 6.4.1; Output DTN: MO0605SPAFABRP.004, <i>Matrix and fracture-fill Ksat for each rock type.xls</i> , worksheet 'fill material1'; Output DTN: MO0605SPABEDRK.005	DTN: GS950708312211.003 [DIRS 146873], Table S98356_004

NOTE: DTN: MO0603GSCGEOMP.000 [DIRS 176585], *ofr-99-0554-e00.tar*, which provides bedrock geology, was prepared by the U.S. Geological Survey in cooperation with the U.S. Department of Energy Nevada Operations Office and was not part of the Yucca Mountain Site Characterization Project. This DTN is identified in the Technical Data Management System as "established fact" because the U.S. Geological Survey Mapping Division is known as the premier source of cartographic information for the United States and is used routinely for government and private sector mapping. This DTN meets the requirements for established fact per LP-3.15Q-BSC, *Managing Technical Product Inputs*.

DTN = data tracking number.

INTENTIONALLY LEFT BLANK

5. ASSUMPTIONS

The following assumptions have been used in this analysis.

5.1 FRACTURE CHARACTERISTICS

Fracture characteristics for many lithostratigraphic units have been determined in 23 surface-based near-vertical boreholes and are based on observations from analog video recordings in DTN: GS950608314211.026 [DIRS 175931]. Data collected in these logs include borehole intercept of the fracture and a calculated azimuth of dip direction; however, no corrections were made to these data. Therefore, the general fracture characteristics and relative abundance determined from the borehole video recordings represent variations between and within different lithostratigraphic units. These fracture data are compared to the depths of lithostratigraphic contacts (BSC 2004 [DIRS 170029]). Information from DTN: GS950608314211.026 [DIRS 175931] has been used to confirm each fracture-characteristic assumption for the units described in this section.

5.1.1 Assumption 1: Fracture Characteristics for the Tptpv3 Vitric Subzone

Fracture characteristics for the Tptpv3 vitric subzone are similar to those for the Tptpv2 vitric subzone. Therefore, the spatial distribution of fracture volume fraction for the Tptpv3 vitric subzone is assumed to be equal to the spatial distribution of fracture volume fraction for the Tptpv2 vitric subzone.

Basis: Assumption 1 is necessary because fracture-mapping data of the type needed to compile fracture characteristics for this analysis are not available for the Tptpv3 subzone. Both the Tptpv3 and the Tptpv2 are zones of welding in the vitric, crystal-poor pyroclastic flow deposit of the Topopah Spring Tuff; the Tptpv3 is densely welded and the Tptpv2 is moderately welded. Evidence from field exposures and boreholes indicate that the densely welded rocks are more fractured than the moderately welded rocks (Buesch et al. 1996 [DIRS 100106]). This assumption, needed to equate the two subzones, results in a potential underrepresentation of fractures for the Tptpv3. Until more data become available, the assumption is considered adequate for assessing the Tptpv3. The Tptpv3 represents less than 0.5% of the infiltration model area (Section 6.2.2, Table 6-3c, IHU 424). Therefore, its contribution to net infiltration is minimal.

Confirmation Status: Assumption 1 does not require further confirmation, because the facts that form the basis of this assumption are well established and documented.

Use in the Analysis: Section 6.3 (Table 6-6).

5.1.2 Assumption 2: Fracture Characteristics for Zeolitic Rock

Fracture characteristics for zeolitic rock are similar to the zeolitic subzone of the Tpp in the Exploratory Studies Facility (ESF) from Station 9+90 to 10+52. Therefore, the spatial distribution of fracture volume fraction for rock types Tptpv2 zeolitic, Tptpv1 zeolitic, Tac zeolitic, Tacbt zeolitic, and Tcuv zeolitic are assumed to be equal to the spatial distribution of fracture volume fraction for the Tpp zeolitic subzone (output DTN: MO0605SPAFABRP.004, *Fracture Volume Fraction for Each Rock Type v7.xls*, worksheet 'Summary of Avg. Fracture Data').

Basis: Assumption 2 is necessary because fracture-mapping data are not available for the zeolitic units. The Tptpv2, Tptpv1, Tac, and TcpuV consist of nonwelded (the Tptpv2 ranges to moderately welded) pyroclastic flow deposits; the Tacbt consists of bedded tuffs (nonwelded pyroclastic flow and fallout deposits); and the Tpp consists of nonwelded pyroclastic flow deposits. Each of these rocks was initially vitric, but was altered to zeolitic minerals at some time after deposition. The amount and pervasiveness of zeolites can vary in these deposits with the Tptpv2, Tptpv1, Tac, Tacbt, and TcpuV typically more zeolitized than the Tpp. Zeolitization can result in some small-scale millimeter- to centimeter-sized variations in the textures that affect properties, such as porosity and saturated hydraulic conductivity, and, typically, zeolitized rocks have more well-developed fractures than do comparable vitric rocks. The zeolitic character of the Tpp in the ESF from Station 9+90 to 10+52 was established only by visual examination and has not been verified by laboratory analysis. The zeolitic rock units represent less than 0.5% of the infiltration model area (Section 6.2.2, Table 6-3c, IHUs 426, 428, 430, 432, and 434). Therefore, their contribution to net infiltration is minimal.

Confirmation Status: Assumption 2 does not require further confirmation, because the facts that form the basis of this assumption are well established and documented.

Use in the Analysis: Section 6.3 (Table 6-6).

5.1.3 Assumption 3: Fracture Characteristics for the TcpuC Zone

Fracture characteristics for crystallized rocks in the TcpuC zone are similar to crystallized rocks in the Tpcrn zone. Therefore, the spatial distribution of fracture volume fraction for the TcpuC zone is assumed to be equal to the spatial distribution of fracture volume fraction from the Tpcrn zone.

Basis: Assumption 3 is necessary because fracture-mapping data are not available for the TcpuC zone. Geologically, the physical processes that formed the rocks in the TcpuC are similar to those that formed the Tpcrn, although they occur in different formations. The Tpcrn consists of densely welded (locally identified as moderately welded) and crystallized pyroclastic flow deposits that underwent vapor-phase corrosion and mineralization during formation of the rocks (Buesch et al. 1996 [DIRS 100106]). The TcpuC consists of partially to moderately welded and crystallized pyroclastic flow deposits that underwent vapor-phase corrosion and mineralization during formation of the rocks (Buesch and Spengler 1999 [DIRS 107905]). Vapor-phase corrosion and mineralization in these rocks can result in some small-scale millimeter- to centimeter-sized variations in the textures and properties of the rocks; however, the overall effect of these processes is to homogenize many of the properties. The TcpuC represents less than 0.5% of the infiltration model area (Section 6.2.2, Table 6-3c, IHU 435). Therefore, its contribution to net infiltration is minimal.

Confirmation Status: Assumption 3 does not require further confirmation, because the facts that form the basis of this assumption are well established and documented.

Use in the Analysis: Section 6.3 (Table 6-6).

5.1.4 Assumption 4: Fracture Characteristics for the Tcpcm Zone

Fracture characteristics for crystallized rocks in the Tcpcm zone are similar to crystallized rocks in the Tpcpmn. Therefore, the spatial distribution of fracture volume fraction for the Tcpcm is assumed to be equal to the spatial distribution of fracture volume fraction from the Tpcpmn.

Basis: Assumption 4 is necessary because fracture-mapping data are not available for the Tcpcm unit. Geologically, the physical processes that formed the rocks in the Tcpcm are similar to those that formed the Tpcpmn, although they occurred in different formations. Both the Tpcpmn and the Tcpcm contain crystallized pyroclastic flow deposits that underwent minimal vapor-phase corrosion and mineralization during formation of the rocks and have abundant steeply dipping fractures (Buesch et al. 1996 [DIRS 100106]; Buesch and Spengler 1999 [DIRS 107905]). One minor difference is that the Tcpcm contains moderately to densely welded tuff, whereas the Tpcpmn has densely welded tuff (Buesch et al. 1996 [DIRS 100106]; Buesch and Spengler 1999 [DIRS 107905]) and this might result in slightly fewer fractures in the Tcpcm. This assumption results in a potential overrepresentation of fractures for the Tcpcm. Until there are data to support quantitative characterization of the fractures, the assumption is considered adequate for assessing the Tcpcm. The Tcpcm represents less than 0.5% of the infiltration model area (Section 6.2.2, Table 6-3c, IHU 436). Therefore, its contribution to net infiltration is minimal.

Confirmation Status: Assumption 4 does not require further confirmation, because the facts that form the basis of this assumption are well established and documented.

Use in the Analysis: Section 6.3 (Table 6-6).

5.1.5 Assumption 5: Fracture Characteristics for the Tcpu vitric Zone

Fracture characteristics for the Tcpu vitric zone and the Tcbt vitric zone are similar to the vitric rocks of the Ttpv1 subzone. Therefore, the spatial distribution of fracture volume fraction for the Tcpu and the Tcbt are equal to the spatial distribution of fracture volume fraction for the Ttpv1 (output DTN: MO0605SPAFABRP.004, *Fracture Volume Fraction for Each Rock Type v7.xls*, worksheet 'Underground Summary').

Basis: Assumption 5 is necessary because fracture-mapping data are not available for the Tcpu and Tcbt zones. Physical processes that formed the rocks in the Tcpu and the Tcbt are similar to those that formed the Ttpv1 and the Tpb1, although they occur in different formations. For an infiltration model, the Ttpv1 (a nonwelded and vitric pyroclastic flow deposit) and the Tpb1 (nonwelded and vitric pyroclastic flow and fallout deposits) are grouped, in part, because the Tpb1 is thin and does not have fracture data. The Tcbt IHU includes the Tcplv, Tcbt, and Tcbuv lithostratigraphic units based on two reasons. The first reason is that the source map (Scott and Bonk 1984 [DIRS 104181]) does not explicitly map comparable units to the Tcpu or Tcbuv; it only maps a unit comparable to the Tcbt. The second reason is that the Tcplv and Tcbuv are nonwelded and vitric pyroclastic flow deposits, whereas the Tcbt consists of nonwelded and vitric pyroclastic flow and fallout deposits. Although in name the Tcbt appears to be of mostly bedded tuffs, it is actually representative of nonwelded vitric pyroclastic flow deposits as is the Ttpv1. The Tcpu represents less than 0.5% of the infiltration model area (Section 6.2.2, Table 6-3c, IHU 437). Therefore, its contribution to net infiltration is minimal.

Confirmation Status: Assumption 5 does not require further confirmation, because the facts that form the basis of this assumption are well established and documented.

Use in the Analysis: Section 6.3 (Table 6-6).

5.1.6 Assumption 6: Fracture Characteristics for the Tcbuc, Tcbm, and Tcblc Zones

Fracture characteristics for the grouping of crystallized rocks in the Tcbuc, Tcbm, and Tcblc are similar to crystallized rocks in the Tcpm. Because the Tcpm is similar to the Tpcpmn (Section 5.1.4, Assumption 4), the spatial distribution of fracture volume fraction for the grouping of the Tcbuc, Tcbm, and Tcblc is assumed to be equal to the spatial distribution of fracture volume fraction from the Tpcpmn.

Basis: Assumption 6 is necessary because fracture-mapping data are not available for the Tcbuc, Tcbm, and Tcblc units. Geologically, the physical processes that formed the rocks in the Tcbuc, Tcbm, and Tcblc are similar to those that formed the Tcpm and Tpcpmn, although they occur in different formations. The Tcbuc, Tcbm, and Tcblc are grouped together for the purposes of the infiltration model and this is consistent with grouping crystallized lithofacies (Buesch and Spengler 1999 [DIRS 107905]). The assumption that fracture characteristics are dominated by the Tcpm is based on the lithostratigraphic descriptions of the exposures of the crystallized Bullfrog Tuff (Scott and Bonk 1984 [DIRS 104181]). It is also based on the fact that, in borehole USW G-2, the Tcpm comprises the majority of the combined thickness of the crystallized rocks (BSC 2004 [DIRS 170029]). The Tcbuc and Tcblc consist of partially to moderately welded and crystallized pyroclastic flow deposits that underwent vapor-phase corrosion and mineralization during formation of the rocks. The Tcbuc, Tcbm, and Tcblc represent less than 0.5% of the infiltration model area (Section 6.2.2, Table 6-3c, IHU 438). Therefore, their contribution to net infiltration is minimal.

Confirmation Status: This assumption does not require further confirmation, because the facts that form the basis of this assumption are well established and documented.

Use in the Analysis: Section 6.3 (Table 6-6).

5.1.7 Assumption 7: Fracture-Volume-Fraction Distribution

Within each geologic unit, fracture volume fraction follows a beta distribution.

Basis: Because fracture volume fraction must fall in the range of zero and one, a beta distribution is suitable to describe the spatial variability of fracture-volume-fraction values.

Confirmation Status: Assumption 7 does not require further confirmation, because the beta distribution is suitable to describe the range of fracture-volume-fraction values. This approach is consistent with the unsaturated zone (UZ) transport abstraction model (BSC 2005 [DIRS 173980], Section 6.5.7), which uses a beta distribution to describe the uncertainty of porosity; fracture volume fraction is a measure of fracture porosity.

Use in the Analysis: Sections 6.3 and 6.5.

5.1.8 Assumption 8: Fracture Proportion

Assumption 8: The proportion of fractures for a given lithostratigraphic zone within a mapped rock mass area is assumed to be the same as the proportion of fractures within the projected volume of the rock mass.

Basis: This assumption considers that fracture occurrence in the rock mass is homogeneous and isotropic. This approach is reasonable because the effects of heterogeneity, such as how the occurrence of fractures is directionally biased, are accounted for through the use of multiple mapped locations for the same lithostratigraphic zone, which provides multiple directions for data collection. That is, fracture mapping data are collected in various horizontal and vertical directions and, therefore, effectively sample any potential directional bias. Additionally, fracture data includes mapping of horizontal pavements on both surface and vertical sections exposed by subsurface tunneling.

Confirmation Status: Assumption 8 was confirmed by comparing calculated fracture-volume-fraction data to available results from previous studies using FracMAN (Section 6.3). The FracMAN program has been used to develop stochastically defined fracture systems that are representative of the host rock mass. FracMAN uses a measure of fracture intensity called P32, which is the ratio of fracture area to rock volume (m^2/m^3) (Anna 1998 [DIRS 144421], p. 16). The comparison of fracture volume fractions, from FracMAN data to the results of this calculation, shows that the simplified approach used herein produces greater fracture volume fractions (Section 6.3).

Use in the Analysis: Assumption 8 is used in Section 6.3.

5.1.9 Assumption 9: Fracture Infill

For the purpose of calculating a lower bound of bedrock saturated hydraulic conductivity, fractures in bedrock, immediately below the soil-bedrock interface, are assumed to be completely filled with caliche.

Basis: By visual inspection of fracture data (Sweetkind et al. 1995 [DIRS 106959], p. 48 and Appendix 2), it is clear that caliche completely fills most of the steeply dipping fractures at pavement 2001, which exposes the Tptpul and the Tptpmn. The caliche is composed principally of pedogenic calcite. Additional field observations indicate that pedogenic calcite filling fractures in surface exposures is ubiquitous at Yucca Mountain (Sanchez 2006 [DIRS 176569], p. 61).

Confirmation Status: This assumption is used (Table 6-9) to calculate the saturated hydraulic conductivity (K_{sat}) of IHU Tpcrl (number 404). The K_{sat} value calculated using this assumption was then compared (Section 6.4.5.3) with the value derived from data from a long-term infiltration test performed at Yucca Mountain. Based on the infiltration test, the mean bulk K_{sat} calculated for IHU number 404 may be underestimated, and the bulk K_{sat} may need to be increased by considering unfilled fractures. The sensitivity of bulk bedrock saturated hydraulic conductivity to unfilled fractures was examined by calculating the K_{sat} of a network of partially filled fractures with the consideration of an additional aperture for each IHU, and comparing this value to the mean K_{sat} of bulk bedrock with completely filled fractures (Section 6.4.5.4). For the

assessment of partially filled fractures, hydraulic apertures ranging from 50 μm to 1 mm were considered with the additional unfilled-fracture proportion varied between 0% and 100%. When 50% of the fractures is considered to have an additional 100 μm hydraulic aperture, then the resulting bulk K_{sat} more closely matches the results of the Alcove 1 infiltration test.

Use in the Analysis: Assumption 9 is used in Sections 6.4.5.1 and 6.4.5.2 in the calculation of K_{sat} of the bulk bedrock material with all fractures completely filled with caliche. This value is taken as a lower bound. K_{sat} of the bulk bedrock material considering partially filled fractures with an additional hydraulic aperture is calculated in Section 6.4.5.4.

5.2 SATURATED HYDRAULIC CONDUCTIVITIES OF ROCK MATRIX AND FRACTURE-FILLING CALICHE

5.2.1 Assumption 10: Representativeness of Boreholes Samples

Matrix saturated hydraulic conductivity measured on samples from boreholes is representative of the same geologic unit where it is exposed as bedrock or where it directly underlies the soil cover.

Basis: Assumption 10 is necessary because most of the saturated hydraulic conductivity data have been measured using borehole samples.

Confirmation Status: This assumption is supported by two studies that compared properties of outcrop samples and borehole samples. The petrologic properties of outcrop samples of Topopah Spring Tuff were examined and were found to be similar to stratigraphically equivalent samples from other boreholes (Price et al. 1987 [DIRS 100173], pp. 1, 16, and 17). This indicates that changes in mineralogy resulting from weathering are small. To assess geologically determined vertical trends for porosity and K_{sat} , as functions of stratigraphic elevation (dimensionless elevation within a lithostratigraphic unit), outcrop samples were used to determine the spatial variability of hydrologic properties of the Tiva Canyon Tuff (Istok et al. 1994 [DIRS 101136]). To validate the relationship between hydrologic properties and stratigraphic elevation, predicted values of porosity and K_{sat} were compared to data for samples from three additional outcrops and five boreholes. The assessment resulted in good predictions of porosity for half the stratigraphic depth for all boreholes, and for the entire stratigraphic depth for one of the five boreholes. The assessment also resulted in good predictions of porosity over the entire stratigraphic elevation for two of the three outcrops. These comparisons between data from borehole samples and from outcrop samples indicate that Assumption 10 needs no further confirmation.

Use in the Analysis: Section 6.4.

5.2.2 Assumption 11: Lognormal Spatial Distributions

Within each geologic unit, matrix and fracture-filling caliche saturated hydraulic conductivities have spatial distributions that are lognormal.

Basis: Assumption 11 is necessary because the infiltration model treats bedrock saturated hydraulic conductivity of each geologic unit as spatially varying.

Confirmation Status: Assumption 11 does not require further confirmation, because standard hydrogeologic practice is to consider matrix saturated hydraulic conductivity, including the saturated hydraulic conductivity of fracture-fill material, as lognormally distributed, based upon extensive experience (Gelhar 1993 [DIRS 101388], p. 2).

Use in the Analysis: Section 6.4.3.

5.2.3 Assumption 12: Similarity of the Tiva Canyon and Topopah Spring Formations

Matrix saturated hydraulic conductivity of the Tiva Canyon formation is similar to that of the Topopah Spring formation, within their respective units; for example, crystal rich or poor, lithophysal or nonlithophysal.

Basis: Assumption 12 is necessary because data are not available for all the units in the Tiva Canyon formation.

Confirmation Status: Assumption 12 does not require further confirmation, because the similarity of these two formations, both pyroclastic flow deposits in the Paintbrush Group resulting from similar eruptive processes, has been demonstrated (Buesch et al. 1996 [DIRS 100106], Figure 2).

Use in the Analysis: Section 6.4.4.1.

5.2.4 Assumption 13: Relationship of Porosity and Saturated Hydraulic Conductivity

Within each geologic unit, samples with greater matrix porosity have greater matrix saturated hydraulic conductivity.

Basis: Assumption 13 is necessary because some units are represented by only one or two measurements of matrix saturated hydraulic conductivity, but by more numerous measurements of porosity.

Confirmation Status: Assumption 13 does not require further confirmation, because saturated hydraulic conductivity is measured by flow through connected pores. The connectivity and the size and shape distributions of pores, and the porosity, determine the saturated hydraulic conductivity. It is reasonable to assume that the connectivity and the size and shape distributions of pores are approximately uniform within each lithologic unit. Porosity data were measured by the method of Archimedes, in which connected pores are saturated; therefore, the porosity data are appropriate for use in this analysis. This assumption is supported by a linear relationship between $\log K_{sat}$ and porosity for Tiva Canyon Tuff, with a correlation coefficient r^2 of 0.824 (Istok et al. 1994 [DIRS 101136], Equation 1a and Figure 5). This assumption is also supported by comparing the rankings of saturated hydraulic conductivity and porosity measurements for several samples within a lithologic unit (Section 6.4.4.2).

Use in the Analysis: Section 6.4.4.2.

5.2.5 Assumption 14: Standard Deviation

Where only one value of matrix saturated hydraulic conductivity is known, the standard deviation of the \log_{10} of saturated hydraulic conductivity is assumed to be one log unit, that is, one order of magnitude.

Basis: Assumption 14 is necessary because some units are represented by only one measured saturated hydraulic conductivity value.

Confirmation Status: Assumption 14 does not require further confirmation, because where sufficient data are available to calculate the standard deviation of the \log_{10} of saturated hydraulic conductivity, the values for various IHUs range between 0.35 and 2.51, with a median of 1.12 (output DTN: MO0605SPAFABRP.004, *Matrix and fracture-fill Ksat for each rock type.xls*, worksheet 'Matrix and fill summary').

Use in the Analysis: Section 6.4.4.2.

5.2.6 Assumption 15: Similarity of Identifying Properties

Matrix saturated hydraulic conductivity of the units in Topopah Spring formation is similar to other units that share an identifying property, such as having been zeolitized, or the presence or absence of lithophysae.

Basis: Assumption 15 is necessary because K_{sat} data are not available for all the units in the Topopah Spring formation.

Confirmation Status: Assumption 15 does not require further confirmation, because the surrogate and the target unit results were formed from the same eruptive process and underwent similar depositional and alteration processes that led to the identifying properties.

Use in the Analysis: Sections 6.4.4.1 and 6.4.5.3 to identify Tcplv(z), Tptpul, and Tptrn3, respectively, as surrogate units for Tptpv2(z), Tpcrnl and Tpcrl, and Tpcrn4.

5.2.7 Assumption 16: Use of Log-Uniform Uncertainty Distributions

Lower and upper limits for bulk bedrock saturated hydraulic conductivity are calculated on the basis of all fractures completely filled and all fractures partially filled with an additional 200 μm hydraulic aperture, respectively. Between these limits, bulk bedrock saturated hydraulic conductivity is assumed to be log-uniformly distributed.

Basis: The saturated hydraulic conductivity distributions for both the matrix material and fracture filling material are assumed to be lognormally distributed (Section 5.2.2, Assumption 11). The lognormal distribution is symmetric in log space and provides for a symmetric distribution of probability across parameters that vary over several orders of magnitude. A log-uniform distribution is appropriate to represent the uncertainty because bedrock K_{sat} , including the effect of partially filled fractures, may cover a large range (orders of magnitude) and little information is known about the shape of the distribution (Mishra 2002 [DIRS 163603], Section 2.3).

Confirmation Status: Assumption 16 does not require further confirmation, because for cases where the parameter limits span a large a range of values (greater than an order of magnitude), and either endpoint is equally likely, the log-uniform uncertainty distribution provides equal probability weighting across the entire scale.

Use in the Analysis: Section 6.4.5.4.

INTENTIONALLY LEFT BLANK

6. SCIENTIFIC ANALYSIS DISCUSSION

6.1 INTRODUCTION

This section documents the technical approach used to calculate bedrock saturated hydraulic conductivity, which is a measure of the ability of a material to transmit water through its connected pores under saturated conditions, typically measured in units of millimeters per day or meters per second. Bedrock saturated hydraulic conductivity is a function of two components: the saturated hydraulic conductivity of the rock matrix and the saturated hydraulic conductivity of fractures within the rock mass. The division of the bedrock between these two components is measured by the fracture volume fraction (f_{vf}) (Section 6.3).

For the purposes of this calculation, fractures are initially assessed as being completely filled with pedogenic caliche. This approach is based upon observations of filled fractures in exposed pavements and is evaluated by comparison with results of an infiltration test (Section 6.4.5.3). Rock matrix saturated hydraulic conductivities, which are variable among the geologic units at Yucca Mountain, and the saturated hydraulic conductivity of fracture-filling caliche were extracted from existing site-specific data. Both the matrix saturated hydraulic conductivities and the filled-fracture saturated hydraulic conductivities are lognormally distributed and characterized by a geometric mean value and a standard deviation in log units. The fracture volume fraction is characterized by a beta distribution. Bedrock saturated hydraulic conductivity is calculated from these quantities and is characterized by a mean value and a variance. The calculation of upper bound saturated hydraulic conductivities based on the presence of partially filled fractures with an additional hydraulic aperture is provided in Section 6.4.5.4, with a summary of the resulting mean saturated hydraulic conductivities provided in Section 6.4.5.5.

This analysis provides bedrock saturated hydraulic conductivity for various rock units at Yucca Mountain. Output from this analysis provides bedrock saturated hydraulic conductivity data that are traceable and transparent and support the development of an infiltration model (BSC 2006 [DIRS 176107], Section 1.1.4). To achieve the goals of this analysis, a hydrogeologic stratigraphic system has been developed consisting of IHU units that have differing hydrogeologic properties with special emphasis on saturated hydraulic conductivity. The IHUs are defined on the basis of lithostratigraphic contacts in boreholes and of saturated hydraulic conductivity values from measurements on the core from boreholes (BSC 2004 [DIRS 170029]), and from various other sources, including boreholes in the UZTT facility at Busted Butte and surface-based samples (Section 6.4).

The correlation of lithostratigraphic units and IHUs enables the extrapolation of the IHUs to exposures at the ground surface where most of the correlated lithostratigraphic units have been documented on the following geologic maps:

- *Preliminary Geologic Map of Yucca Mountain, Nye County, Nevada, with Geologic Sections* (Scott and Bonk 1984 [DIRS 104181])
- *Bedrock Geologic Map of the Central Block Area, Yucca Mountain, Nye County, Nevada* (Day et al. 1998 [DIRS 101557])

- *Digital Geologic Map of the Nevada Test Site and Vicinity, Nye, Lincoln and Clark Counties, Nevada, and Inyo County, California, Revision 4; Digital Aeromagnetic Map of the Nevada Test Site and Vicinity, Nye, Lincoln, and Clark Counties, Nevada, and Inyo County, California; and Digital Isostatic Gravity Map of the Nevada Test Site and Vicinity, Nye, Lincoln, and Clark Counties, Nevada, and Inyo County, California* (Slate et al. 2000 [DIRS 150228], Open-File Report 99-554-A), hereafter referred to as the digital geologic map.

For map units that do not have any correlative IHU, proxy IHUs have been proposed that are based on similarities in lithostratigraphic characteristics. These correlations of IHUs to lithostratigraphic units to map units are the basis for a bedrock saturated hydraulic conductivity map (Section 6.2). Symbols for the IHUs are unique compared to other stratigraphic systems on the Yucca Mountain Project and they contain a nomenclature hierarchy based on the lithostratigraphic unit from which the saturated hydraulic conductivity data were used as the “type section” of the IHU. In the IHU symbol nomenclature, all symbols are lower case, begin with ‘h’, and contain the letters of the formation and subdivision (zone or unit). For example, the crystal-poor, middle nonlithophysal zone of the Topopah Spring Tuff with the lithostratigraphic symbol Tptpmn, has an IHU symbol of “htmn” (Section 6.2).

In the conceptual model for infiltration, water percolates downward through the soil column and is released into the unsaturated zone (UZ) only when the saturation of the overlying soil at its interface with the bedrock exceeds field capacity, at a flux rate limited by the saturated hydraulic conductivity of the bedrock. In the conceptual model, the bedrock acts as a skin at the bottom of the soil column. The bedrock at its interface with the overlying soils is a composite material consisting of rock matrix and fractures, which are treated as being filled with caliche. Filled fractures occupy a certain fraction of the bulk volume, which is herein termed the fracture volume fraction.

In general, the area of any plane cutting a volume of fractured material is divided into fracture and matrix in the same ratio as the bulk rock. Therefore, for the purpose of limiting the flux into the UZ, bedrock saturated hydraulic conductivity is calculated as the mean of matrix and filled-fracture saturated hydraulic conductivities, each weighted by its respective volume fraction, which is the same as the area fraction. The spatial distributions of the fracture volume fraction and the saturated hydraulic conductivities of both the matrix material and fracture-filling material are described as probability distribution functions; saturated hydraulic conductivity of composite material is described and calculated in Section 6.4.5; spatial variability propagated is described in Section 6.4.5.1, with a general discussion of the propagation of variability with lognormal distributions provided in Appendix B.

Technical inputs used directly in the calculation of bedrock saturated hydraulic conductivity are listed in Table 4-1. Indirect inputs of corroborative or supporting information are listed in Table 6-1. The bedrock saturated hydraulic conductivity data set developed herein describes the spatial variability of the saturated hydraulic conductivity at the interface between the soil and bedrock and is only intended for use as input to an infiltration model for Yucca Mountain. Inputs to this analysis are limited by a lack of data on the extent to which fractures in the bedrock at the interface between the soil and bedrock are incompletely filled with pedogenic caliche, as discussed in Section 6.4.5.4.

Table 6-1. Indirect Inputs

Indirect Input Description	Location in This Analysis	Source
Technical work plan	Sections 1, 2, 3, 4.3, 6.1, 6.2.2	BSC 2006 [DIRS 176107]
Q-List	Section 2	BSC 2005 [DIRS 175539]
Acceptance criteria	Sections 4.2, 7	NRC 2003 [DIRS 163274], Section 2.2.1.3.5.3
Description of regional geology and fracture characteristics at Yucca Mountain	Section 5.1	DTN: GS950608314211.026 [DIRS 175931]
	Sections 1, 5.1, 5.1.6, 6.1, 6.2.2; Appendix A	BSC 2004 [DIRS 170029]
	Section 6.3	National Research Council 1996 [DIRS 139151], pp. 108, 111, 118, and 126
	Sections 1, 5.1.5, 5.1.6, 6.1, 6.2.2; Appendix A	Scott and Bonk 1984 [DIRS 104181]
	Section 6.2.1; Appendix A	Broxton et al. 1993 [DIRS 107386]
	Sections 1, 5.1.3, 5.1.6, 6.2.2; Appendix A	Buesch and Spengler 1999 [DIRS 107905]
	Sections 1, 5.1.1, 5.1.3, 5.1.4, 5.2.3, 6.2.1, 6.2.2, 6.4.4.1; Appendix A	Buesch et al. 1996 [DIRS 100106], Figure 2 and Table 1
	Section 6.2.1	Byers et al. 1976 [DIRS 104639]
	Section 6.2.1	Christiansen et al. 1977 [DIRS 157236]
	Section 6.2.1; Appendix A	Day et al. 1998 [DIRS 100027]
	Sections 1, 6.1, 6.2.2, 6.4.5.3; Appendix A	Day et al. 1998 [DIRS 101557]
	Section 6.2.1	Gibson et al. 1990 [DIRS 157245]
	Section 6.2.1	Lipman et al. 1966 [DIRS 100773]
	Section 6.2.2; Appendix A	Moyer and Geslin 1995 [DIRS 101269]
	Section 6.2.1	Ortiz et al. 1985 [DIRS 101280], Table 1
	Section 6.2.1	Sawyer et al. 1994 [DIRS 100075]
	Section 6.2.1	Schuraytz et al. 1989 [DIRS 107248]
	Sections 1, 6.1, 6.2.2; Appendix A	Slate et al. 2000 [DIRS 150228], Open-File Report 99-554-A
	Section 6.2.2; Appendix A	Dickerson and Drake 1998 [DIRS 102929]
	Appendix A	Geslin et al. 1995 [DIRS 103330]
	Appendix A	Otto and Buesch 2003 [DIRS 170727]
	Appendix A	Geslin and Moyer 1995 [DIRS 101226]
	Appendix A	Moyer et al. 1995 [DIRS 103777]
	Appendix A	DTN: MO0101XRDDRILC.002 [DIRS 163795]
	Sections 5.2.1, 5.2.4	Istok et al. 1994 [DIRS 101136], Equation 1a and Figure 5
	Section 5.2.1	Price et al. 1987 [DIRS 100173], pp. 1, 16, and 17
Supporting surface fracture mapping data	Section 6.3	Sweetkind et al. 1997 [DIRS 177047], pp. 22, 25, and 85
	Output DTN: MO0605SPAFABRP.004, <i>Fracture Volume Fraction for Each Rock Type v7.xls</i> , worksheet 'Surface Calculation'	Sweetkind and Williams-Stroud 1996 [DIRS 100182], pp. 41 and 43
	Sections 5.1.9, 6.4.5.4, 6.4.5.5, 6.5.2	Sweetkind et al. 1995 [DIRS 106959], p. 48, Figure 2, Appendix 2
	Sections 6.4.5.4, 6.4.5.4.2, 6.4.5.5, 6.5.2	Sweetkind et al. 1995 [DIRS 106958], pp. 12 and 34

Table 6-1. Indirect Inputs (Continued)

Indirect Input Description	Location in This Analysis	Source
Supporting surface fracture mapping data (Continued)	Sections 5.1.9, 6.4.5.4.2, 6.4.5.5, 6.5.2	Sanchez 2006 [DIRS 176569], pp. 26 to 61
Lithostratigraphic contacts for underground fracture mapping data	Section 6.3	Beason et al. 1996 [DIRS 101191], pp. 16 to 26
	Section 6.3	Barr et al. 1996 [DIRS 100029], Table 1, p. 76
	Section 6.3	Eatman et al. 1997 [DIRS 101219], Table 1
	Section 6.3	DTN: GS981108314224.005 [DIRS 109070], Table S98481_001
	Section 6.3	DTN: GS990708314224.007 [DIRS 164604], Table S00076_001
Stochastically defined fracture systems developed using FracMAN	Sections 5.1.8, 6.3	Anna 1998 [DIRS 144421], Figures 3 and 8, p. 16
	Section 6.3	Anna 1998 [DIRS 138501], Figure 2 and Table 2
	Section 6.3	BSC 2004 [DIRS 166107], Figure 6-18
Analysis of hydrologic properties data	Section 1	BSC 2004 [DIRS 170007], Table B-3
	Sections 6.2.1, 6.4.1, 6.4.3, 6.4.5.4	BSC 2004 [DIRS 170038]
	Sections 6.2.1, 6.2.2, and 6.4.4; Appendix A	BSC 2004 [DIRS 169855], Table 6-5
Flow through rock	Sections 6.4.3, 6.4.5.4.1, 6.5.1	Freeze and Cherry 1979 [DIRS 101173], Section 2.4, Equations 2.28 and 2.87
	Section 6.4.5.3	Liu et al. 2003 [DIRS 162470]
	Section 6.4.5.3	DTN: GS000808312242.006 [DIRS 162980]
	Section 6.4.5.3	DTN: GS990108312242.006 [DIRS 162979]
	Section 6.4.5.3	DTN: MO0512SPASURFD.000 [DIRS 175870]
	Section 6.4.5.3	DTN: MO0605SPASOILS.005 [DIRS 176922]
	Section 6.4.5.4.2	Glass et al. 2002 [DIRS 176044], Sections 2 and 3.4
	Section 6.4.5.4	Anna 1998 [DIRS 144421], pp. 28 and 29, Tables 14 and 15
	Section 6.4.5.4	Anna 1998 [DIRS 138501], Table 11
	Section 6.4.5.4.2	DTN: GS970183122410.001 [DIRS 105580]
	Section 6.4.5.4.2	LeCain 1998 [DIRS 100052], pp. 17 to 20
	Section 5.2.2	Gelhar 1993 [DIRS 101388], p. 2
Lithology for hydrologic properties data	Sections 6.4.2, 6.4.5.3	BSC 2004 [DIRS 170004], Figures 1-1 and 1-2
Supporting saturated hydraulic conductivity data	Section 6.4.1	DTN: GS000408312231.003 [DIRS 149461]
	Section 6.4.1	DTN: GS960808312231.001 [DIRS 108998]
	Section 6.4.1	DTN: GS960808312231.005 [DIRS 108995]
	Section 6.4.1	DTN: GS990408312231.001 [DIRS 148711]
Statistical evaluation and uncertainty assessment	Section 6.4.3	Helsel and Hirsch 1995 [DIRS 175683], Chapters 2 and 13
	Sections 5.1.7, 6.3	BSC 2005 [DIRS 173980], Section 6.5.7
	Sections 6.4, 6.5.2	Hahn and Shapiro 1967 [DIRS 146529], Equations 3-28a and 3-28b, p. 128
	Appendix B	Gilbert 1987 [DIRS 163705], pp. 27 to 28, 152, 156, 159, 167 to 168, and 259 to 261
	Section 6.5.2; Appendix B	ANSI/NCSL Z540-2-1997 [DIRS 157394], pp. 3, 9, 19, 32, and 33

Table 6-1. Indirect Inputs (Continued)

Indirect Input Description	Location in This Analysis	Source
Statistical evaluation and uncertainty assessment (Continued)	Sections 5.2.7, 6.4.5.4, 6.5.2	Mishra 2002 [DIRS 163603], Section 2.3
Software validation	Section 3	CRWMS M&O 2000 [DIRS 153526]

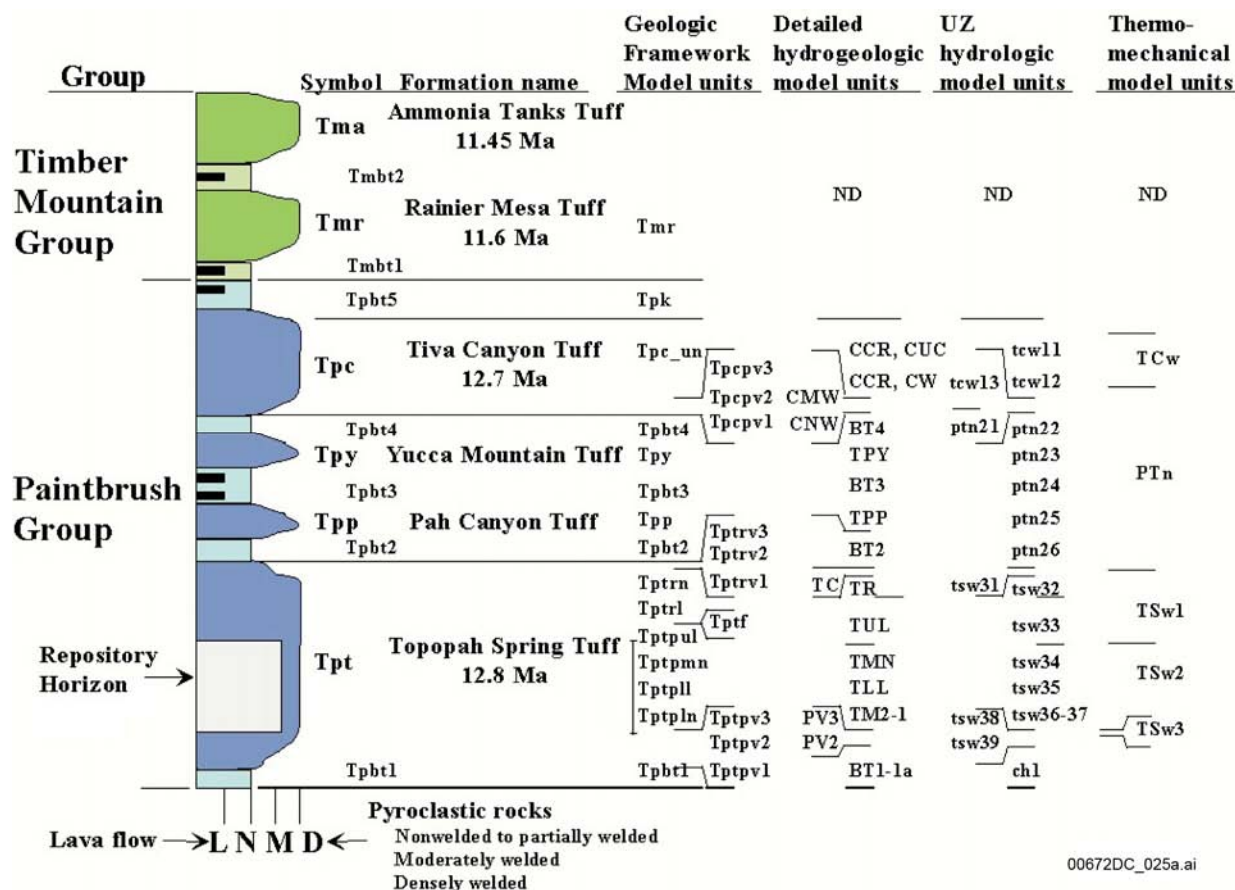
6.2 ASSESSMENT OF BEDROCK GEOLOGY

6.2.1 Regional Geology

Yucca Mountain lies in southern Nevada, in the Great Basin, which is part of the Basin and Range structural/physiographic province. In the Yucca Mountain area, pre-Tertiary rocks, consisting of a thick sequence of Proterozoic and Paleozoic sedimentary rocks, underlie approximately 1,000 to 3,000 m of Miocene volcanic rocks (Gibson et al. 1990 [DIRS 157245]). The Miocene volcanic sequence exposed at Yucca Mountain includes units of the Paintbrush and Timber Mountain groups (Sawyer et al. 1994 [DIRS 100075]); the entire section dips five to 10 degrees east (Day et al. 1998 [DIRS 100027]).

The Paintbrush Group consists of pyroclastic rocks and lavas that originate from the Claim Canyon caldera approximately 6 km north of the study area and are from 12.7 to 12.8 million years old (Byers et al. 1976 [DIRS 104639]; Sawyer et al. 1994 [DIRS 100075]). The Paintbrush Group includes a sequence of four formations: the Tiva Canyon, Yucca Mountain, Pah Canyon, and Topopah Spring Tuffs (Figure 6-1), each of which consist primarily of large-volume, pyroclastic-flow deposits with minor amounts of pyroclastic-fall deposits (Broxton et al. 1993 [DIRS 107386]; Buesch et al. 1996 [DIRS 100106]; Byers et al. 1976 [DIRS 104639]; Christiansen et al. 1977 [DIRS 157236]). At Yucca Mountain, two of these formations, the Topopah Spring and Tiva Canyon Tuffs, are voluminous, mostly densely welded, compositionally zoned, outflow sheet, pyroclastic-flow deposits – also referred to as ignimbrites – that grade upward from rhyolite composition to quartz latite composition (Byers et al. 1976 [DIRS 104639]; Lipman et al. 1966 [DIRS 100773]; Schuraytz et al. 1989 [DIRS 107248]). Formations of the Paintbrush Group are interbedded with bedded tuffs, which consist of thinner pyroclastic-flow and pyroclastic-fall deposits, and, locally, a few lava flows (Broxton et al. 1993 [DIRS 107386]; Buesch et al. 1996 [DIRS 100106]; Byers et al. 1976 [DIRS 104639]; Christiansen et al. 1977 [DIRS 157236]; Day et al. 1998 [DIRS 100027]).

The 11.45 to 11.6 million year old rocks of the Timber Mountain Group were erupted from the Timber Mountain caldera complex and consist of the Ammonia Tanks Tuff and the Rainer Mesa Tuff (Sawyer et al. 1994 [DIRS 100075]) and interbedded tuffaceous rocks and lava flows.



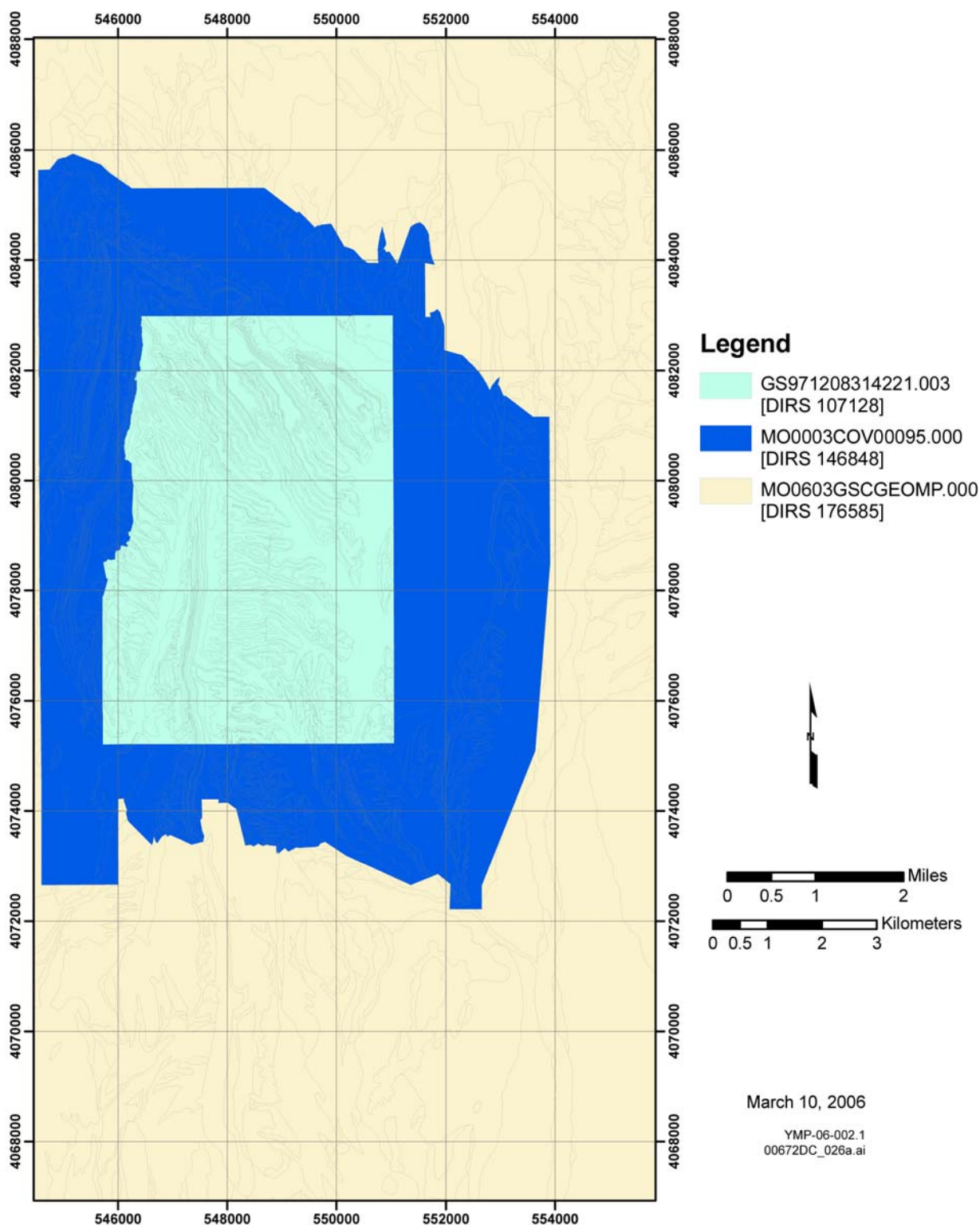
Sources: BSC 2004 [DIRS 170029], Table 6-2 (geologic framework model units); BSC 2004 [DIRS 170038], Table 6-1 (hydrogeologic model units); BSC 2004 [DIRS 169855], Table 6-5 (UZ hydrologic model units); Ortiz et al. 1985 [DIRS 101280], Table 1 (thermo-mechanical model units).

UZ = unsaturated zone.

Figure 6-1. Simplified Lithostratigraphic Column of Timber Mountain Group and Paintbrush Group at Yucca Mountain

6.2.2 Development of Bedrock Hydrogeologic Units for Infiltration Modeling

The infiltration model (BSC 2006 [DIRS 176107], Section 1.1.4) uses 253,597 records of data with each record corresponding to a 30×30 m grid cell in the model area. The model area includes the entire Busted Butte 7.5 min quadrangle and the southern half of the Topopah Spring NW 7.5 min quadrangle. Because bedrock hydrologic properties are assigned on the basis of lithology, the proper bedrock geologic unit was assigned to each grid cell. This was accomplished with digital manipulation of existing geologic mapping data covering the area. Three coverage files were selected for this process; the area covered by each source file is shown on Figure 6-2.



Sources: DTNs: GS971208314221.003 [DIRS 107128], *cb6k.ps*; MO0003COV00095.000 [DIRS 146848], *scotbons.e00*; MO0603GSCGEOMP.000 [DIRS 176585], *ofr-99-0554-e00.tar*.

NOTE: The outer figure boundary is the boundary for the infiltration model.

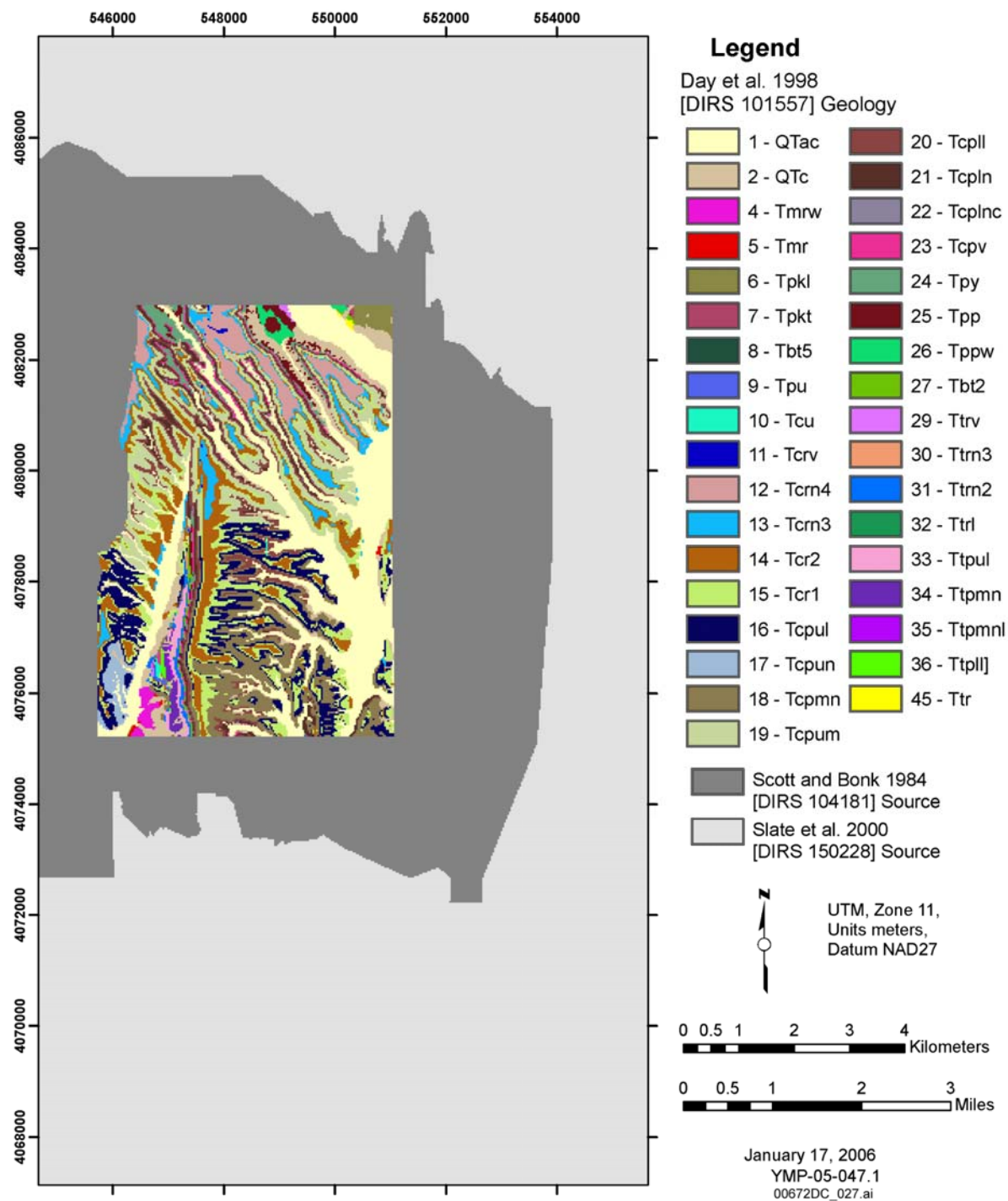
Figure 6-2. Bedrock Geology Coverage Supplied by Source Files for the Infiltration Model Area

Three source files contain the three geologic maps evaluated in this analysis. The first map is contained in DTN: GS971208314221.003 [DIRS 107128], *cb6k.ps*, which represents detailed mapping of the central block area at Yucca Mountain (Figure 6-3) (Day et al. 1998 [DIRS 101557]). The original publication scale for this mapping is 1:6,000. The second map, contained in DTN: MO0003COV00095.000 [DIRS 146848], *scotbons.e00*, covers a larger area (Scott and Bonk 1984 [DIRS 104181]) and was, therefore, used for the area (Figure 6-4) outside the limits of DTN: GS971208314221.003 [DIRS 107128], *cb6k.ps*. The original publication scale for mapping in DTN: MO0003COV00095.000 [DIRS 146848], *scotbons.e00*, is 1:12,000. These two source files do not provide coverage for the northern, eastern, and southern edges of the model area. Thus, bedrock geology for the edges of the model area is from the third map, which is the digital geologic map contained in DTN: MO0603GSCGEOMP.000 [DIRS 176585], *ofr-99-0554-e00.tar*, as developed by Slate et al. (2000 [DIRS 150228], Open-File Report 99-554-A). This version is the current map for the Nevada Test Site and vicinity. This coverage represents a compilation and synthesis of previous geologic mapping in the region and has an original publication scale of 1:120,000 (Figure 6-5).

In output DTN: MO0603SPAGRIDD.003, each comma-delimited record includes fields representing x- and y-coordinates for the center of the associated 30 × 30 m cell. The lithologic mapping unit corresponding to the center-cell coordinates was determined from source polygon coverages using ARCINFO. The source files use a number code to designate stratigraphic units in the digital coverage files. These original unit identification numbers for the areas of interest are listed in Table 6-2. In addition, the stratigraphic unit identified is shown at the point at the center of the cell in the “Geology” field of output DTN: MO0603SPAGRIDD.003. Modified geologic identifier numbers were used for this designation, because they provided unique identifiers for instances where the same code numbers were used in the three coverage files to represent different stratigraphic units. The stratigraphic units and the original source identification numbers corresponding to these modified code numbers in output DTN: MO0603SPAGRIDD.003 are listed in Table 6-2.

The use of the center point of a grid cell to determine lithology can result in a generalization of the bedrock geology from that shown on source maps. Cells that contain contacts between two or more units have been generalized to the unit found at the center of the cell. This means that thin units may occasionally be underrepresented or overrepresented in the file or that contacts may be displaced by up to 15 m. Given that the infiltration model contains over 250,000 cells, this level of precision is considered acceptable for the purposes of the infiltration model when the natural variation within each lithologic unit and the uncertainties regarding the properties assigned to each unit are considered.

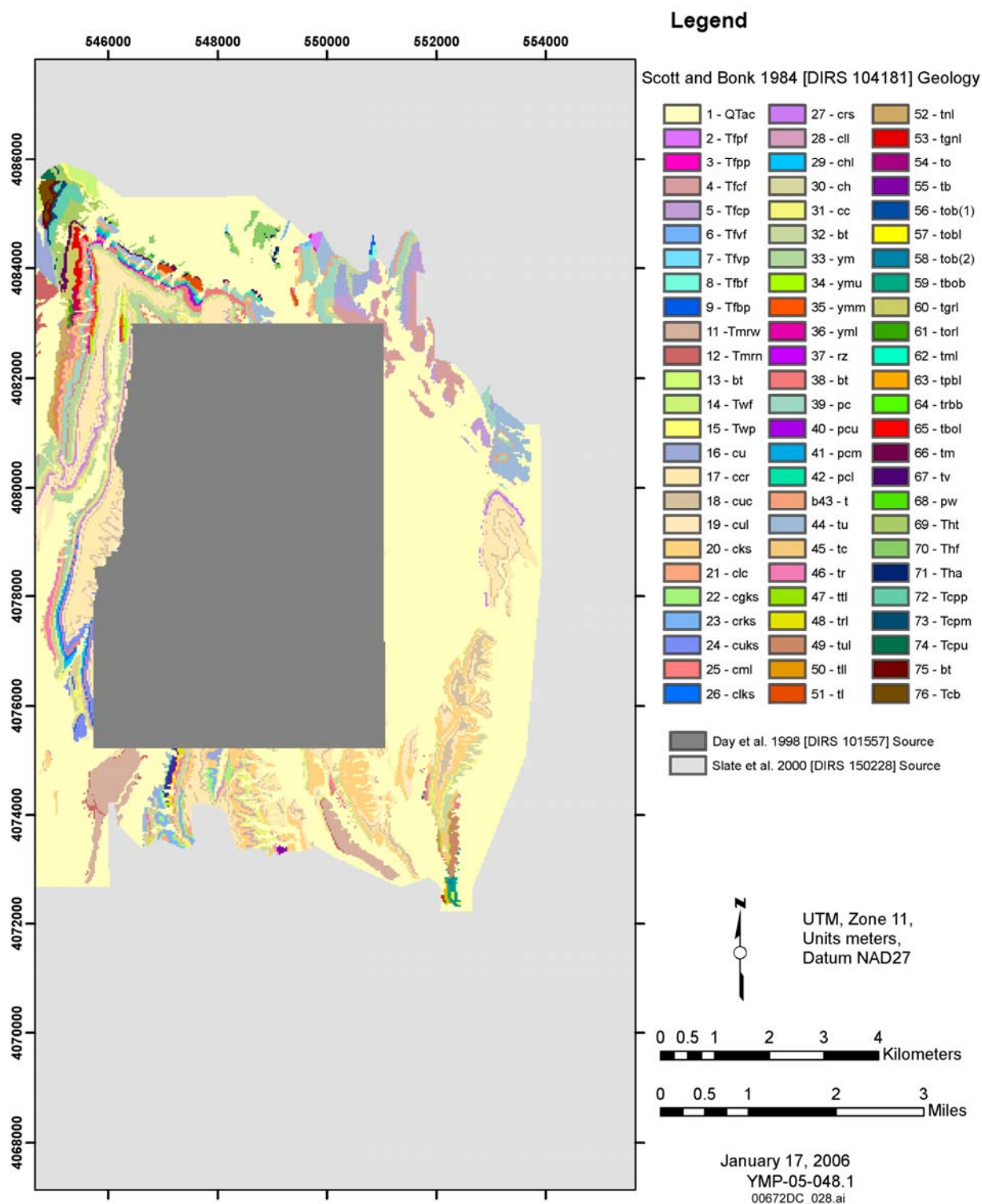
Map units are correlated to a common set of lithostratigraphic units and symbols (Tables 6-3a and A-1), because the same stratigraphic nomenclature to define mapping units (Table 6-2) is not used in the three source coverage files: DTNs: GS971208314221.003 [DIRS 107128], *cb6k.ps*; MO0003COV00095.000 [DIRS 146848], *scotbons.e00*; and MO0603GSCGEOMP.000 [DIRS 176585], *ofr-99-0554-e00.tar*. Details of the names, descriptions, and symbols for map units, in the three map source files, and the associated lithostratigraphic names and symbols are included as a correlation table in output DTN: MO0605SPAFABRP.004, *Infiltrate Ap-A Bedrock Correlation 14Feb06.xls*.



Source: DTN: GS971208314221.003 [DIRS 107128], *cb6k.ps*.

NOTES: The outer figure boundary is the boundary for the infiltration model. Unit identification numbers are from the source file and are listed in Table 6-2.

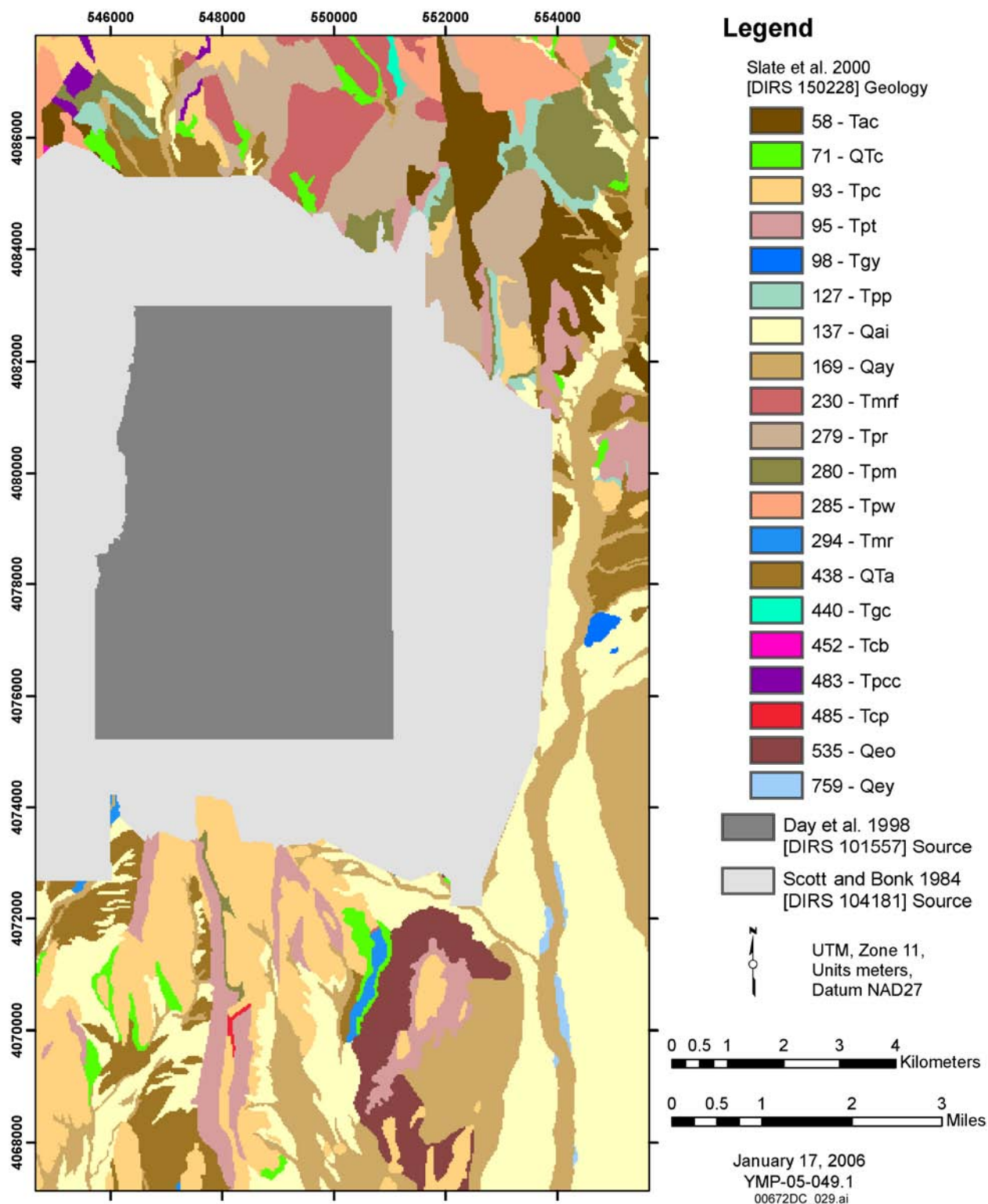
Figure 6-3. Revised Bedrock Geologic Map of the Central Block Area



Source: DTN: MO0003COV00095.000 [DIRS 146848], *scotbons.e00*.

NOTES: The outer figure boundary is the boundary for the infiltration model. Unit identification numbers are from the source file and are listed in Table 6-2.

Figure 6-4. Geology Coverage: Scotbons



Source: DTN: MO0603GSCGEOMP.000 [DIRS 176585], *ofr-99-0554-e00.tar*.

NOTES: The outer figure boundary is the boundary for the infiltration model. Unit identification numbers are from the source file and are listed in Table 6-2.

Figure 6-5. Digital Geologic Map

Table 6-2. Bedrock Mapping Units Used in the Source File

Modified Geologic ID Number	Formation	Lithology/Subdivision (Symbol)	Source DTNs:	ID Number Used in Source File
101	Alluvium and Colluvium	(Qtac)	GS971208314221.003 [DIRS 107128]	1
102	Colluvium	(QTc)	GS971208314221.003 [DIRS 107128]	2
103	Rainier Mesa Tuff	Welded (Tppw)	GS971208314221.003 [DIRS 107128]	4
104	Rainier Mesa Tuff	Nonwelded (Tmr)	GS971208314221.003 [DIRS 107128]	5
105	Rhyolite of Comb Peak	Lava flows (TpkI)	GS971208314221.003 [DIRS 107128]	6
106	Rhyolite of Comb Peak	Ash-flow tuff (Tbkt)	GS971208314221.003 [DIRS 107128]	7
107	Bedded tuff	(Tpbt5)	GS971208314221.003 [DIRS 107128]	8
108	Paintbrush Group	Undivided, highly brecciated (Tpu)	GS971208314221.003 [DIRS 107128]	9
109	Tiva Canyon Tuff (crystal rich)	Undivided, tectonically brecciated (Tcu)	GS971208314221.003 [DIRS 107128]	10
110	Tiva Canyon Tuff (crystal rich)	Crystal-rich vitric zone (Tcrv)	GS971208314221.003 [DIRS 107128]	11
111	Tiva Canyon Tuff (crystal rich)	Subvitric transition zone (Tcrn4)	GS971208314221.003 [DIRS 107128]	12
112	Tiva Canyon Tuff (crystal rich)	Pumice-poor zone (Tcrn3)	GS971208314221.003 [DIRS 107128]	13
113	Tiva Canyon Tuff (crystal rich)	Mixed-pumice zone (Tcrn2)	GS971208314221.003 [DIRS 107128]	14
114	Tiva Canyon Tuff (crystal rich)	Crystal transition zone (Tcrn1)	GS971208314221.003 [DIRS 107128]	15
115	Tiva Canyon Tuff (crystal poor)	Upper lithophysal zone (Tcpl)	GS971208314221.003 [DIRS 107128]	16
116	Tiva Canyon Tuff (crystal poor)	Upper nonlithophysal zone (Tcpun)	GS971208314221.003 [DIRS 107128]	17
117	Tiva Canyon Tuff (crystal poor)	Middle nonlithophysal zone (Tcpmn)	GS971208314221.003 [DIRS 107128]	18
118	Tiva Canyon Tuff (crystal poor)	Upper and middle nonlithophysal zones, undivided (Tcpum)	GS971208314221.003 [DIRS 107128]	19
119	Tiva Canyon Tuff (crystal poor)	Lower lithophysal zone (TcplI)	GS971208314221.003 [DIRS 107128]	20
120	Tiva Canyon Tuff (crystal poor)	Lower nonlithophysal zone (Tcpln)	GS971208314221.003 [DIRS 107128]	21
121	Tiva Canyon Tuff (crystal poor)	Columnar subzone (Tcplnc)	GS971208314221.003 [DIRS 107128]	22
122	Tiva Canyon Tuff (crystal poor)	Crystal-poor vitric zone (Tcpv)	GS971208314221.003 [DIRS 107128]	23
123	Pre-Tiva Canyon Tuff, Yucca Mountain Tuff	Nonwelded tuffs, undivided (Tpy)	GS971208314221.003 [DIRS 107128]	24
124	Pah Canyon Tuff	Nonwelded to moderately welded (Tpp)	GS971208314221.003 [DIRS 107128]	25
125	Pah Canyon Tuff	Welded (Tppw)	GS971208314221.003 [DIRS 107128]	26
126	Pre-Pah Canyon bedded tuff	(Tpbt2)	GS971208314221.003 [DIRS 107128]	27
127	Topopah Spring Tuff (crystal rich)	Vitric and densely welded zones (Ttrv)	GS971208314221.003 [DIRS 107128]	29
128	Topopah Spring Tuff (crystal rich)	Densely welded zone (Ttrn3)	GS971208314221.003 [DIRS 107128]	30
129	Topopah Spring Tuff (crystal rich)	Pumice-rich zone (Ttrn2)	GS971208314221.003 [DIRS 107128]	31
130	Topopah Spring Tuff (crystal rich)	Crystal transition zone (Ttr1)	GS971208314221.003 [DIRS 107128]	32

Table 6-2. Bedrock Mapping Units Used in the Source File (Continued)

Modified Geologic ID Number	Formation	Lithology/Subdivision (Symbol)	Source DTNs:	ID Number Used in Source File
131	Topopah Spring Tuff (crystal poor)	Upper lithophysal zone (Ttpul)	GS971208314221.003 [DIRS 107128]	33
132	Topopah Spring Tuff (crystal poor)	Middle nonlithophysal zone (Ttpmn)	GS971208314221.003 [DIRS 107128]	34
133	Topopah Spring Tuff (crystal poor)	Lithophysal subzone of Ttpmn (Ttpmnl)	GS971208314221.003 [DIRS 107128]	35
134	Topopah Spring Tuff (crystal poor)	Lower lithophysal zone (Ttpll)	GS971208314221.003 [DIRS 107128]	36
135	Topopah Spring Tuff (crystal rich)	Undivided (Ttr)	GS971208314221.003 [DIRS 107128]	45
201	Alluvium and Colluvium	(Qtac)	MO0003COV00095.000 [DIRS 146848] GS930283117461.001 [DIRS 107027]	1
202	Rhyolite of Pinnacles Ridge	Lava flows (Tfpf)	MO0003COV00095.000 [DIRS 146848] GS930283117461.001 [DIRS 107027]	2
203	Rhyolite of Pinnacles Ridge	Pyroclastic rocks (Tfpp)	MO0003COV00095.000 [DIRS 146848] GS930283117461.001 [DIRS 107027]	3
204	Rhyolite of Comb Peak	Lava flows (Tfcf)	MO0003COV00095.000 [DIRS 146848] GS930283117461.001 [DIRS 107027]	4
205	Rhyolite of Comb Peak	Pyroclastic rocks (Tfcp)	MO0003COV00095.000 [DIRS 146848] GS930283117461.001 [DIRS 107027]	5
206	Rhyolite of Vent Pass	Lava flows (Tlvf)	MO0003COV00095.000 [DIRS 146848] GS930283117461.001 [DIRS 107027]	6
207	Rhyolite of Vent Pass	Pyroclastic rocks (Tfvp)	MO0003COV00095.000 [DIRS 146848] GS930283117461.001 [DIRS 107027]	7
208	Rhyolite of Black Glass Canyon	Lava flows (Tfbf)	MO0003COV00095.000 [DIRS 146848] GS930283117461.001 [DIRS 107027]	8
209	Rhyolite of Black Glass Canyon	Pyroclastic rocks (Tfbp)	MO0003COV00095.000 [DIRS 146848] GS930283117461.001 [DIRS 107027]	9
210	Rainier Mesa Tuff	Welded ash-flow tuff (Tmrw)	MO0003COV00095.000 [DIRS 146848] GS930283117461.001 [DIRS 107027]	11
211	Rainier Mesa Tuff	Nonwelded ash-flow tuff (Tmrn)	MO0003COV00095.000 [DIRS 146848] GS930283117461.001 [DIRS 107027]	12
212	Bedded tuff	(bt)	MO0003COV00095.000 [DIRS 146848] GS930283117461.001 [DIRS 107027]	13
213	Rhyolite of Windy Wash	Lava flows (Twf)	MO0003COV00095.000 [DIRS 146848] GS930283117461.001 [DIRS 107027]	14
214	Rhyolite of Windy Wash	Pyroclastic rocks (Twp)	MO0003COV00095.000 [DIRS 146848] GS930283117461.001 [DIRS 107027]	15
215	Tiva Canyon Tuff	Undivided (cu)	MO0003COV00095.000 [DIRS 146848] GS930283117461.001 [DIRS 107027]	16
216	Tiva Canyon Tuff	Caprock (ccr) south of UTM northing 4079520	MO0003COV00095.000 [DIRS 146848] GS930283117461.001 [DIRS 107027]	17
217	Tiva Canyon Tuff	Upper cliff (cuc)	MO0003COV00095.000 [DIRS 146848] GS930283117461.001 [DIRS 107027]	18

Table 6-2. Bedrock Mapping Units Used in the Source File (Continued)

Modified Geologic ID Number	Formation	Lithology/Subdivision (Symbol)	Source DTNs:	ID Number Used in Source File
218	Tiva Canyon Tuff	Upper lithophysal (cul)	MO0003COV00095.000 [DIRS 146848] GS930283117461.001 [DIRS 107027]	19
219	Tiva Canyon Tuff	Clinkstone (cks)	MO0003COV00095.000 [DIRS 146848] GS930283117461.001 [DIRS 107027]	20
220	Tiva Canyon Tuff	Lower cliff (clc)	MO0003COV00095.000 [DIRS 146848] GS930283117461.001 [DIRS 107027]	21
221	Tiva Canyon Tuff	Gray clinkstone (cgks)	MO0003COV00095.000 [DIRS 146848] GS930283117461.001 [DIRS 107027]	22
222	Tiva Canyon Tuff	Red clinkstone (crks)	MO0003COV00095.000 [DIRS 146848] GS930283117461.001 [DIRS 107027]	23
223	Tiva Canyon Tuff	Upper clinkstone (cuks)	MO0003COV00095.000 [DIRS 146848] GS930283117461.001 [DIRS 107027]	24
224	Tiva Canyon Tuff	Middle lithophysal (cml)	MO0003COV00095.000 [DIRS 146848] GS930283117461.001 [DIRS 107027]	25
225	Tiva Canyon Tuff	Lower clinkstone (clks)	MO0003COV00095.000 [DIRS 146848] GS930283117461.001 [DIRS 107027]	26
226	Tiva Canyon Tuff	Rounded step (crs)	MO0003COV00095.000 [DIRS 146848] GS930283117461.001 [DIRS 107027]	27
227	Tiva Canyon Tuff	Lower lithophysal (cll)	MO0003COV00095.000 [DIRS 146848] GS930283117461.001 [DIRS 107027]	28
228	Tiva Canyon Tuff	Lower lithophysal and hackly undifferentiated (chl)	MO0003COV00095.000 [DIRS 146848] GS930283117461.001 [DIRS 107027]	29
229	Tiva Canyon Tuff	Hackly zone (ch)	MO0003COV00095.000 [DIRS 146848] GS930283117461.001 [DIRS 107027]	30
230	Tiva Canyon Tuff	Columnar (cc)	MO0003COV00095.000 [DIRS 146848] GS930283117461.001 [DIRS 107027]	31
231	Bedded tuff	(bt)	MO0003COV00095.000 [DIRS 146848] GS930283117461.001 [DIRS 107027]	32
232	Yucca Mountain Tuff	Undivided (ym)	MO0003COV00095.000 [DIRS 146848] GS930283117461.001 [DIRS 107027]	33
233	Yucca Mountain Tuff	Upper (ymu)	MO0003COV00095.000 [DIRS 146848] GS930283117461.001 [DIRS 107027]	34
234	Yucca Mountain Tuff	Middle (ymm)	MO0003COV00095.000 [DIRS 146848] GS930283117461.001 [DIRS 107027]	35
235	Yucca Mountain Tuff	Lower (yml)	MO0003COV00095.000 [DIRS 146848] GS930283117461.001 [DIRS 107027]	36
236	Rhyolite Flows	(rz)	MO0003COV00095.000 [DIRS 146848] GS930283117461.001 [DIRS 107027]	37

Table 6-2. Bedrock Mapping Units Used in the Source File (Continued)

Modified Geologic ID Number	Formation	Lithology/Subdivision (Symbol)	Source DTNs:	ID Number Used in Source File
237	Bedded tuff	(bt)	MO0003COV00095.000 [DIRS 146848] GS930283117461.001 [DIRS 107027]	38
238	Pah Canyon Tuff	Undivided (pc)	MO0003COV00095.000 [DIRS 146848] GS930283117461.001 [DIRS 107027]	39
239	Pah Canyon Tuff	Upper (pcu)	MO0003COV00095.000 [DIRS 146848] GS930283117461.001 [DIRS 107027]	40
240	Pah Canyon Tuff	Middle (pcm)	MO0003COV00095.000 [DIRS 146848] GS930283117461.001 [DIRS 107027]	41
241	Pah Canyon Tuff	Lower (pcl)	MO0003COV00095.000 [DIRS 146848] GS930283117461.001 [DIRS 107027]	42
242	Bedded tuff	—	MO0003COV00095.000 [DIRS 146848] GS930283117461.001 [DIRS 107027]	43
243	Topopah Spring Tuff	Undivided (tu)	MO0003COV00095.000 [DIRS 146848] GS930283117461.001 [DIRS 107027]	44
244	Topopah Spring Tuff	Caprock (tc)	MO0003COV00095.000 [DIRS 146848] GS930283117461.001 [DIRS 107027]	45
245	Topopah Spring Tuff	Rounded (tr)	MO0003COV00095.000 [DIRS 146848] GS930283117461.001 [DIRS 107027]	46
246	Topopah Spring Tuff	Thin lithophysal (ttl)	MO0003COV00095.000 [DIRS 146848] GS930283117461.001 [DIRS 107027]	47
247	Topopah Spring Tuff	Red lithophysal (trl)	MO0003COV00095.000 [DIRS 146848] GS930283117461.001 [DIRS 107027]	48
248	Topopah Spring Tuff	Upper lithophysal (tul)	MO0003COV00095.000 [DIRS 146848] GS930283117461.001 [DIRS 107027]	49
249	Topopah Spring Tuff	Lower lithophysal (tll)	MO0003COV00095.000 [DIRS 146848] GS930283117461.001 [DIRS 107027]	50
250	Topopah Spring Tuff	Lithophysal (tl)	MO0003COV00095.000 [DIRS 146848] GS930283117461.001 [DIRS 107027]	51
251	Topopah Spring Tuff	Nonlithophysal (tnl)	MO0003COV00095.000 [DIRS 146848] GS930283117461.001 [DIRS 107027]	52
252	Topopah Spring Tuff	Gray nonlithophysal (tgnl)	MO0003COV00095.000 [DIRS 146848] GS930283117461.001 [DIRS 107027]	53
253	Topopah Spring Tuff	Orange (to)	MO0003COV00095.000 [DIRS 146848] GS930283117461.001 [DIRS 107027]	54
254	Topopah Spring Tuff	Brick (tb)	MO0003COV00095.000 [DIRS 146848] GS930283117461.001 [DIRS 107027]	55
255	Topopah Spring Tuff	Orange brick (tob)	MO0003COV00095.000 [DIRS 146848] GS930283117461.001 [DIRS 107027]	56

Table 6-2. Bedrock Mapping Units Used in the Source File (Continued)

Modified Geologic ID Number	Formation	Lithology/Subdivision (Symbol)	Source DTNs:	ID Number Used in Source File
256	Topopah Spring Tuff	Orange brick lithophysal (tobl)	MO0003COV00095.000 [DIRS 146848] GS930283117461.001 [DIRS 107027]	57
257	Topopah Spring Tuff	Orange brick (tob)	MO0003COV00095.000 [DIRS 146848] GS930283117461.001 [DIRS 107027]	58
258	Topopah Spring Tuff	Brownish-orange brick (tbob)	MO0003COV00095.000 [DIRS 146848] GS930283117461.001 [DIRS 107027]	59
259	Topopah Spring Tuff	Grayish-red lithophysal (tgrl)	MO0003COV00095.000 [DIRS 146848] GS930283117461.001 [DIRS 107027]	60
260	Topopah Spring Tuff	Orangish-red lithophysal (torl)	MO0003COV00095.000 [DIRS 146848] GS930283117461.001 [DIRS 107027]	61
261	Topopah Spring Tuff	Mottled lithophysal (tml)	MO0003COV00095.000 [DIRS 146848] GS930283117461.001 [DIRS 107027]	62
262	Topopah Spring Tuff	Purplish-brown lithophysal (tpbl)	MO0003COV00095.000 [DIRS 146848] GS930283117461.001 [DIRS 107027]	63
263	Topopah Spring Tuff	Reddish-brown brick (trbb)	MO0003COV00095.000 [DIRS 146848] GS930283117461.001 [DIRS 107027]	64
264	Topopah Spring Tuff	Brownish-orange lithophysal (tbol)	MO0003COV00095.000 [DIRS 146848] GS930283117461.001 [DIRS 107027]	65
265	Topopah Spring Tuff	Mottled (tm)	MO0003COV00095.000 [DIRS 146848] GS930283117461.001 [DIRS 107027]	66
266	Topopah Spring Tuff	Vitrophyre (tv)	MO0003COV00095.000 [DIRS 146848] GS930283117461.001 [DIRS 107027]	67
267	Topopah Spring Tuff	Partially welded (tpw)	MO0003COV00095.000 [DIRS 146848] GS930283117461.001 [DIRS 107027]	68
268	Calico Hills Formation	Pyroclastic rocks (Tht)	MO0003COV00095.000 [DIRS 146848] GS930283117461.001 [DIRS 107027]	69
269	Calico Hills Formation	Lava flows (Thf)	MO0003COV00095.000 [DIRS 146848] GS930283117461.001 [DIRS 107027]	70
270	Calico Hills Formation	Autobrecciated lavas (Tha)	MO0003COV00095.000 [DIRS 146848] GS930283117461.001 [DIRS 107027]	71
271	Prow Pass Tuff	Partially welded (Tcpp)	MO0003COV00095.000 [DIRS 146848] GS930283117461.001 [DIRS 107027]	72
272	Prow Pass Tuff	Moderately welded (Tcpm)	MO0003COV00095.000 [DIRS 146848] GS930283117461.001 [DIRS 107027]	73
273	Prow Pass Tuff	Undivided (Tcpu)	MO0003COV00095.000 [DIRS 146848] GS930283117461.001 [DIRS 107027]	74
274	Bedded tuff	(bt)	MO0003COV00095.000 [DIRS 146848] GS930283117461.001 [DIRS 107027]	75

Table 6-2. Bedrock Mapping Units Used in the Source File (Continued)

Modified Geologic ID Number	Formation	Lithology/Subdivision (Symbol)	Source DTNs:	ID Number Used in Source File
275	Bullfrog Tuff	Ash-flow tuff (Tcb)	MO0003COV00095.000 [DIRS 146848] GS930283117461.001 [DIRS 107027]	76
276	Tiva Canyon Tuff	Caprock (ccr) north of UTM northing 4079520	MO0003COV00095.000 [DIRS 146848] GS930283117461.001 [DIRS 107027]	17
301	Calico Hills Formation	Undivided (Tac)	MO0603GSCGEOMP.000 [DIRS 176585]	58
302	Colluvium	(QTc)	MO0603GSCGEOMP.000 [DIRS 176585]	71
303	Tiva Canyon Tuff	Undivided (Tpc)	MO0603GSCGEOMP.000 [DIRS 176585]	93
304	Topopah Spring Tuff	Undivided (Tpt)	MO0603GSCGEOMP.000 [DIRS 176585]	95
305	Basin Fill sediments (Pliocene and upper Miocene)	(Tgy)	MO0603GSCGEOMP.000 [DIRS 176585]	98
306	Pah Canyon Tuff	Undivided (Tpp)	MO0603GSCGEOMP.000 [DIRS 176585]	127
307	Intermediate alluvial deposits	(Qai)	MO0603GSCGEOMP.000 [DIRS 176585]	137
308	Young alluvial deposits	(Qay)	MO0603GSCGEOMP.000 [DIRS 176585]	169
309	Rhyolite of Fluorspar Canyon (Rhyolite of Pinnacles Ridge)	Undivided (Tmrf)	MO0603GSCGEOMP.000 [DIRS 176585]	230
310	Rhyolite of Comb Peak	Undivided (Tpr)	MO0603GSCGEOMP.000 [DIRS 176585]	279
311	Middle Paintbrush Group rhyolites	Undivided (Tpm)	MO0603GSCGEOMP.000 [DIRS 176585]	280
312	Rhyolite of Windy Wash	Undivided (Tpw)	MO0603GSCGEOMP.000 [DIRS 176585]	285
313	Rainier Mesa Tuff	Undivided (Tmr)	MO0603GSCGEOMP.000 [DIRS 176585]	294
314	Old alluvial deposits	(Qta)	MO0603GSCGEOMP.000 [DIRS 176585]	438
315	Caldera moat-filling sediments (Miocene)	(Tgc)	MO0603GSCGEOMP.000 [DIRS 176585]	440
316	Bullfrog Tuff	Undivided (Tcb)	MO0603GSCGEOMP.000 [DIRS 176585]	452
317	Caldera-collapse breccia of Claim Canyon Caldera	(Tpcc)	MO0603GSCGEOMP.000 [DIRS 176585]	483
318	Coded as Prow Pass Tuff in source, but should be bedded tuff	(bt)	MO0603GSCGEOMP.000 [DIRS 176585]	485
319	Old eolian sand deposits	(Qeo)	MO0603GSCGEOMP.000 [DIRS 176585]	535
320	Young eolian sand deposits	(Qey)	MO0603GSCGEOMP.000 [DIRS 176585]	759

NOTE: Files used from source DTNs are as follows: GS930283117461.001 [DIRS 107027], Records Package MOY-940125-02-18, ACC: HQS.19880517.1443; GS971208314221.003 [DIRS 107128], *cb6k.ps*; MO0003COV00095.000 [DIRS 146848], *scotbons.e00*; MO0603GSCGEOMP.000 [DIRS 176585], *ofr-99-0554-e00.tar*.

DTNs: data tracking numbers; ID = identification.

Table 6-3a. Assignment of Infiltration Hydrogeologic Units

Lithostratigraphic Name	Lithostratigraphic Unit Symbol	Source of Symbol	Equivalent IHU	IHU Number	Source Map Unit Numerical Identifiers	Source Map Lithostratigraphic Units	Comments	UZ Flow Model Layer
Tiva Canyon Tuff—crystal-rich nonlithophysal zone, subvitrophyre transition subzone	Tpcrn4	Buesch et al. 1996 [DIRS 100106]	hcr4	401	111, 276	Tcrn4, ccr	—	tcw11
Tiva Canyon Tuff—crystal-rich nonlithophysal zone, pumice-poor subzone	Tpcrn3	Buesch et al. 1996 [DIRS 100106]	hcr3	402	112	Tcrn3, ccr	—	tcw11
Tiva Canyon Tuff—crystal-rich nonlithophysal zone, mixed pumice subzone	Tpcrn2	Buesch et al. 1996 [DIRS 100106]	hcr2	403	113, 216, 217	Tcr2, ccr, cuc	—	tcw11
Tiva Canyon Tuff—crystal-rich lithophysal zone	Tpcrl	Buesch et al. 1996 [DIRS 100106]	hcr1	404	114	Tcr1	—	tcw11
Tiva Canyon Tuff—crystal-poor upper lithophysal zone	Tpcpul	Buesch et al. 1996 [DIRS 100106]	hcul	405	115, 108, 109, 215, 218, 303	Tcpul, Tpu, Tcu, cu, cul, Tpc	—	tcw12
Tiva Canyon Tuff—crystal-poor middle nonlithophysal zone	Tpcpmn	Buesch et al. 1996 [DIRS 100106]	hcmn	406	116, 117, 118, 219, 220, 221, 222, 223, 224, 225, 226	Tcpun, Tcpmn, Tcpum, cks, clc, cgks, crks, cuks, cml, clks, crs	—	tcw12
Tiva Canyon Tuff—crystal-poor lower lithophysal zone	Tpcpll	Buesch et al. 1996 [DIRS 100106]	hcll	407	119, 105, 125, 227, 213, 204, 234, 208, 240, 312	Tcpll, TpkI, Tppw, cll, Twf, Tfcl, ymm, Tfcl, pcm, Tpw	—	tcw12
Tiva Canyon Tuff—crystal-poor lower nonlithophysal zone	Tpcpln	Buesch et al. 1996 [DIRS 100106]	hcln	408	120, 121, 228, 229	Tcpln, Tcplnc, chl, ch	—	tcw12

Table 6-3a. Assignment of Infiltration Hydrogeologic Units (Continued)

Lithostratigraphic Name	Lithostratigraphic Unit Symbol	Source of Symbol	Equivalent IHU	IHU Number	Source Map Unit Numerical Identifiers	Source Map Lithostratigraphic Units	Comments	UZ Flow Model Layer
Tiva Canyon Tuff—crystal-poor vitric moderately welded subzone	Tpcpv2	Buesch et al. 1996 [DIRS 100106]	hcv2	409	122, 230	Tcpv, cc, includes cc1, cc2, cc3	—	tcw13
Tiva Canyon Tuff—crystal-poor vitric nonwelded subzone	Tpcpv1	Buesch et al. 1996 [DIRS 100106]	hcv1	410	104, 211	Tmr, Tmrn	—	ptn21
Pre-Tiva Canyon bedded tuff	Tpbt4	Buesch et al. 1996 [DIRS 100106]	hbt4	411	NM, 231	Tbt, bt	—	ptn22
Yucca Mountain Tuff (not divided, total formation)	Tpy	Buesch et al. 1996 [DIRS 100106]	hym	412	123, 232, 233, 235	Tpy, ym, ymu, yml	—	ptn23
Pre-Yucca Mountain bedded tuff	Tpbt3	Buesch et al. 1996 [DIRS 100106]	hbt3	413	NM, 106, 107, 237, 203, 214, 205, 207, 212, 209	Tbt, Tpkt, Tpbt5, bt, Tfpp, Twp, Tfcp, Tfvp, bt, Tfbp	—	ptn24
Pah Canyon Tuff (not divided, total formation)	Tpp	Buesch et al. 1996 [DIRS 100106]	hpc	414	124, 238, 239, 241, 306	Tpp, pc, pcu, pcl, Tpp	—	ptn25
Pre-Pah Canyon bedded tuff	Tpbt2	Buesch et al. 1996 [DIRS 100106]	hbt2	415	126, 242, 318	Tbt2, bt	—	ptn26
Topopah Spring Tuff, crystal-rich vitric nonwelded to moderately welded subzones	Tptrv3-2	Buesch et al. 1996 [DIRS 100106]	htrv3	416	not used	—	Not mapped separately, typically included with Tpbt2	ptn26
Topopah Spring Tuff, crystal-rich vitric densely welded subzone	Tptrv1	Buesch et al. 1996 [DIRS 100106]	htrv1	417	127, 128, 110, 244, 202, 236, 311	Ttrv, Trn3, Tcrv, tc, ccr1 and ccr2, Tfpf, rz, Tpm	—	tsw31
Topopah Spring Tuff, crystal-rich nonlithophysal, vapor-phase corroded subzone	Tptrn2	Buesch et al. 1996 [DIRS 100106]	htrn	418	129, 135, 103, 245, 210	Ttrn2, Ttr, Tmrw, tr, Tmrw	—	tsw32
Topopah Spring Tuff, crystal-rich transition subzone	Tptrn1, Tptrl1	Buesch et al. 1996 [DIRS 100106]	htrl	419	130, 246	Ttr1, ttl	—	tsw33

Table 6-3a. Assignment of Infiltration Hydrogeologic Units (Continued)

Lithostratigraphic Name	Lithostratigraphic Unit Symbol	Source of Symbol	Equivalent IHU	IHU Number	Source Map Unit Numerical Identifiers	Source Map Lithostratigraphic Units	Comments	UZ Flow Model Layer
Topopah Spring Tuff, crystal-poor upper lithophysal zone	Ttpul	Buesch et al. 1996 [DIRS 100106]	htul	420	131, 247, 248, 249, 250	Ttpul, trl, tul, tll, tl	—	tsw33
Topopah Spring Tuff, crystal-poor middle nonlithophysal zone	Ttpmn	Buesch et al. 1996 [DIRS 100106]	htmn	421	132, NOOM, 251, 252, 253, 254, 255, 257, 258	Ttpmn, Td, tnl, tgnl, to, tb, tob 1 and 2, tbob	—	tsw34
Topopah Spring Tuff, crystal-poor lower lithophysal zone	Ttpll	Buesch et al. 1996 [DIRS 100106]	htll	422	134, 133, 259, 260, 261, 262, 263, 264, 256, 243, 206, 269, 304, 317, 309, 310, 301	Ttpll, Ttpmnl, tgrl, torl, tml, tpbl, trbb, tbol, tobl, tu, Tfvf, Thf, Tpt, Tpcc, Tmrf, Tpr, Tpm, Tac	—	tsw35
Topopah Spring Tuff, crystal-poor lower nonlithophysal zone	Ttpln	Buesch et al. 1996 [DIRS 100106]	htln	423	265	tm	—	tsw36, tsw37
Topopah Spring Tuff, crystal-poor, vitric, densely welded subzone	Ttpv3	Buesch et al. 1996 [DIRS 100106]	htpv3	424	266	tv	—	tsw38
Topopah Spring Tuff, crystal-poor, vitric, moderately welded subzone	Ttpv2	Buesch et al. 1996 [DIRS 100106]	htv2v	425	not used	—	Not mapped separately from Ttpv1, see Ttpv1v.	tsw39 (V)
Topopah Spring Tuff, crystal-poor, zeolitic, moderately welded subzone	Ttpv2	Buesch et al. 1996 [DIRS 100106]	htv2z	426	267	—	Not mapped separately from Ttpv1, see Ttpv1z.	tsw39 (Z)
Topopah Spring Tuff, crystal-poor, vitric, nonwelded subzone	Ttpv1	Buesch et al. 1996 [DIRS 100106]	htv1v	427	not used	tpw	Not mapped separately from Tpb1 and typically included with Ttpv2. Exposures near Busted Butte are vitric.	ch1

Table 6-3a. Assignment of Infiltration Hydrogeologic Units (Continued)

Lithostratigraphic Name	Lithostratigraphic Unit Symbol	Source of Symbol	Equivalent IHU	IHU Number	Source Map Unit Numerical Identifiers	Source Map Lithostratigraphic Units	Comments	UZ Flow Model Layer
Topopah Spring Tuff, crystal-poor, zeolitic, nonwelded subzone	Ttpv1	Buesch et al. 1996 [DIRS 100106]	htv1z	428	not used	tpw	Not mapped separately from Tpbt1 and typically included with Ttpv2. Exposures along the north end of Yucca Mountain and north of Yucca Wash are zeolitic.	ch1
Calico Hills Formation, pyroclastic rocks flow	Tac	Moyer and Geslin 1995 [DIRS 101269]	hacv	429	not used	Tht	Exposures near Busted Butte are vitric.	ch2, ch3, ch4, ch5 (V)
Calico Hills Formation, pyroclastic rocks flow	Tac	Moyer and Geslin 1995 [DIRS 101269]	hacz	430	268, 270	Tht, Tha	Exposures along the north end of Yucca Mountain and north of Yucca Wash are zeolitic.	ch2, ch3, ch4, ch5 (Z)
Pre-Calico Hills bedded tuff	Tacbt	Moyer and Geslin 1995 [DIRS 101269]	habtv	431	not used	—	Not mapped separately from Tac.	ch6 (V)
Pre-Calico Hills bedded tuff	Tacbt	Moyer and Geslin 1995 [DIRS 101269]	habtz	432	not used	—	Not mapped separately from Tac.	ch6 (Z)
Prow Pass Tuff, upper vitric	Tcpuv	Buesch and Spengler 1999 [DIRS 107905]	hpuvv	433	not used	—	The Tcpuv was probably mapped as part of the lowermost Tac.	pp4 (V)

Table 6-3a. Assignment of Infiltration Hydrogeologic Units (Continued)

Lithostratigraphic Name	Lithostratigraphic Unit Symbol	Source of Symbol	Equivalent IHU	IHU Number	Source Map Unit Numerical Identifiers	Source Map Lithostratigraphic Units	Comments	UZ Flow Model Layer
Prow Pass Tuff, upper vitric	Tcpuv	Buesch and Spengler 1999 [DIRS 107905]	hpuvz	434	not used	—	The Tcpuv was probably mapped as part of the lowermost Tac.	pp4 (Z)
Prow Pass Tuff, upper crystallized	Tcpuc	Buesch and Spengler 1999 [DIRS 107905]	hpuc	435	271, 313	Tcpp, Tmr	—	pp3
Prow Pass Tuff, moderately welded and crystallized	Tcpm	Buesch and Spengler 1999 [DIRS 107905]	hpmc	436	272, 273	Tcpm, Tcpu	Includes Tcplc.	pp2
Pre-Prow Pass bedded tuff	Tcpbt	Buesch and Spengler 1999 [DIRS 107905]	hpbvz	437	274	bt	Includes Tcplv, Tcpbt, and Tcbuv, and all are zeolitic.	pp1
Bullfrog Tuff, welded and crystallized	Tcbuc, Tcbm, Tcblc	Buesch and Spengler 1999 [DIRS 107905]	hbucm	438	275, 316	Tcb, Tcb	The base is not exposed in the infiltration map area.	bf3
Alluvium/Colluvium	QTac	Day et al. 1998 [DIRS 101557]	NA	490	101, 102, 201, 302, 308, 307, 314, 319, 320	QTac, QTc, Qtac, QTc, Qay, Qai, QTa, Qeo, Qey	NA	Alluvium/Colluvium
Basin-fill sediments, undivided and Caldera moat-filling sediments	Tgy, Tgc	Slate et al. 2000 [DIRS 150228], Open-File Report 99-554-A	NA	491	305, 315	Tgy, Tgc	NA	Basin-fill sediments, undivided and Caldera moat-filling sediments

NOTE: The UZ flow model layer is identified in *Development of Numerical Grids for UZ Flow and Transport Modeling* (BSC 2004 [DIRS 169855], Table 6-5). UZ flow model layer ptn22 also includes the top portion of the Tpy lithostratigraphic unit; UZ flow model layer ptn24 also includes the bottom portion of the Tpy.

IHU = infiltration hydrogeologic unit; NA = not applicable; UZ = unsaturated zone.

A simplified version of the correlation table (Table 6-2) is provided in Appendix A where only the map symbols and lithostratigraphic names and symbols are displayed. Lithostratigraphic names and symbols used as a common lithostratigraphic system are (1) from previously published names and symbols, (2) from a more detailed geologic map of the area north of Yucca Wash than was included in the digital geologic map (Slate et al. 2000 [DIRS 150228], Open-File Report 99-554-A), or (3) updated to be consistent with the type of naming and symbol nomenclature for lithostratigraphic units as described by Buesch and Spengler (1999 [DIRS 107905]).

For map units such as the lava flow and pyroclastic rocks exposed north of Yucca Wash, the digital geologic map (Slate et al. 2000 [DIRS 150228], Open-File Report 99-554-A) only uses names and symbols from regional correlations; therefore, symbols for the exposures within the infiltration model area are from *Geologic Map of the Paintbrush Canyon Area, Yucca Mountain, Nevada* (Dickerson and Drake 1998 [DIRS 102929]).

For three formations, the Rainier Mesa, Yucca Mountain, and Pah Canyon Tuffs, the lithostratigraphic names and symbols have been updated to be consistent with the type of nomenclature system described by Buesch and Spengler (1999 [DIRS 107905]), and these symbols are identified in output DTN: MO0605SPAFABRP.004, *Infiltrate Ap-A Bedrock Correlation 14Feb06.xls*, and in Table A-1 by footnote “f,” to indicate the use of nomenclature style. In the lithostratigraphic nomenclature described by Buesch and Spengler (1999 [DIRS 107905]), there are five lithostratigraphic zones:

- Upper vitric (uv) that is nonwelded to partially welded and vitric
- Upper crystallized (uc) that is partially to moderately welded and crystallized
- Moderately welded (m) that is moderately to densely welded and crystallized
- Lower crystallized (lc) that is partially to moderately welded and crystallized
- Lower vitric (lv) that is nonwelded to partially welded and vitric.

For example, “Tmrm” represents moderately welded and crystallized rocks and “Tmrlv” represents the lower nonwelded and vitric rocks in the Rainier Mesa Tuff.

To compile a map of the distribution of hydrogeologic properties, map units (Table 6-2) were grouped into correlative lithostratigraphic units (Table 6-3a), as described in output DTN: MO0605SPAFABRP.004, *Infiltrate Ap-A Bedrock Correlation 14Feb06.xls*, worksheet ‘Short Correlation Tables’, with details of the lithostratigraphic correlations and the correlation to associated IHUs described in worksheet ‘Map and IHU Correlation’ and in Appendix A.

Some modifications were made to source files to create a better correlation or to correct errors. To better characterize and group lithologic characteristics, the Tiva Canyon Tuff caprock unit (ccr) (DTN: MO0003COV00095.000 [DIRS 146848], *scotbons.e00*) was divided along an east-west line defined by UTM northing coordinate 4079520 into units 216 and 276 (Table 6-2), because this unit correlates to several units used by DTN: GS971208314221.003 [DIRS 107128], *cb6k.ps*. The ccr unit south of this line was determined to correlate best, on an exposed area basis, with the Tcr2 unit in DTN: GS971208314221.003 [DIRS 107128], *cb6k.ps*. The ccr unit north of this line was determined to correlate to the Tcrn4 unit in DTN: GS971208314221.003 [DIRS 107128], *cb6k.ps*.

Another correction was made after reviewing a plot of the digital geologic map (DTN: MO0603GSCGEOMP.000 [DIRS 176585], *ofr-99-0554-e00.tar*), which showed an area mapped as the Prow Pass Tuff, unit 485 (Figure 6-5), in the southern portion of the model area. A check of larger-scale source maps for this area indicated that this exposure should be mapped as bedded tuff. This appears to be a coding error in the compilation of the source digital file. In generating IHU assignments, this exposure was assigned to a bedded tuff IHU. Table 6-3a lists the groupings of modified code numbers that have been assigned to each IHU (output DTN: MO0603SPAGRIDD.003).

Output DTN: MO0603SPAGRIDD.003 was further modified to show the bedrock types buried under the deeper alluvium. The three source maps (DTNs: GS971208314221.003 [DIRS 107128], *cb6k.ps*; MO0003COV00095.000 [DIRS 146848], *scotbons.e00*; MO0603GSCGEOMP.000 [DIRS 176585], *ofr-99-0554-e00.tar*) each show significant areas covered by deep Quaternary alluvium (Figures 6-3, 6-4, and 6-5). The intent is to provide the infiltration model with the bedrock types underlying this alluvium to allow the calculation of infiltration into the bedrock from any water that percolates through the alluvium and reaches the bedrock contact. To determine the bedrock types underlying the alluvium, the geologic framework model (DTN: MO0012MWDGFM02.002 [DIRS 153777]) was used to determine the rock units predicted to underlie the alluvium.

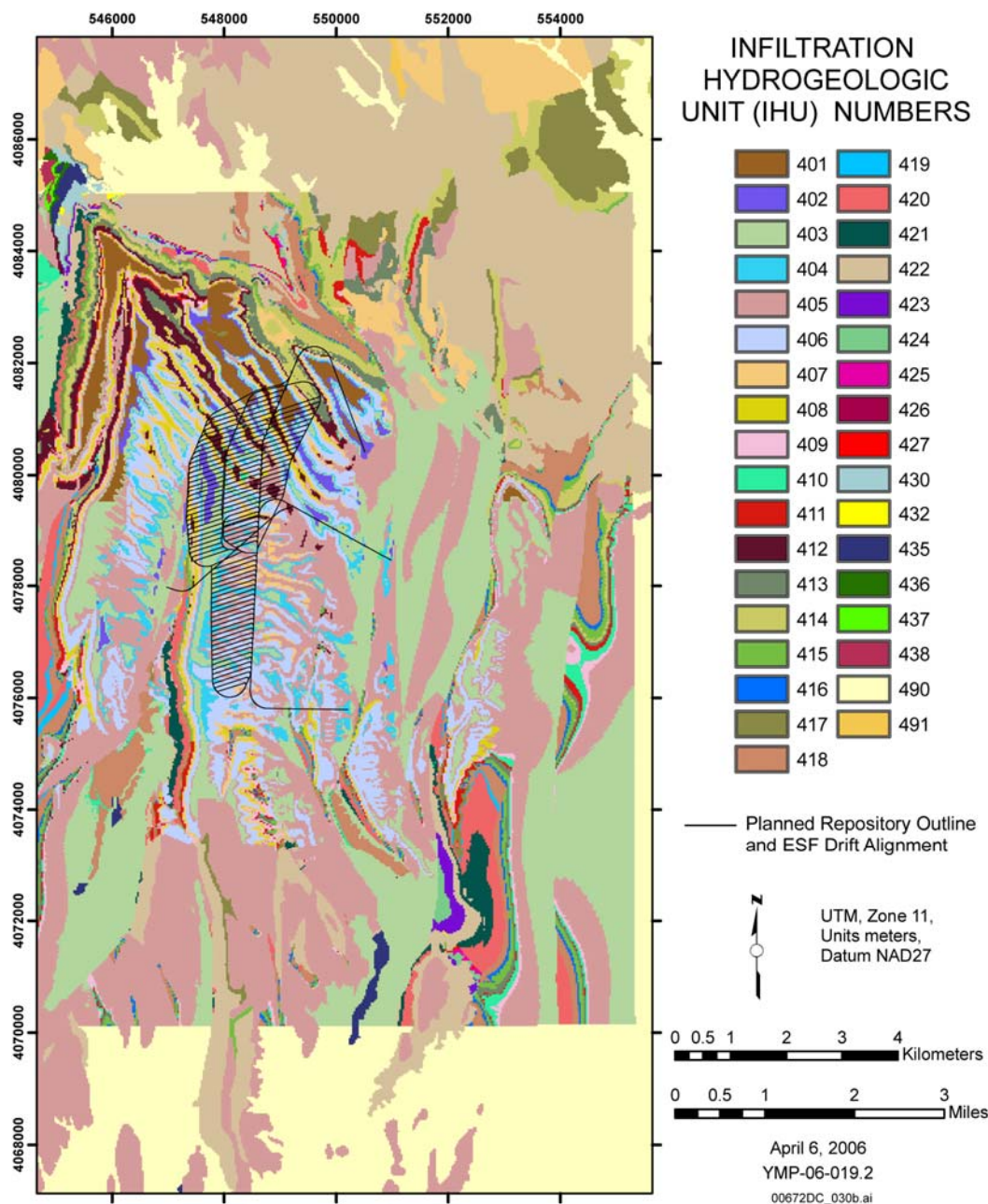
The geologic framework model (DTN: MO0012MWDGFM02.002 [DIRS 153777]) was queried using EARTHVISION® for each cell that was classified as alluvial type and for the bedrock type predicted by the model to underlie the alluvium. The geologic framework model also uses a different stratigraphic nomenclature to define some of the units it models and, therefore, IHU numbers were assigned using the correlation information listed in Tables 6-3a and A-1 in a similar manner to that used for the surface mapping for the bedrock assignments added using the geologic framework model. Table 6-3b lists the correlation used to assign IHU numbers for this operation. Areas on the north, east, and south edges of the model area are not covered by the geologic framework model and are still shown as alluvium (IHUs 490 and 491) in the final file. Extrapolation from the area covered by the geologic framework model suggests that most of this alluvium is predominantly underlain by the Tiva Canyon Tuff (IHUs 403 and 405) with IHU 405 more likely in the shallower alluvial areas. It is, therefore, recommended that the saturated hydraulic conductivity value for IHU 405 be used as the bedrock saturated hydraulic conductivity value for areas mapped as IHUs 490 and 491 in output DTN: MO0603SPAGRIDD.003.

The final distribution of IHUs, in output DTN: MO0603SPAGRIDD.003, across the model area after the alluvial areas were removed is illustrated on Figure 6-6. The IHU number for each cell in output DTN: MO0603SPAGRIDD.003 can be used to look up associated hydrologic properties for each cell (Section 6.4). The percentage of each IHU within the total model area is provided in Table 6-3c.

Table 6-3b. Assignment of Infiltration Hydrogeologic Units to Geologic Framework Model Stratigraphic Units

Geologic Framework Model Stratigraphic Unit	Corresponding Infiltration Hydrogeologic Unit Number
Post-Tiva North	422
Crystal-Rich Tiva and Rainier	403
Tpcp	405
TpcLD	408
Tpcpv3	409
Tpcpv2	409
Tpcpv1	410
Tpbt4	411
Yucca	412
Tpbt3_dc	413
Pah	414
Tpbt2	415
Tptrv3	416
Tptrv2	416
Tptrv1	417
Tptrn	418
Tptrl	419
Tptf	422
Tptpul	420
RHHtop	420
Tptpmn	421
Tptpll	422
Tptpln	423
Tptpv3	424
Tptpv2	425
Tptpv1	427
Tpbt1	415
Calico	422
Calicobt	432
Prowuv	433
Prowuc	435
Prowmd	436
Prowlc	436
Prowlv	437
Prowbt	437
Bullfroguv	437
Bullfroguc	438
Bullfrogmd	438
Bullfroglc	438
Bullfroglv	437
Bullfrogbt	437

NOTE: Geologic framework model stratigraphic units are from
DTN: MO0012MWDGRM02.002 [DIRS 153777].



Source: Output DTN: MO0603SPAGRIDD.003.

NOTES: The outer figure boundary is the boundary for the infiltration model. IHU numbers are described in Table 6-3a. The IHU numbers in this figure are not sequential because some IHUs identified in Table 6-3a do not occur on this map. For each cell classified as alluvium in the source maps (DTNs: GS971208314221.003 [DIRS 107128], *cb6k.ps*; MO0003COV00095.000 [DIRS 146848], *scothons.e00*; MO0603GSCGEOMP.000 [DIRS 176585], *ofr-99-0554-e00.tar*), the bedrock types underlying this alluvium are provided based on the geologic framework model (DTN: MO0012MWDGFM02.002 [DIRS 153777]). Areas on the north, east, and south edges of the infiltration model area, however, are not covered by the geologic framework model and are still shown as alluvium (IHUs 490 and 491).

ESF = Exploratory Studies Facility; IHU = infiltration hydrogeologic unit.

Figure 6-6. Distribution of Infiltration Hydrogeologic Units across the Infiltration Model Area

Table 6-3c. Percentage of Each Infiltration Hydrogeologic Unit Within the Total Model Area

IHU Number	Number of Cells	Area (m ²)	Percent
401	3,259	2,933,100	1.29
402	1,651	1,485,900	0.65
403	37,286	33,557,400	14.70
404	3,921	3,528,900	1.55
405	55,658	50,092,200	21.95
406	12,266	11,039,400	4.84
407	8,937	8,043,300	3.52
408	2,896	2,606,400	1.14
409	3,022	2,719,800	1.19
410	1,757	1,581,300	0.69
411	1,790	1,611,000	0.71
412	3,221	2,898,900	1.27
413	3,677	3,309,300	1.45
414	5,998	5,398,200	2.37
415	2,655	2,389,500	1.05
416	931	837,900	0.37
417	5,948	5,353,200	2.35
418	7,536	6,782,400	2.97
419	482	433,800	0.19
420	3,836	3,452,400	1.51
421	2,053	1,847,700	0.81
422	41,994	37,794,600	16.56
423	579	521,100	0.23
424	581	522,900	0.23
425	142	127,800	0.06
426	20	18,000	0.01
427	96	86,400	0.04
430	506	455,400	0.20
432	45	40,500	0.02
435	791	711,900	0.31
436	124	111,600	0.05
437	77	69,300	0.03
438	127	114,300	0.05
490	39,556	35,600,400	15.60
491	179	161,100	0.07
Total	253,597	228,237,300	100.00

Source: Output DTN: MO0605SPAFA BRP.004, *IHU_map_file2.xls*.

NOTE: The IHU numbers in this table are not sequential because some IHUs identified in Table 6-3a do not occur on the bedrock map (Figure 6-6).

IHU = infiltration hydrogeologic unit.

6.3 CALCULATION OF FRACTURE VOLUME FRACTION

The fracture volume fraction (f_{vf}) is the portion of the rock mass that consists of fractures in the bedrock saturated hydraulic conductivity calculation. In this analysis, a simplified approach has been applied that calculates fracture area over a given mapped rock mass area. The proportion of fractures for a given lithostratigraphic zone within a mapped rock mass area is assumed to be the same as the proportion of fractures within the projected volume of the rock mass (Section 5.1.8, Assumption 8). That is, this approach considers that fracture occurrence in the rock mass is homogeneous and isotropic. This approach is reasonable because the effects of heterogeneity, such as how the occurrence of fractures is directionally biased, are included with the use of multiple mapped locations for the same lithostratigraphic zone, when available, which provides multiple directions. Additionally, fracture data includes mapping of the horizontal pavements on both the surface sections and the vertical sections exposed by subsurface tunneling.

Fracture data are typically provided as a range consisting of a minimum and maximum value. Thus, when an infill thickness range is provided, then a mean value is calculated as the average of the minimum and maximum value. This calculation approach is conservative because fracture aperture/infill widths are typically lognormally distributed along the fracture length (National Research Council 1996 [DIRS 139151], pp. 108, 111, 118, and 126), with values near the lower end of the range more likely, and the maximum value represents an extreme, low-occurrence value.

Surface fracture mapping data used in this analysis include: minimum and maximum fracture aperture/infill width in millimeters; fracture length in feet or meters; and mapped area in feet or meters. The area in square meters of each mapped fracture is calculated as the average fracture aperture/infill width converted to meters multiplied by the fracture length converted to meters. The fracture area in square meters is the sum of all mapped fracture areas. The percent fractures within the rock mass is calculated as follows:

$$\text{percent fractures} = \frac{\text{fracture area}}{\text{mapped area}} \times 100 \quad (\text{Eq. 6-1})$$

The calculation of percent fractures from surface mapping data is documented in output DTN: MO0605SPAFABRP.004, *Fracture Volume Fraction for Each Rock Type v7.xls*, worksheet 'Surface Calculation'. The surface mapping results are listed for each location in Table 6-4.

Underground mapping data used in this analysis include tunnel mapping data from the North Ramp, Cross Drift, and South Ramp of the ESF, and mapping data from the underground test facility at Busted Butte. Underground fracture mapping data include: minimum and maximum fracture aperture in millimeters; minimum and maximum fracture infill thickness in millimeters; fracture length above the traceline in meters; and fracture length below the traceline in meters. The mapping traceline is the detailed line survey that runs along the tunnel below the springline. Fractures typically greater than 1 m that cross the traceline are mapped. The total fracture thickness in millimeters is the sum of the aperture and the infill thickness in millimeters. The fracture length in meters is the sum of the length above and below the traceline.

Table 6-4. Summary of Percent Fracture Results from Surface Mapping

Location	Lithostratigraphic Unit	Mapped Area (m ²)	Average Fracture Area (m ²)	Average Percent Fractures	Source DTN:
Antler Ridge Pavement (ARP-1)	Tpcpul, Tpcpmn, Tpcpll	1,530	13.87	0.91	GS940308314222.001 [DIRS 175720], Table S96400_001 and Records Package MOY-010123-26-09, ACC: MOL.19950123.0094
Fran Ridge Pavement (P2001)	Tptpmn, Tptpul	1,300	10.16	0.78	GS950108314222.001 [DIRS 175708], Tables S96319_001 and S96319_002, Records Package MOY-950817-21-02, ACC: MOL.19960213.0253, p. 13
UZ-7A Drill Pad	Tpcpmn	245	0.44	0.18	GS960808314222.001 [DIRS 175721], Table S98071_001, Records Package MOY-010119-16-07, ACC: MOL.19980305.0108, Figure 2
NRG-1 Pavement	Tpcpul, Tpcpmn, Tpcpll, Tpcpln	470	8.33	1.77	GS060208314222.001 [DIRS 176825], Table S06034_001
North Ramp Starter Tunnel Drainage Cut	Tpcrl, Tpcrn	1,000	21.74	2.17	GS980608314224.004 [DIRS 175707], Table S04374_001, <i>DRAINAGE.xls</i> ; GS940408314224.004 [DIRS 157228], <i>channel.PDF</i>
FS-1, PTn Section of Solitario Canyon	Tpy, Tpb3, Tpb4, Tpb2, Tptrv, Tpcpv	245	0.39	0.16	GS950508314222.003 [DIRS 175723], Table S97370_001 and Records Package MOY-010110-14-01, ACC: MOL.19960129.0083, pp. 1, 34, and 67
FS-2, PTn Section of Solitario Canyon	Tpp, Tpy, Tpb3	168	0.24	0.14	
FS-3, PTn Section of Solitario Canyon	Tpcpv, Tpb3, Tpp	116	0.16	0.14	

NOTES: The percent fractures within the rock mass is calculated using Equation 6-1. Calculations associated with mapped and fracture areas are documented in output DTN: MO0605SPAFABRP.004, *Fracture Volume Fraction for Each Rock Type v7.xls*, worksheet 'Surface Calculation'. The assignment of geologic units at location NRG-1 Pavement is documented in *Administrative Report: Integrated Fracture Data in Support of Process Models, Yucca Mountain, Nevada* (Sweetkind et al. 1997 [DIRS 177047], pp. 22, 25, and 85). The number of significant figures presented does not represent the degree of accuracy or precision in the estimate, but simply represents a choice made by the analyst as to how many figures to report.

DTN = data tracking number.

The area in square meters of each mapped fracture is calculated as the average fracture thickness converted to meters multiplied by the fracture length in meters. The fracture area in square meters is the sum of all mapped fracture areas. Underground fracture mapping is not defined by a specified mapping area. Instead, mapping includes all fractures that are greater than 1 m and that cross the mapping trace line. This approach is known as the detailed line survey.

The mapped area in square meters is set equal to the length of tunnel run mapped in meters multiplied by the average fracture length in meters. This approach for determining the mapped area is appropriate because fractures are predominately vertically oriented. A maximum fracture length of 4 m was used in this analysis; if the fracture length was greater than 4 m, then the fracture length was set equal to 4 m. The fracture length cutoff of 4 m was used to avoid biasing the average fracture length toward long continuous fractures that would skew the width of the mapped area, because the mapped area is calculated as the average fracture length multiplied by the length of tunnel mapped. The 4 m fracture length cutoff is appropriate because fracture lengths are predominately less than 4 m (output DTN: MO0605SPAFABRP.004, *Fracture Volume Fraction for Each Rock Type v7.xls*, worksheets ‘Underground Calculation 1’, ‘Underground Calculation 2’, and ‘Underground Calculation 3’; spreadsheet columns labeled “Total Length”). For underground mapping in the North Ramp, 79% of the fracture trace lengths are less than 3 m, with an average fracture trace length of 2.3 m (Barr et al. 1996 [DIRS 100029], p. 76).

The percent fractures within the rock mass is calculated using Equation 6-1. The calculation of percent fractures from underground mapping data is documented in output DTN: MO0605SPAFABRP.004, *Fracture Volume Fraction for Each Rock Type v7.xls*, worksheets ‘Underground Calculation 1’, ‘Underground Calculation 2’, and ‘Underground Calculation 3’. The underground mapping results are listed for various tunnel locations in Table 6-5.

Surface and underground fracture data were grouped according to lithostratigraphic units as listed in Table 6-3a. Wherever multiple locations exist for the same rock type, the percent fracture data were averaged using both the surface locations and the underground locations. The standard deviation of the percent fracture data was also determined. For rock types in which no fracture data were available, then a fracture volume fraction was assigned using the assumptions of fracture similarity listed in Section 5.1. While it is recognized that surface and underground fracture exposures have been subjected to different physical phenomena that could affect fracture characteristics (for example, weathering effects on surface exposures and stress effects on underground exposures due to stress redistribution resulting from tunnel excavation), these effects are determined to be not significant. Because fracture volume fraction must fall in the range of zero and one, a beta distribution is suitable to describe the spatial variability of the fracture-volume-fraction values (Section 5.1.7, Assumption 7). This approach is consistent with the unsaturated zone (UZ) transport abstraction model (BSC 2005 [DIRS 173980], Section 6.5.7), which uses a beta distribution to describe the uncertainty of porosity; fracture volume fraction is essentially a measure of fracture porosity. The summary of fracture-volume-fraction data for each rock type is listed in Table 6-6. The calculation of fracture-volume-fraction data is documented in output DTN: MO0605SPAFABRP.004, *Fracture Volume Fraction for Each Rock Type v7.xls*, worksheet ‘Summary of Avg. Fracture Data’.

Table 6-5. Summary of Percent Fracture Results from Underground Mapping

Location	Lithostratigraphic Unit	Mapped Area (m ²)	Average Fracture Area (m ²)	Average Percent Fractures	Source DTNs:
ESF Station 0+61.7 to 0+99.5	Tpcpul	61	1.32	2.16	GS971108314224.020 [DIRS 105561], Table S98062_001
ESF Station 0+99.5 to 1+90.0	Tpcpmn	138	1.29	0.93	GS971108314224.020 [DIRS 105561], Table S98062_001
ESF Station 1+90.0 to 1+99.8	Tpcpll	8	0.02	0.21	GS971108314224.020 [DIRS 105561], Table S98062_001
ESF Station 2+63.5 to 3+35.0	Tpki	206	0.44	0.21	GS971108314224.020 [DIRS 105561], Table S98062_001
ESF Station 3+35.0 to 3+46.0	Tpbt5	14	0.00	0.00	GS971108314224.020 [DIRS 105561], Table S98062_001
ESF Station 3+46.0 to 3+59.5	Tpcrv	18	0.01	0.05	GS971108314224.020 [DIRS 105561], Table S98062_001
ESF Station 3+59.5 to 4+34.0	Tpcrn	168	0.88	0.53	GS971108314224.020 [DIRS 105561], Table S98062_001 GS971108314224.021 [DIRS 106007], Table S98076_001
ESF Station 4+34.0 to 4+38.0	Tpcrl	2	0.00	0.04	GS971108314224.021 [DIRS 106007], Table S98076_001
ESF Station 4+38.0 to 5+52.0	Tpcpul	203	5.88	2.90	GS971108314224.021 [DIRS 106007], Table S98076_001
ESF Station 5+52.0 to 5+87.0	Tpcpmn	55	0.84	1.53	GS971108314224.021 [DIRS 106007], Table S98076_001
ESF Station 5+87.0 to 6+20.0	Tpcpll	48	0.79	1.63	GS971108314224.021 [DIRS 106007], Table S98076_001
ESF Station 6+20.0 to 7+77.0	Tpcpln	258	3.12	1.21	GS971108314224.021 [DIRS 106007], Table S98076_001
ESF Station 7+77.0 to 8+69.0	Tpcpv	179	0.91	0.51	GS971108314224.021 [DIRS 106007], Table S98076_001 GS971108314224.022 [DIRS 106009], Table S98063_001
ESF Station 8+69.0 to 9+10.0	Tpy, Tpbt4, Tpbt3	99	0.13	0.13	GS971108314224.022 [DIRS 106009], Table S98063_001
ESF Station 9+10.0 to 10+21.0	Tpp	334	2.08	0.62	GS971108314224.022 [DIRS 106009], Table S98063_001 GS971108314224.023 [DIRS 106010], Table S98064_001
ESF Station 9+90.0 to 10+21.0	Tpp (zeolitic subzone)	95	1.02	1.08	GS971108314224.022 [DIRS 106009], Table S98063_001 GS971108314224.023 [DIRS 106010], Table S98064_001
ESF Station 10+21.0 to 10+52.0	Tpbt2	62	0.01	0.01	GS971108314224.023 [DIRS 106010], Table S98064_001
ESF Station 10+52.0 to 10+66.0	Tptrv3	18	0.24	1.35	GS971108314224.023 [DIRS 106010], Table S98064_001
ESF Station 10+66.0 to 10+76.0	Tptrv2	24	0.19	0.78	GS971108314224.023 [DIRS 106010], Table S98064_001
ESF Station 10+76.0 to 11+84.0	Tptrv1	117	1.52	1.30	GS971108314224.023 [DIRS 106010], Table S98064_001
ESF Station 11+84.0 to 17+16.0	Tptrn	1,067	19.94	1.87	GS971108314224.023 [DIRS 106010], Table S98064_001
ESF Station 17+60.0 to 17+97, 64+55 to 64+93, 68+47 to 68+65.5, 73+02 to 73+27.5	Tptrl1	242	1.11	0.46	GS971108314224.023 [DIRS 106010], Table S98064_001 GS970208314224.003 [DIRS 106048], Table S97164_001 GS970808314224.008 [DIRS 106049], Table S97510_001 GS970808314224.010 [DIRS 106050], Table S97511_001
ESF Station 65+07.0 to 65+25.0, 65+27.0 to 66+34.0, 68+85.0 to 69+90.5, 73+41.0 to 74+40.0	Tptrn	811	14.83	1.83	GS970808314224.008 [DIRS 106049], Table S97510_001 GS970808314224.010 [DIRS 106050], Table S97511_001
ESF Station 66+34.0 to 66+37.5	Tptrv1	4	0.00	0.06	GS970808314224.008 [DIRS 106049], Table S97510_001

Table 6-5. Summary of Percent Fracture Results from Underground Mapping (Continued)

Location	Lithostratigraphic Unit	Mapped Area (m ²)	Average Fracture Area (m ²)	Average Percent Fractures	Source DTNs:
ESF Station 66+37.5 to 66+49.0	Tptrv2, Tptrv3	24	0.06	0.27	GS970808314224.008 [DIRS 106049], Table S97510_001
ESF Station 66+49.0 to 66+98.0, 70+07 to 70+58, 74+50.5 to 74+96.4	Tpbt2, Tpbt3, Tpbt4	383	0.48	0.13	GS970808314224.008 [DIRS 106049], Table S97510_001 GS970808314224.010 [DIRS 106050], Table S97511_001
ESF Station 66+98.0 to 67+25.0, 67+62.0 to 67+70.0, 74+96.4 to 75+14.6	Tpcpv	102	0.70	0.68	GS970808314224.008 [DIRS 106049], Table S97510_001 GS970808314224.010 [DIRS 106050], Table S97511_001 GS970808314224.012 [DIRS 106057], Table S97512_001
ESF Station 67+25.0 to 67+62.0, 67+70.0 to 67+88.0, 75+14.6 to 76+03.0	Tpcpln	289	10.26	3.55	GS970808314224.008 [DIRS 106049], Table S97510_001 GS970808314224.012 [DIRS 106057], Table S97512_001
ESF Station 69+90.5 to 69+96.0	Tptrv1	7	0.01	0.12	GS970808314224.008 [DIRS 106049], Table S97510_001
ESF Station 69+96.0 to 70+07.0	Tptrv3	18	0.09	0.50	GS970808314224.008 [DIRS 106049], Table S97510_001 GS970808314224.010 [DIRS 106050], Table S97511_001
ESF Station 76+03.0 to 78+40.0	Tpcpmn	528	12.81	2.43	GS970808314224.012 [DIRS 106057], Table S97512_001
ESF Station 78+40.0 to 78+77.0	Tpcpul	69	0.27	0.39	GS970808314224.012 [DIRS 106057], Table S97512_001
Cross Drift Station 0+0 to 10+15	Tptpul	2,468	4.36	0.18	GS990408314224.001 [DIRS 108396], Table S99426_001
Cross Drift Station 10+15 to 14+44	Tptpmn	976	10.70	1.10	GS990408314224.001 [DIRS 108396], Table S99426_001
Cross Drift Station 14+44 to 23+26	Tptpll	2,039	15.40	0.75	GS990408314224.001 [DIRS 108396], Table S99426_001 GS990408314224.002 [DIRS 105625], Table S99427_001
Cross Drift Station 23+26 to 25+85	Tptpln	613	12.91	2.10	GS990408314224.002 [DIRS 105625], Table S99427_001
Busted Butte: Access Drift Station 0+00 to 0+18	Tptpv2	38	0.02	0.05	GS990708314224.007 [DIRS 164604], Table S00076_001
Busted Butte: Access Drift Station 0+18 to 0+49 and Cross Drift 0+00 to 0+18	Tptpv1	117	0.10	0.09	GS990708314224.007 [DIRS 164604], Table S00076_001
Busted Butte: Access Drift Station 0+49 to 0+70	Tac	65	0.01	0.01	GS990708314224.007 [DIRS 164604], Table S00076_001

NOTES: The percent fractures within the rock mass is calculated using Equation 6-1. Calculations associated with both the mapped area and the fracture area are documented in output DTN: MO0605SPAFABRP.004, *Fracture Volume Fraction for Each Rock Type v7.xls*, worksheets 'Underground Calculation 1', 'Underground Calculation 2', and 'Underground Calculation 3'. Supplemental information for lithostratigraphic contacts in the underground excavations is provided by Beason et al. (1996 [DIRS 101191], pp. 16 to 26), Barr et al. (1996 [DIRS 100029], Table 1), Eatman et al. (1997 [DIRS 101219], Table 1), and DTNs: GS981108314224.005 [DIRS 109070], Table S98481_001 and GS990708314224.007 [DIRS 164604], Table S00076_001. Fracture data from the ESF North Ramp, Main Drift, and South Ramp for the Tptpul and Tptpmn were not used because they were not in a readily available format to extract fracture thickness data.

The number of significant figures presented does not represent the degree of accuracy or precision in the estimate, but simply represents a choice made by the analyst as to how many figures to report.

DTNs = data tracking numbers; ESF = Exploratory Studies Facility.

Table 6-6. Summary of Fracture-Volume-Fraction Results for Each Rock Type

IHU Number	Lithostratigraphic Unit	Percent Fractures at Various Locations		Average Fracture Volume Fraction, f_{vf}			
		Underground	Surface	Mean	Standard Deviation	Beta-Distribution Parameters	
						α	β
401	Tpcrn4	0.53	2.17	0.0135	0.0116	1.31	95.96
402	Tpcrn3	0.53	2.17	0.0135	0.0116	1.31	95.96
403	Tpcrn2	0.53	2.17	0.0135	0.0116	1.31	95.96
404	Tpcrl	0.04	2.17	0.0111	0.0151	0.52	46.73
405	Tpcpul	2.16, 2.90, 0.39	0.91, 1.77	0.0130	0.0100	1.64	124.93
406	Tpcpmn	0.93, 1.53, 2.43	0.91, 0.18, 1.77	0.0120	0.0069	3.00	246.26
407	Tpcpll	0.21, 1.63	0.91, 1.77	0.0106	0.0065	2.63	246.32
408	Tpcpln	1.21, 3.55	1.77	0.0216	0.0100	4.56	206.72
409	Tpcpv2	0.51, 0.68	0.16, 0.14	0.0037	0.0027	1.91	510.83
410	Tpcpv1	0.51, 0.68	0.16, 0.14	0.0037	0.0027	1.91	510.83
411	Tpbt4	0.13, 0.13	0.16	0.0014	0.0002	55.84	40,605.16
412	Tpy	0.13	0.16, 0.14	0.0014	0.0002	82.58	57,483.55
413	Tpbt3	0.13, 0.13	0.16, 0.14, 0.14	0.0014	0.0001	107.31	77,160.73
414	Tpp	0.56	0.14, 0.14	0.0030	0.0028	1.17	385.43
415	Tpbt2	0.01, 0.13	0.16	0.0010	0.0008	1.52	1557.74
416	Tptrv3, Tptrv2	1.35, 0.78, 0.27, 0.50	0.16	0.0061	0.0048	1.63	264.67
417	Tptrv1	1.30, 0.06, 0.12	0.16	0.0041	0.0060	0.46	113.04
418	Tptrn2	1.87, 1.83	—	0.0185	0.0003	3,937.52	209,072.14
419	Tptrn1, Tptrl1	1.87, 1.83, 0.46	—	0.0138	0.0080	2.92	207.80
420	Tptpul	0.18	0.78	0.0130	0.0100	1.64	124.93
421	Tptpmn	1.10	0.78	0.0120	0.0069	3.00	246.26
422	Tptpll	0.75	—	0.0106	0.0065	2.63	246.32
423	Tptpln	2.10	—	0.0216	0.0100	4.56	206.72
424	Tptpv3	No data — see Section 5.1.1, Assumption 1		0.0005	0.0003	2.30	4762.72
425	Tptpv2 vitric	0.05	—	0.0005	0.0003	2.30	4762.72
426	Tptpv2 zeolitic	No data — see Section 5.1.2, Assumption 2		0.0108	0.0071	2.26	207.06
427	Tptpv1 vitric	0.09	—	0.0009	0.0006	2.30	2618.78
428	Tptpv1 zeolitic	No data — see Section 5.1.2, Assumption 2		0.0108	0.0071	2.26	207.06
429	Tac vitric	0.01	—	0.0001	0.0001	2.30	15,462.77
430	Tac zeolitic	No data — see Section 5.1.2, Assumption 2		0.0108	0.0071	2.26	207.06

Table 6-6. Summary of Fracture-Volume-Fraction Results for Each Rock Type (Continued)

IHU Number	Lithostratigraphic Unit	Percent Fractures at Various Locations		Average Fracture Volume Fraction, f_{vf}			
		Underground	Surface	Mean	Standard Deviation	Beta-Distribution Parameters	
						α	β
431	Tacbt vitric	0.01	—	0.0001	0.0001	2.30	15,462.77
432	Tacbt zeolitic	No data — see Section 5.1.2, Assumption 2		0.0108	0.0071	2.26	207.06
433	Tcpuv vitric	No data — see Section 5.1.5, Assumption 5		0.0009	0.0006	2.30	2,618.78
434	Tcpuv zeolitic	No data — see Section 5.1.2, Assumption 2		0.0108	0.0071	2.26	207.06
435	Tcpuc	No data — see Section 5.1.3, Assumption 3		0.0135	0.0116	1.31	95.96
436	Tcpm	No data — see Section 5.1.4, Assumption 4		0.0120	0.0069	3.00	246.26
437	Tcpbt	No data — see Section 5.1.5, Assumption 5		0.0009	0.0006	2.30	2,618.78
438	Tcbuc, Tcbm, Tcbic	No data — see Section 5.1.6, Assumption 6		0.0120	0.0069	3.00	246.26

NOTES: The data in the columns for “Percent Fractures at Various Locations” are from Table 6-4 (surface) and Table 6-5 (underground).

The “Mean” is the average of the available data from the columns “Percent Fractures at Various Locations,” for the corresponding lithostratigraphic zone. The “Standard Deviation” is the standard deviation of the available data from the columns “Percent Fractures at Various Locations,” for the corresponding lithostratigraphic zone. The calculation of beta-distribution parameters (Section 5.1.7, Assumption 7) is based on the approach described in *Statistical Models in Engineering* (Hahn and Shapiro 1967 [DIRS 146529], Equations 3-28a and 3-28b) and is documented in output DTN: MO0605SPAFABRP.004, *Fracture Volume Fraction for Each Rock Type v7.xls*, worksheet ‘Summary of Avg. Fracture Data’.

Based on the similarity of the fracture characteristic in the Tiva Canyon Tuff and the Topopah Spring Tuff, the data from these units are combined as follows to calculate the average fracture volume fraction: 405 and 420, 406 and 421, 407 and 422, 408 and 423. The average fracture-volume-fraction data for IHUs 426, 428, 430, 432, and 434 are based on Assumption 2 (Section 5.1.2) and are documented in output DTN: MO0605SPAFABRP.004, *Fracture Volume Fraction for Each Rock Type v7.xls*, worksheet ‘Summary of Avg. Fracture Data’.

When only one data point was available, this value is considered the average value, and the standard deviation was determined using the average ratio of standard deviation to mean for all available data in this table. The details of this calculation are provided in output DTN: MO0605SPAFABRP.004, *Fracture Volume Fraction for Each Rock Type v7.xls*, worksheet ‘Summary of Avg. Fracture Data’. For rock types in which no fracture data were available, a fracture volume fraction was assigned using the assumptions of fracture similarity listed in Section 5.1.

The number of significant figures presented does not represent the degree of accuracy or precision in the estimate, but simply represents a choice made by the analyst as to how many figures to report.

IHU = infiltration hydrogeologic unit.

An alternative approach not used in this fracture-volume-fraction calculation is discrete fracture modeling based on field fracture mapping data. FracMAN has been used to develop stochastically defined fracture systems that are representative of the host rock mass to support preliminary hydrologic modeling of Yucca Mountain for estimation of rock mass permeability (Anna 1998 [DIRS 144421]; Anna 1998 [DIRS 138501]). FracMAN has also been used for drift degradation analyses at Yucca Mountain to analyze the seismic response of fractured, nonlithophysal rock (BSC 2004 [DIRS 166107], Section 6.1.6).

FracMAN was not selected for use in this calculation because it requires a complex assemblage of three-dimensional fractures that is beyond the scope of this analysis. Instead, available results from previous studies using FracMAN are used to corroborate the fracture-volume-fraction results from this calculation. FracMAN uses a measure of fracture intensity called P32, which is the ratio of fracture area to rock volume (m^2/m^3) (Anna 1998 [DIRS 144421], p. 16). In FracMAN, fracture planes are typically modeled as flat, elliptically shaped discs in three-dimensional space. The fracture area is the area of the elliptical disc. To estimate fracture volume fraction, f_{vf} , which is equivalent to the ratio of fracture volume to rock volume, from a FracMAN P32 value, the thickness of the fracture is needed to convert fracture area to fracture volume:

$$f_{vf} = \text{P32} \times \text{fracture thickness in meters} \quad (\text{Eq. 6-2})$$

Consolidated FracMAN P32 data (Anna 1998 [DIRS 144421], Figures 3 and 8; Anna 1998 [DIRS 138501], Figure 2 and Table 2) are available for IHU numbers 405, 406, 407, 408, and 421 (Table 6-3a). Average fracture thickness data from either surface or underground mapping (output DTN: MO0605SPAFABRP.004, *Fracture Volume Fraction for Each Rock Type v7.xls*, worksheet 'Fracture Thickness Calculation') were used to calculate fracture volume fractions from FracMAN P32 data (Table 6-7). The comparison of the fracture volume fractions, from FracMAN data to the results of this calculation (Table 6-7), shows that the simplified approach used herein produces fracture volume fractions that are approximately two to five times greater than the FracMAN approach. Given that fracture conductivity is generally much larger than matrix conductivity, the resulting bulk bedrock K_{sat} (Section 6.4) could be overestimated by a factor of 2 to 5. This uncertainty, however, is small compared with the uncertainty in the number and aperture of partially filled fractures, which is accounted for by establishing upper and lower bounds in the bulk bedrock K_{sat} that results in an uncertainty range of over two orders of magnitude for some IHUs (Section 6.4.5.5).

6.4 CALCULATION OF BEDROCK SATURATED HYDRAULIC CONDUCTIVITY

Bulk saturated hydraulic conductivity (K_{sat}) data were developed for each of 38 rock types, or IHUs, that form the bedrock at Yucca Mountain. Bulk saturated hydraulic conductivity is calculated for a composite porous medium consisting of rock matrix and fractures filled with permeable caliche. Bulk saturated hydraulic conductivity is also calculated based on the consideration of partially filled fractures in the bedrock.

Table 6-7. Comparison of Fracture-Volume-Fraction Results to an Alternative FracMAN Approach

IHU Number	Litho-stratigraphic Unit	FracMAN P32 (m^2/m^3)	Source of P32 Values	Average Fracture Thickness (mm)	Fracture Volume Fraction	
					From FracMAN	From Table 6-6 (Mean)
405	Tpcpul	0.59	Anna 1998 [DIRS 144421], Figures 3 and 8	11.55	0.0068	0.0130
406	Tpcpmn			7.38	0.0044	0.0120
407	Tpcpll			7.15	0.0042	0.0106
408	Tpcpln			7.76	0.0046	0.0216
421	Tptpmn	0.43	Anna 1998 [DIRS 138501], Figure 2 and Table 2	6.84	0.0029	0.0120
		0.40	BSC 2004 [DIRS 166107], Figure 6-18 (Intensity)		0.0027	

NOTES: The FracMAN P32 value is the ratio of fracture area to rock volume (m^2/m^3). The calculation of average fracture thickness data is documented in output DTN: MO0605SPAFABRP.004, *Fracture Volume Fraction for Each Rock Type v7.xls*, worksheet 'Fracture Thickness Calculation'. Fracture-volume-fraction data from FracMAN are calculated using Equation 6-2. The number of significant figures presented does not represent the degree of accuracy or precision in the estimate, but simply represents a choice made by the analyst as to how many figures to report.

IHU = infiltration hydrogeologic unit.

6.4.1 Input Data

The basis for calculation of the saturated hydraulic conductivity of fracture-filling caliche is DTN: GS950708312211.003 [DIRS 146873]. Saturated hydraulic conductivity was measured on 15 subsamples from five samples of fracture-filling material. The caliche is formed by precipitation of minerals from water on the fracture walls as it evaporates. As a result, it is layered and measurements taken both parallel to and perpendicular to the layers are reported. Only four of the measurements are in the parallel direction and these values are used here; the method of data analysis is described in Section 6.4.3. The same values for fracture-filling material were used for each rock type; that is, for each IHU. The use of such a limited number of samples to determine the properties of the fracture fill material introduces a significant source of uncertainty in the resulting bulk K_{sat} for each of the IHUs presented in this analysis. The contribution of the limited sample size to the overall uncertainty in the bulk K_{sat} is discussed in Section 6.5.2. This contribution to the uncertainty in results of the present analysis, as well as other sources of uncertainty, are reported in Section 6.4.5, and must be carried forward by the users of this analysis.

The use of parallel-direction K_{sat} values of the fracture fill material is based on the physical characteristics of fracture flow. The flow of water through fractures is bound by the bedrock surface on each side of the fracture. As the fracture is subjected to the repeated evaporation and rewetting required for the formation of the caliche precipitate, the layers of precipitate are deposited first on the fracture walls. As a result, the precipitation process proceeds in layers parallel to the preferred path of water flow through the cracks, regardless of the orientation of the crack. When a crack becomes completely filled with the layered calcitic deposits,

the preferred path for water flow (now through the less permeable fill material) remains bound by the less permeable fracture walls, and will proceed along the most permeable path parallel to the layers of precipitate.

The basis for calculation of matrix saturated hydraulic conductivity for each rock type is the database of measurements made on core samples from 33 vertical surface boreholes and 16 horizontal boreholes from the UZTT at Busted Butte, and from measurements made on samples collected from the ESF. The vertical boreholes represent nearly all rock types, while the UZTT and ESF samples represent only rock units at and below the repository host horizon. Because the data from the vertical boreholes are generally equally distributed, and because some of the bedrock layers that are exposed on the surface are not represented in each borehole, data are sparser for thinner layers and some bedrock units are represented by few measurements, only one, or none. Methods used for those cases are described in Section 6.4.4. The approach taken to summarize and analyze hydraulic conductivity data is similar to that taken in *Analysis of Hydrologic Properties Data* (BSC 2004 [DIRS 170038]), hereafter referred to as the hydrologic properties analysis; the following sources were summarized in output DTN: MO0605SPAFABRP.004, *Matrix and fracture-fill Ksat for each rock type.xls*, worksheet ‘Original DTNs(1)’:

- Matrix hydraulic conductivity data measured on core samples are from DTN: MO0109HYMXPROP.001 [DIRS 155989], Table S01144_001, which summarizes data from 31 boreholes. Those data were then supplemented by DTNs: GS980708312242.011 [DIRS 107150], Table S98249_006; GS980908312242.038 [DIRS 107154], Table S98388_004; and GS980908312242.041 [DIRS 107158], Table S98386_004; which provided additional data from some of the 31 boreholes and from two additional surface boreholes.
- Data for samples from the UZTT and ESF are from DTNs: GS971008312231.006 [DIRS 107184], Table S98373_005; GS990308312242.007 [DIRS 107185], Table S99180_003; and GS990708312242.008 [DIRS 109822], Tables S99391_001 and S99391_002.
- Porosity data used in the analysis of K_{sat} (Section 6.4.4.2) are from DTNs: GS980708312242.010 [DIRS 106752], Table S98248_006, and GS980808312242.014 [DIRS 106748], Table S98285_002.

The use of multiple DTNs resulted in some duplicate K_{sat} measurements that were identified by borehole and depth data, and were then eliminated from the analysis. The following DTNs also contain K_{sat} data not used here, because they repeat data in output DTN: MO0109HYMXPROP.001 [DIRS 155989], Table S01144_001:

- GS000408312231.003 [DIRS 149461]
- GS960808312231.001 [DIRS 108998]
- GS960808312231.005 [DIRS 108995]
- GS990408312231.001 [DIRS 148711].

6.4.2 Assignment of Samples to Lithologic Units

The K_{sat} data were grouped according to rock type for averaging. Porosity data and the lithologic unit for each of about 4,900 samples, and K_{sat} data for about 600 of those samples, are listed in DTN: MO0109HYMXPROP.001 [DIRS 155989], Table S01144_001. The K_{sat} data for each sample, identified by borehole and sample depth, but not by lithologic unit, are reported in DTNs: GS980708312242.011 [DIRS 107150], Table S98249_006, GS980908312242.038 [DIRS 107154], Table S98388_004, and GS980908312242.041 [DIRS 107158], Table S98386_004. To assign rock types for these data, the data in output DTN: MO0605SPAFABRP.004, *Matrix and fracture-fill Ksat for each rock type.xls*, worksheet 'Original DTNs(1)', were sorted by borehole and depth. The rock types for those samples, as well as those in DTN: MO0109HYMXPROP.001 [DIRS 155989], Table S01144_001, were identified by depth-to-contact data in DTN: MO0012MWDGFM02.002 [DIRS 153777], *contacts00md.dat*. In some cases, rock type assignments by this method did not agree with assignments in DTN: MO0109HYMXPROP.001 [DIRS 155989], Table S01144_001. These discrepancies were resolved in favor of the assignments made according to the depth in a borehole, except where a more specific rock type in the Tiva Canyon Tuff (Tpc) was provided in DTN: MO0109HYMXPROP.001 [DIRS 155989], Table S01144_001.

Samples from the ESF were assigned to Tptpmn based on *In Situ Field Testing of Processes* (BSC 2004 [DIRS 170004], Figure 1-1). Samples from the UZTT at Busted Butte were assigned to Tptpv1, Tptpv2, or Tac based on geologic logs. Where noncrystalline vitric rock units have been zeolitized, the zeolitic rock properties are different from the parent vitric material. DTN: MO0012MWDGFM02.002 [DIRS 153777] identifies the depth of the vitric-zeolitic boundary for many of the vertical boreholes; samples in rock types Tptpv1, Tptpv2, Tac, Tacbt, and Tpbtl were separated into vitric and zeolitic subsets and averaged separately.

6.4.3 Analysis of K_{sat} Data

The spatial distributions of K_{sat} of matrix and of fracture-filling caliche are assumed to be lognormal (Section 5.2.2, Assumption 11). The method to determine the geometric mean of K_{sat} and the standard deviation of $\log_{10} K_{sat}$ is described in *Statistical Methods in Water Resources* (Helsel and Hirsch 1995 [DIRS 175683], Chapter 2). Measurements that differed by more than an order of magnitude from the nearest-ranked value were eliminated as outliers. Within each rock type, the K_{sat} data were ranked and assigned percentiles, and the percentiles were converted to normal quantiles, that is, standard deviations, above and below the mean using the NORMSINV function in Excel®. When $\log_{10} K_{sat}$ is plotted against normal quantiles, which is equivalent to plotting $\log_{10} K_{sat}$ on probability paper, the intercept and slope of a straight-line fit through the data give the geometric mean of K_{sat} and the standard deviation of $\log_{10} K_{sat}$.

For lognormally distributed properties, the logarithm of the geometric mean is also the median of the log-transformed values. This also follows the approach used in the hydrologic properties analysis (BSC 2004 [DIRS 170038]). For each rock type, except IHUs hcv1 (410) and hpc (414), $\log_{10} K_{sat}$ fitted a straight line better than K_{sat} , supporting the assumption of lognormal distribution. For many rock types, several or a majority of samples had K_{sat} too low to measure by the method used, considering that the lower limit of measurability is approximately 10^{-13} m/s.

These “no-flow” values were included in data point ranking to determine the geometric mean of K_{sat} and the standard deviation of $\log_{10} K_{sat}$ (Helsel and Hirsch 1995 [DIRS 175683], Chapter 13). In output DTN: MO0605SPAFABRP.004, *Matrix and fracture-fill Ksat for each rock type.xls*, results are presented for each IHU in individual worksheets; for example: worksheets ‘fill material 2’, ‘Tpcpll (407)’, and ‘Tpcpln (408)’; results are summarized in worksheet ‘Matrix and fill summary’ and are listed in Table 6-8. Uncalibrated matrix K_{sat} values derived from the same DTNs as those used in the hydrologic properties analysis (BSC 2004 [DIRS 170038], Table 6-6) are also listed in Table 6-8. These values were converted from intrinsic permeability k to K_{sat} for comparison, using:

$$K_{sat} = kg\rho/\mu \quad (\text{Eq. 6-3})$$

where g is the acceleration of gravity, and ρ and μ are the density and viscosity of water (Freeze and Cherry 1979 [DIRS 101173], Equation 2.28).

For IHUs 401 through 404, the value in the hydrologic properties analysis (BSC 2004 [DIRS 170038], Table 6-6) is based upon three measurements of K_{sat} in borehole N27; for traceability, these are rows 99, 103, and 117 in output DTN: MO0605SPAFABRP.004, *Matrix and fracture-fill Ksat for each rock type.xls*, worksheet ‘Original DTNs(1)’. Under the present scheme, the strata are more finely divided and, thus, the three points were assigned to IHUs 402, 403, and 404, which resulted in values for these IHUs that do not bracket the value reported in the hydraulic properties analysis (BSC 2004 [DIRS 170038], Table 6-6). Nevertheless, the values derived herein are reasonable. This difference results from methods that were used for analysis of sparse data (Sections 6.4.4.1 and 6.4.4.2). For IHUs 402 and 403, the geometric mean K_{sat} was extrapolated from a single value (Section 6.4.4.2), yielding a smaller and more representative value for geometric mean K_{sat} . For IHU 404, this extrapolation method could not be used because K_{sat} and density were only measured on one sample; rather, the values for surrogate 420 were used. No data were available for 401, so a surrogate unit Tptrn3 was used.

6.4.4 Analysis of Sparse Matrix K_{sat} Data

Matrix K_{sat} data for several rock types are sparse because of the following:

- Rock units are thin and not well represented among the data, or
- Rock units are not present or their core was not recovered at the location of many boreholes, or
- The specific unit within the Tiva Canyon Tuff is not specified where rock type assignments were made based on the depth within boreholes (Section 6.4.2).

For some rock types, surrogate units were identified whose properties could be inferred to be similar to the rock type with sparse data. For others, where no surrogate could be identified, the more numerous porosity data were used to adjust the median and standard deviation of $\log_{10} K_{sat}$.

Table 6-8. Matrix Saturated Hydraulic Conductivity for Each Rock Type, Fracture-Filling Caliche Saturated Hydraulic Conductivity, and Comparison with an Alternative Calculation

IHU Symbol	IHU Number	Lithostratigraphic Unit(s) (from Table 6-3a)	Data for Lithostratigraphic Unit Analyzed	Equivalent UZ Flow Model Layer ^a	HGU ^a	Log ₁₀ K _{sat} (m/s)			
						This Analysis		BSC 2004 [DIRS 170038], Table 6-6 ^b	
						Log ₁₀ Geometric Mean K _{sat} ^m	Log ₁₀ Standard Deviation K _{sat}	Log ₁₀ Geometric Mean K _{sat} ^m	Log ₁₀ Standard Deviation K _{sat}
hcr4	401	Tpcrn4	Tptrn3 ^c	tcw11	CCR, CUC	-9.47 ^c	1.51 ^c	-7.34	0.47
hcr3	402	Tpcrn3	Tpcrn3 ^d	tcw11	CCR, CUC	-9.27 ^d	1.00 ^d	-7.34	0.47
hcr2	403	Tpcrn2	Tpcrn2 ^e	tcw11	CCR, CUC	-7.90 ^e	1.00 ^e	-7.34	0.47
hcr1	404	Tpcrl	Tptpul ^f	tcw11	CCR, CUC	-10.73 ^f	1.37 ^f	-7.34	0.47
hcul	405	Tpcpul	Tpcpul ^g	tcw12	CUL, CW	-8.30 ^g	0.94 ^g	-12.21	2.74
hcmn	406	Tpcpmn	Tptpmn ^h	tcw12	CUL, CW	-11.64 ^h	0.91 ^h	-12.21	2.74
hcll	407	Tpcpll	Tpcpll	tcw12	CUL, CW	-13.41 ⁱ	2.25 ⁱ	-12.21	2.74
hcln	408	Tpcpln	Tpcpln	tcw12	CUL, CW	-13.42 ⁱ	1.93 ⁱ	-12.21	2.74
hcv2	409	Tpcpv2	Tpcpv2	tcw13	CMW	-10.86	0.90	-8.75	2.38
hcv1	410	Tpcpv1	Tpcpv1	ptn21	CNW	-6.76	0.70	-6.41	2.05
hbt4	411	Tpbt4	Tpbt4	ptn22	BT4	-5.20	0.50	-5.40	1.41
hym	412	Tpy	Tpy	ptn23	TPY	-6.79	1.09	-7.91	0.64
hbt3	413	Tpbt3	Tpbt3	ptn24	BT3	-5.78	0.35	-5.88	1.09
hpc	414	Tpp	Tpp	ptn25	TPP	-6.02	0.36	-5.97	0.39
hbt2	415	Tpbt2	Tpbt2	ptn26	BT2	-5.48	0.55	-5.18	1.12
htrv3	416	Tptrv3-2	Tptrv3-2	ptn26	BT2	-5.15	0.51	-5.18	1.12
htrv1	417	Tptrv1	Tptrv1	tsw31	TC	-9.37	2.16	-9.37	3.02
htrn	418	Tptrn2	Tptrn2	tsw32	TR	-9.17	1.06	-8.51	0.94
htrl	419	Tptrn1, Tptrl1	Tptpul ^f	tsw33	TUL	-10.73	1.37 ^f	-9.57	1.61
htul	420	Tptpul	Tptpul	tsw33	TUL	-10.73	1.37	-9.57	1.61
htmn	421	Tptpmn	Tptpmn	tsw34	TMN	-11.64	0.91	-11.35	0.97
htll	422	Tptpll	Tptpll	tsw35	TLL	-10.61	1.62	-9.45	1.65
htln	423	Tptpln	Tptpln	tsw36, tsw37	TM2, TM1	-13.35 ⁱ	2.51 ⁱ	-12.64	3.67
htpv3	424	Tptpv3	Tptpv3	tsw38	PV3	-11.59	1.44	-10.55	1.57
htv2v	425	Tptpv2	Tptpv2(v)	tsw39 (v)	PV2	-5.65	0.55	-5.38	1.38
htv2z	426	Tptpv2	Tptpv2(z)	tsw39 (z)	PV2	-10.36	1.00 ^j	-9.46 ^j	2.74
htv1v	427	Tptpv1	Tptpv1(v)	ch1 (v)	BT1	-6.14	0.98	-5.68	1.11
htv1z	428	Tptpv1	Tptpv1(z)	ch1 (z)	BT1	-11.83	1.35	-9.46	2.74
hacv	429	Tac	Tac(v)	ch2 to ch5 (v)	CHV	-5.86	1.37	-4.82	1.62
hacz	430	Tac	Tac(z)	ch2 to ch5 (z)	CHZ	-10.66	0.75	-10.29	0.91
habtv	431	Tacbt	Tacbt(v)	ch6 (v)	BT	—	—	-4.82	1.62

Table 6-8. Matrix Saturated Hydraulic Conductivity for Each Rock Type, Fracture-Filling Caliche Saturated Hydraulic Conductivity, and Comparison with an Alternative Calculation (Continued)

IHU Symbol	IHU Number	Lithostratigraphic Unit(s) (from Table 6-3a)	Data for Lithostratigraphic Unit Analyzed	Equivalent UZ Flow Model Layer ^a	HGU ^a	Log ₁₀ K_{sat} (m/s)			
						This Analysis		BSC 2004 [DIRS 170038], Table 6-6 ^b	
						Log ₁₀ Geometric Mean K_{sat} ^m	Log ₁₀ Standard Deviation K_{sat}	Log ₁₀ Geometric Mean K_{sat} ^m	Log ₁₀ Standard Deviation K_{sat}
habtz	432	Tacbt	Tacbt(z)	ch6 (z)	BT	-12.83 ⁱ	1.85 ^l	-10.29	0.91
hpuvv	433	Tcpuv	Tcpuv(v)	pp4 (v)	PP4	—	—	—	—
hpuvz	434	Tcpuv	Tcpuv(z)	pp4 (z)	PP4	-10.66	2.50	-8.82	2.74
hpuc	435	Tcpuc	Tcpuc(v)	pp3	PP3	-7.29	0.37	-7.21	0.75
hpmic	436	Tcpm	Tcpm(v)	pp2	PP2	-9.82	1.12	-9.28	1.18
hpbvz	437	Tcpbt	Tcbuv, Tcbiv	pp1	PP1	-10.14 ^k	1.54 ^k	-9.10	1.52
Hbucm	438	Tcbuc, Tcbm, Tcbic	Tcb	bf3	BF3	-9.11	1.48	-7.96	1.64
Fracture-filling caliche						-5.84 ^l	0.28 ^l	—	—

Source: Output DTN: MO0605SPAFABRP.004, *Matrix and fracture-fill Ksat for each rock type.xls*, worksheet 'Matrix and fill summary'.

^a Each rock type is identified with a UZ flow model layer in Table 6-3a. Each flow model layer is identified with an HGU in *Development of Numerical Grids for UZ Flow and Transport Modeling* (BSC 2004 [DIRS 169855], Table 6-5). These columns are needed to identify the HGUs in the hydrologic properties analysis (BSC 2004 [DIRS 170038], Table 6-6) for comparison.

^b Values from the hydrologic properties analysis (BSC 2004 [DIRS 170038], Table 6-6) have been converted from upscaled log₁₀ permeability (m²) values to log₁₀ K_{sat} values for comparison.

^c Data averaged from Tptrn3 measurements. Tptrn3 data were identified among undifferentiated Tptrn data by selecting bulk density of 2.27 g/cm³ or greater.

^d One K_{sat} measurement reported, but the porosity of that sample was extremely high (0.431), the greatest of 48 porosity measurements. Therefore, that measured K_{sat} was taken to be 2.13 standard deviations above the median, and the standard deviation of 1 log unit was assumed.

^e One K_{sat} measurement reported; porosity was near the median of porosity. Standard deviation = 1 log unit was assumed.

^f Tptpul was used as surrogate for Tptrl and Tpcrl.

^g Two K_{sat} measurements reported. They were assigned quantiles based upon the associated porosity (105°C oven) values. Then the median K_{sat} (which is also the geometric mean K_{sat}) and standard deviation in log units were calculated from those two points.

^h Ttpmn was used as surrogate for Tpcpm.

ⁱ For these IHUs more than half the matrix K_{sat} measurements were non-detects. The values herein were not used for calculation of bedrock K_{sat} (Table 6-9).

^j Tcplv(z) was used as a surrogate for Ttpv2(z).

^k K_{sat} values from Tcplv and Tcbuv (no K_{sat} data for Tcbbt).

^l Output DTN: MO0605SPAFABRP.004, *Matrix and fracture-fill Ksat for each rock type.xls*, worksheet 'fill material 2'.

^m For lognormally distributed quantities, the median of log₁₀ K_{sat} is the log₁₀ of the geometric mean K_{sat} .

NOTE: The number of significant figures presented does not represent the degree of accuracy or precision in the estimate, but simply represents a choice made by the analyst as to how many figures to report.

IHU = infiltration hydrogeologic unit; HGU = hydrogeologic unit; UZ = unsaturated zone.

6.4.4.1 Identification of Surrogate Lithologic Units

Surrogate units are identified for lithologic units for which no K_{sat} data are available. The K_{sat} data for Tptpv2 (IHUs 425 and 426) are from samples above the vitric-zeolitic boundary; therefore, no data are available for analysis of Tptpv2(z). The data for Tcplv are from samples below the vitric-zeolitic boundary and, therefore, zeolitic. Tcplv(z) is used as a surrogate for Tptpv2(z) (IHU 426). Both rocks are zeolitic. Tcplv(z) rocks are typically nonwelded to partially welded and locally moderately welded; Tptpv2(z) rocks are moderately welded (Section 5.2.6, Assumption 15).

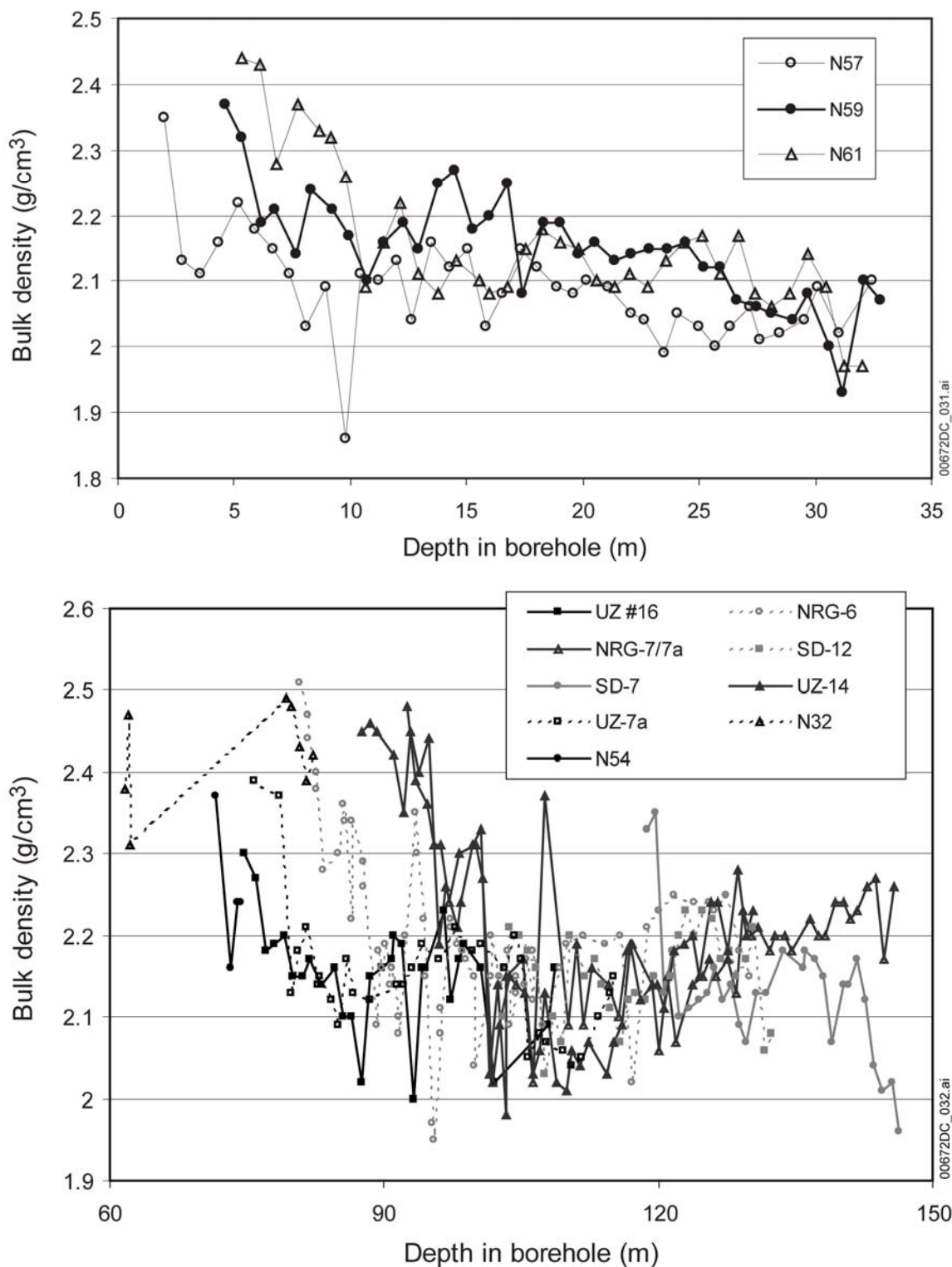
IHU hcr1 (404) combines Tpcrn1 and Tpcrl. These are both crystal-transition subzones with smaller porosity than their respective overlying zones; the phenocrysts that distinguish crystal-rich subzones from crystal-poor subzones do not constitute a large enough fraction of the rock mass to affect the K_{sat} significantly. No K_{sat} data are available for these units. Tptpul, another lithophysal subzone, is used as a surrogate for these two units (Section 5.2.6, Assumption 15).

Tpcrn4 and Tptrn3 are low-porosity, high-density subzones, densely welded and crystallized at the top of the crystal-rich nonlithophysal zone in their respective formations. No data are available for Tpcrn4; hence, Tptrn3 is identified as a surrogate (Section 5.2.6, Assumption 15). Bulk density data of several boreholes from Tptrn are plotted in Figure 6-7. Samples with bulk density greater than 2.26 g/cm^3 near the top of Tptrn, in their respective boreholes, were selected and K_{sat} data for those samples were analyzed. The similarity of Tpcpmn and Tptpmn has been demonstrated; for example, both formations are pyroclastic flow deposits in the Paintbrush Group resulting from similar eruptive processes (Buesch et al. 1996 [DIRS 100106], Figure 2). No data are available for Tpcpmn; hence, Tptpmn is used as a surrogate (Section 5.2.3, Assumption 12).

6.4.4.2 Use of Porosity Data to Analyze Sparse Matrix K_{sat} Data

In the data available for analysis, most samples for which K_{sat} has been measured also have data for porosity. There are many more samples, however, for which porosity data, but not K_{sat} data, are available. For units for which no surrogate could be identified, and for which only one or two K_{sat} values were available, the associated porosity value determined by weighing after drying at 105°C was used to determine the representativeness of the K_{sat} value.

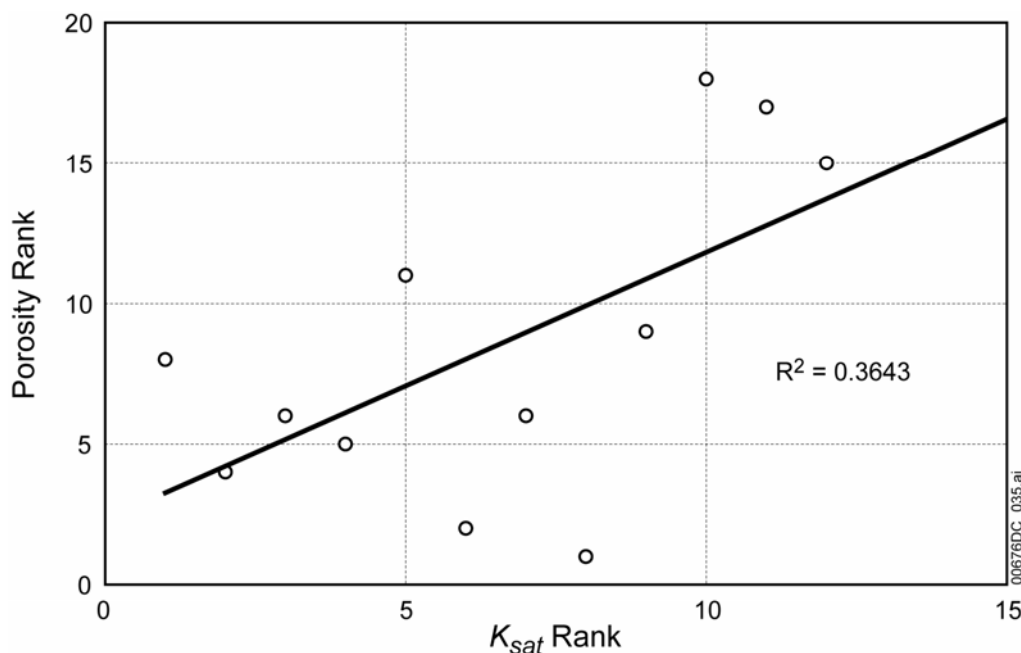
In addition, it is assumed that the more porous samples within a lithologic unit have greater K_{sat} (Section 5.2.4). The validity of this assumption is demonstrated by ranking samples in order of porosity and in order of K_{sat} , and plotting the two rankings against each other. As an example, data for the Tptpln samples with measurable K_{sat} were ranked and plotted in this manner (Figure 6-8); samples for which porosity was not measured are not represented in the figure. The two rankings are sufficiently correlated to justify the assumption. The data are from output DTN: MO0605SPAFABRP.004, *Matrix and fracture-fill Ksat for each rock type.xls*, worksheet 'Sorted by unit(3)'.



Source: Output DTN: MO0605SPAFABRP.004, *Matrix and fracture-fill Ksat for each rock type.xls*, worksheet 'Bulk dens of Tptrn'.

NOTE: The low-porosity, high-density Tptprn3 subzone occurs near the top of the Tptprn.

Figure 6-7. Density Versus Depth in Borehole for Samples in Tptrn



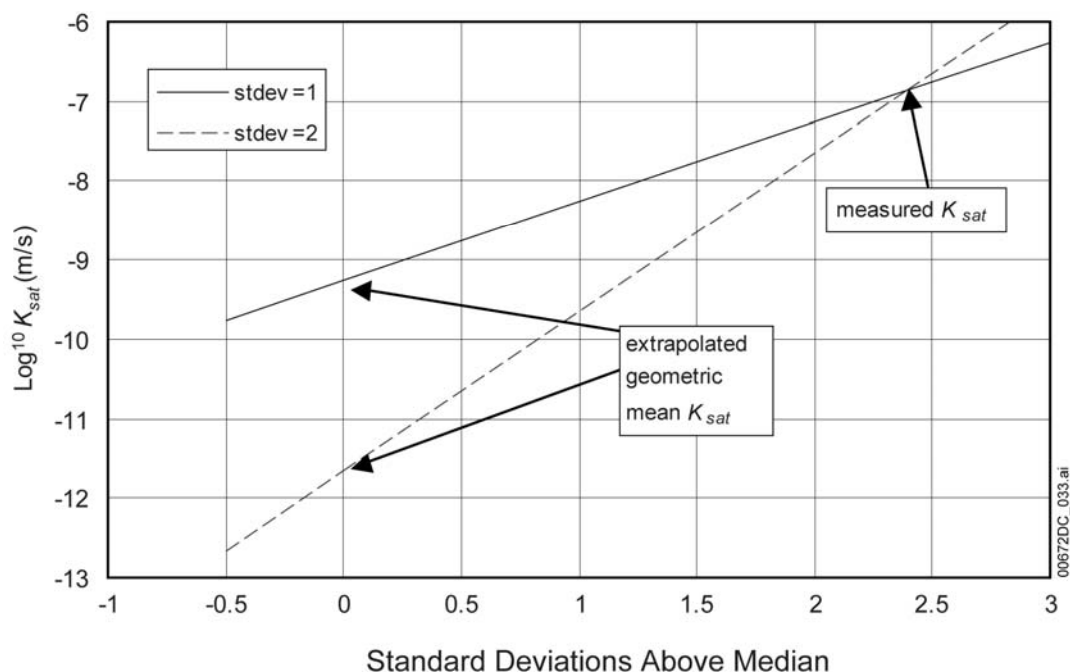
Source: Output DTN: MO0605SPAFABRP.004, *Matrix and fracture-fill Ksat for each rock type.xls*, worksheet 'Sorted by unit(3)', cell AE3575.

Figure 6-8. Ranking of Porosity and K_{sat} for Tptpln Samples

The method used to analyze K_{sat} data (Section 6.4.3) is equivalent to fitting $\log_{10} K_{sat}$ with a straight line on probability paper; the line cannot be determined with only one point. Therefore, the porosity data were ranked and standard quantiles were determined. The quantile for the porosity value was assigned to the single observed saturated hydraulic conductivity value and a standard deviation of one \log_{10} unit was assumed; that is, a slope of 1. The slope of 1 and the single point were used to estimate the median value of $\log_{10} K_{sat}$, equivalently the geometric mean K_{sat} , by extrapolation. This assumption (Section 5.2.5, Assumption 14) is made for Tpcrn3 and Tpcrn2 (IHUs 402 and 403).

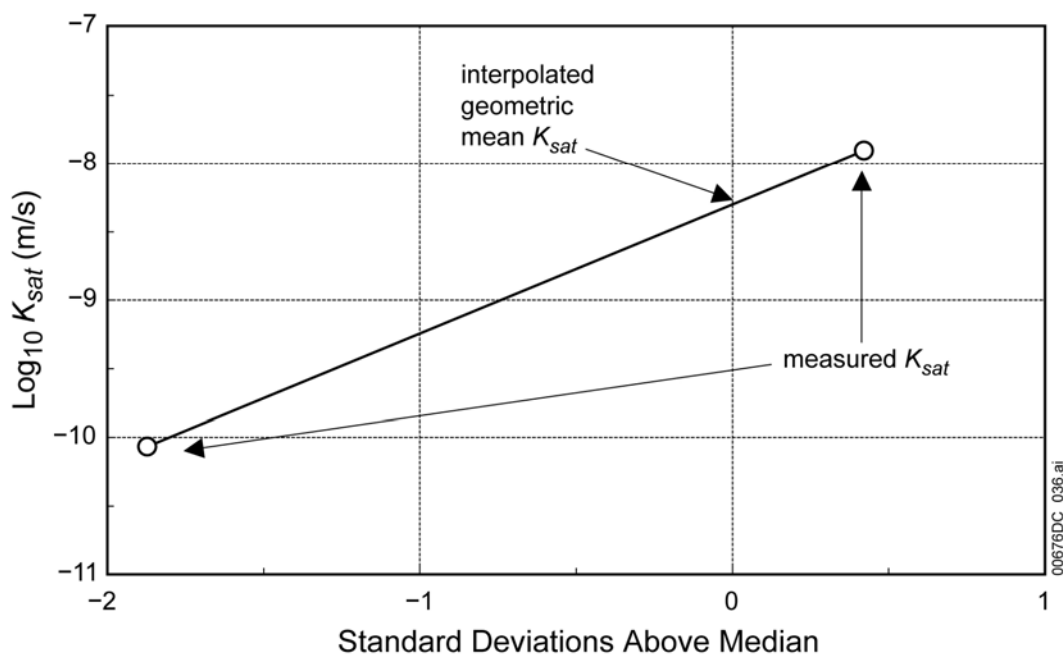
The calculation for Tpcrn3 is illustrated in Figure 6-9, for which the only K_{sat} measurement is made on a sample of extremely high porosity so that the measured K_{sat} is much greater than the geometric mean. Figure 6-9 also shows that the estimated geometric mean is, in this case, sensitive to the assumed standard deviation (Section 5.2.5).

Where two values of K_{sat} are available, and no nondetects, the same approach is used to assign standard quantiles to the K_{sat} values; these two points then determine the line for calculation of the geometric mean of K_{sat} and standard deviation of $\log_{10} K_{sat}$. This is considered more representative than assigning percentiles of 0.25 and 0.75 and calculating the standard quantiles from those numbers. This approach is used for Tpcpul (IHU 405) (Figure 6-10).



Source: Output DTN: MO0605SPAFABRP.004, *Matrix and fracture-fill Ksat for each rock type.xls*, worksheet 'Tpcrn3 (402) from porosity'.

Figure 6-9. Method of Estimating Geometric Mean K_{sat} from One K_{sat} Measurement and Several Porosity Measurements



Source: Output DTN: MO0605SPAFABRP.004, *Matrix and fracture-fill Ksat for each rock type.xls*, worksheet 'Tpcpul (405) from porosity'.

Figure 6-10. Method of Estimating Geometric Mean K_{sat} from Two K_{sat} Measurements and Several Porosity Measurements

6.4.5 K_{sat} of the Bulk Bedrock Material

In this section, the K_{sat} of the bulk bedrock material is calculated. In section 6.4.5.1, the K_{sat} of the bulk bedrock material is calculated considering all fractures as being completely filled with caliche (Section 5.1.9, Assumption 9). For input to the infiltration model, both the spatial variability of bulk bedrock K_{sat} and the uncertainty of its mean value must be quantified for each IHU. This section presents the approaches used to calculate these quantities from the data shown in Tables 6-6 and 6-8. Bulk K_{sat} calculated using Assumption 9 constitutes a lower bound for bulk K_{sat} . In Section 6.4.5.2, the uncertainty of the mean of this lower bound value is calculated.

In Section 6.4.5.3, the bulk K_{sat} calculated with all fractures completely filled is compared to the steady infiltration flux measured in an infiltration test at Alcove 1. This infiltration flux can be considered as a measure of the bulk K_{sat} . The comparison indicates that partially filled fractures also contribute to the bulk bedrock K_{sat} . In Section 6.4.5.4, the contribution of partially filled fractures to the bulk bedrock K_{sat} is calculated assuming that some portion (between 0 and 100%) of the fractures are incompletely filled, and the unfilled portion has a hydraulic (effective parallel-plate) aperture ranging between 50 and 1,000 μm . The calculation is shown in Section 6.4.5.4.1. Based on comparisons with data in Section 6.4.5.4.2, the upper bound for bulk bedrock K_{sat} is calculated for partially filled fractures with an additional 200 μm unfilled aperture along all fractures. The calculation of bulk bedrock K_{sat} is summarized in Section 6.4.5.5. The terms “bulk bedrock K_{sat} ,” “bedrock K_{sat} ,” “bulk K_{sat} ,” and “ K_{bulk} ” are used interchangeably, depending upon context.

6.4.5.1 Spatial Variability of Bulk Bedrock K_{sat} Based on the Consideration of Filled Fractures

In the conceptual model (Section 6.1), bedrock saturated hydraulic conductivity is the last resistance to flow before water enters the UZ model. As conceptualized, the bedrock has no thickness in the infiltration model; it only acts as a skin, limiting the portion of the flux reaching the bedrock that is allowed to infiltrate into the UZ model. The spatial distributions of the matrix and the filled-fracture K_{sat} are each described as lognormal, characterized by a median and a standard deviation of the logarithm. For lognormally distributed quantities, the median of $\log_{10} K_{sat}$ is the \log_{10} of the geometric mean K_{sat} . This section describes the method that was used to combine the data presented in Tables 6-6 and 6-8 to calculate the statistics to describe the K_{sat} of the bulk bedrock. A general discussion of the propagation of variability or uncertainty of lognormal distributions is provided in Appendix B.

Fractures in the bedrock, immediately below the soil-bedrock interface, are assumed filled with caliche (Section 5.1.9, Assumption 9). The area available for infiltration through the bedrock is divided between the matrix material and the filled-fracture material, proportional to their respective volume fractions. For each of these materials, the spatial variability of K_{sat} is expressed by a lognormal distribution and characterized by the median and the standard deviation of $\log_{10} (K_{sat})$. Fracture volume fraction f_{vf} is characterized by a beta distribution because its value cannot exceed one. Matrix volume fraction is defined as $(1 - f_{vf})$ and its spatial variability is ignored because matrix volume fraction is always a value close to one.

Conceptually, flow in the matrix and filled-fracture material is through parallel flow paths. Bulk K_{sat} for the composite porous medium of matrix and fractures filled with permeable caliche is, therefore, calculated as the arithmetic mean of the two K_{sat} (not $\log K_{sat}$) values, weighted by volume fraction:

$$K_{bulk} = f_{vf} K_{ff} + (1 - f_{vf}) K_m \quad (\text{Eq. 6-4})$$

where f_{vf} is the fracture volume fraction listed in Table 6-6; K_{ff} is the K_{sat} of the fracture-filling material and K_m is the K_{sat} of the matrix (Table 6-8); K_{bulk} is the K_{sat} of the composite bedrock.

As shown in Equation 6-4, K_{bulk} is the sum of two terms, of which the first is the product of a lognormal and a beta distribution. This multiplication does not lead to any classical distribution. Moreover, the addition of the two resulting distributions is difficult to estimate analytically, because they are not independent, because of f_{vf} . Therefore, a Monte Carlo approach was used to estimate the shape of the resulting distribution: 30,000 values were sampled from the distribution of each input variable of f_{vf} , K_{ff} , and K_m , from which K_{bulk} is estimated.

The resulting distribution is close to a lognormal distribution in shape for most of the 38 infiltration units. In output DTN: MO0605SPAFABRP.004, the Monte Carlo calculations in *Spatial Variability for Bedrock Permeability_v1.4_04_12_2006.xmcd* use input data from *Fracture_Volume_Fraction_Results.xls* and *Matrix_Ksat_results.xls*; both Excel® files use data from *Fracture Volume Fraction for Each Rock Type v7.xls*, worksheet ‘Summary of Avg. Fracture Data’, and from *Matrix and fracture fill Ksat for each rock type.xls*, worksheet ‘Matrix and fill summary’.

The resulting Monte Carlo distribution of K_{bulk} values, representing the spatial variability, was fitted with two lognormal distributions. The first fitting is called parameter fitting because it fits the mean and the standard deviation of the $\ln K_{bulk}$, which are the parameters of a lognormal distribution. It matches most of the calculated distribution and preserves the first two moments of the logarithm of K_{bulk} , but results in a poor estimate of mean K_{bulk} , which is either lower or greater than that of the calculated distribution. The second fitting is called moment fitting because it fits the moments of the distribution; specifically, the mean and the standard deviation of K_{bulk} . It preserves the mean and the variance of K_{bulk} . Because the mean is strongly influenced by the right-hand tail of a lognormal distribution, this second fitting matches the right-hand tail of the distribution, but does not match most of the calculated distribution. The results of these two fittings are shown in Table 6-9.

The distribution of mean bulk bedrock saturated hydraulic conductivity, from the moment-fitting approach, over the infiltration model is shown in Figure 6-11, depicting the distribution of IHUs (Figure 6-6) with colors for various IHUs representing their respective mean bulk saturated hydraulic conductivities. For most of the model area, the mean bulk bedrock saturated hydraulic conductivity is 2.4×10^{-7} m/s or less.

Table 6-9. Bulk Bedrock K_{sat} Based on the Consideration of Filled Fractures

IHU		Bulk K_{sat}									
		Approach 1: Parameter Fitting				Approach 2: Moment Fitting					
		Spatial Variability		Uncertainty in the Mean of Ln Bulk K_{sat} ^a		Spatial Variability				Uncertainty in the Mean of Bulk K_{sat} ^a	
Number	Symbol	Mean of Ln Bulk K_{sat}	Standard Deviations of Ln Bulk K_{sat}	Minimum	Maximum	Mean of Ln of Moment-Fitting Lognormal Distribution of Bulk K_{sat}	Standard Deviation of Ln of Moment-Fitting Lognormal Distribution of Bulk K_{sat}	Mean of Bulk K_{sat} ^b (m/s)	Standard Deviation of Bulk K_{sat}	Minimum (m/s)	Maximum (m/s)
401	hcr4	-17.7	1.4	-18.6	-16.9	-19.2	2.8	2.1E-07	9.4E-06	9.38E-08	4.71E-07
402	hcr3	-17.9	1.1	-18.6	-17.3	-18.4	1.5	3.2E-08	9.9E-08	1.67E-08	6.09E-08
403	hcr2	-16.9	1.4	-18.3	-15.6	-17.6	2.1	2.0E-07	1.7E-06	5.00E-08	7.65E-07
404	hcr1	-18.9	2.0	-19.6	-18.3	-18.6	1.3	2.2E-08	4.9E-08	1.14E-08	4.09E-08
405	Hcul	-17.3	1.2	-18.4	-16.3	-18.2	1.9	7.6E-08	4.5E-07	2.70E-08	2.16E-07
406	hcmn	-18.0	0.9	-18.6	-17.5	-18.0	0.8	2.1E-08	2.2E-08	1.20E-08	3.83E-08
407 ^c	Hcll	-18.2	0.9	-18.8	-17.6	-18.1	0.8	1.9E-08	1.9E-08	1.07E-08	3.29E-08
408 ^c	Hcln	-17.4	0.8	-17.9	-16.9	-17.4	0.8	3.8E-08	3.5E-08	2.23E-08	6.51E-08
409	Hcv2	-19.3	1.0	-19.9	-18.7	-19.2	0.9	6.7E-09	7.6E-09	3.73E-09	1.22E-08
410	Hcv1	-15.5	1.5	-16.1	-14.8	-15.5	1.6	6.4E-07	2.2E-06	3.37E-07	1.23E-06
411	hbt4	-12.0	1.1	-12.9	-11.1	-12.0	1.1	1.2E-05	2.0E-05	4.84E-06	3.01E-05
412	hym	-15.5	2.3	-16.3	-14.7	-15.2	2.3	3.4E-06	4.5E-05	1.53E-06	7.51E-06
413	hbt3	-13.3	0.8	-13.6	-13.0	-13.3	0.8	2.3E-06	2.2E-06	1.65E-06	3.19E-06
414	hpc	-13.9	0.8	-14.1	-13.6	-13.8	0.8	1.3E-06	1.3E-06	1.02E-06	1.79E-06
415	hbt2	-12.6	1.3	-13.0	-12.2	-12.7	1.3	7.4E-06	1.6E-05	4.94E-06	1.12E-05
416	htrv3	-11.9	1.2	-12.5	-11.2	-11.8	1.2	1.4E-05	2.4E-05	7.49E-06	2.61E-05
417	htrv1	-18.6	2.8	-20.7	-16.4	-14.6	2.9	3.1E-05	2.2E-03	3.71E-06	2.58E-04
418	htrn	-17.3	0.7	-17.8	-16.7	-17.8	1.3	4.5E-08	9.6E-08	2.52E-08	7.90E-08
419	htrl	-17.8	0.9	-18.5	-17.2	-19.2	1.9	2.8E-08	1.8E-07	1.51E-08	5.36E-08
420	htul	-18.1	1.1	-18.7	-17.4	-19.0	1.8	2.6E-08	1.2E-07	1.38E-08	5.02E-08
421	htmn	-18.0	0.9	-18.6	-17.4	-18.0	0.8	2.1E-08	2.2E-08	1.17E-08	3.91E-08
422	htll	-18.1	1.0	-18.7	-17.5	-19.8	2.3	3.3E-08	4.5E-07	1.83E-08	6.11E-08
423 ^c	htln	-17.4	0.8	-18.0	-16.8	-17.4	0.8	3.8E-08	3.5E-08	2.17E-08	6.73E-08
424	htpv3	-21.2	1.0	-21.8	-20.6	-23.0	2.3	1.5E-09	2.1E-08	8.15E-10	2.76E-09
425	htv2v	-13.0	1.3	-13.3	-12.7	-13.1	1.3	4.9E-06	1.0E-05	3.58E-06	6.67E-06

Table 6-9. Bulk Bedrock K_{sat} Based on the Consideration of Filled Fractures (Continued)

IHU		Bulk K_{sat}									
		Approach 1: Parameter Fitting				Approach 2: Moment Fitting					
		Spatial Variability		Uncertainty in the Mean of Ln Bulk K_{sat} ^a		Spatial Variability				Uncertainty in the Mean of Bulk K_{sat} ^a	
Number	Symbol	Mean of Ln Bulk K_{sat}	Standard Deviations of Ln Bulk K_{sat}	Minimum	Maximum	Mean of Ln of Moment-Fitting Lognormal Distribution of Bulk K_{sat}	Standard Deviation of Ln of Moment-Fitting Lognormal Distribution of Bulk K_{sat}	Mean of Bulk K_{sat} ^b (m/s)	Standard Deviation of Bulk K_{sat}	Minimum (m/s)	Maximum (m/s)
426	htv2z	-18.2	1.0	-18.7	-17.6	-18.1	0.9	2.0E-08	2.2E-08	1.11E-08	3.59E-08
427	htv1v	-14.1	2.2	-14.5	-13.7	-13.6	2.0	8.9E-06	6.1E-05	5.97E-06	1.32E-05
428	htv1z	-18.2	1.0	-18.8	-17.6	-18.2	0.9	1.9E-08	2.1E-08	1.03E-08	3.60E-08
429	hacv	-13.5	3.1	-13.9	-13.0	-11.8	2.6	2.0E-04	5.2E-03	1.23E-04	3.31E-04
430	hacz	-18.2	1.0	-18.8	-17.6	-18.1	0.9	1.9E-08	2.1E-08	1.09E-08	3.42E-08
431	habtv	—	—	—	—	—	—	—	—	—	—
432 ^c	habtz	-18.2	1.0	-18.8	-17.6	-18.2	0.9	1.9E-08	2.1E-08	1.06E-08	3.50E-08
433	hpuvv	—	—	—	—	—	—	—	—	—	—
434	hpuvz	-17.7	1.6	-18.3	-17.2	-15.7	2.8	7.0E-06	3.1E-04	3.92E-06	1.26E-05
435	hpuc	-16.4	0.7	-16.6	-16.2	-16.4	0.7	9.6E-08	8.0E-08	7.78E-08	1.19E-07
436	hpmic	-17.9	0.9	-18.5	-17.4	-18.2	1.2	2.6E-08	4.8E-08	1.47E-08	4.42E-08
437	hpbvz	-20.1	1.4	-20.6	-19.6	-21.1	2.8	3.5E-08	1.8E-06	2.07E-08	5.85E-08
438	hbucm	-17.5	1.3	-18.2	-16.9	-18.6	2.6	2.4E-07	6.6E-06	1.25E-07	4.56E-07

Source: Output DTN: MO0605SPABEDRK.005.

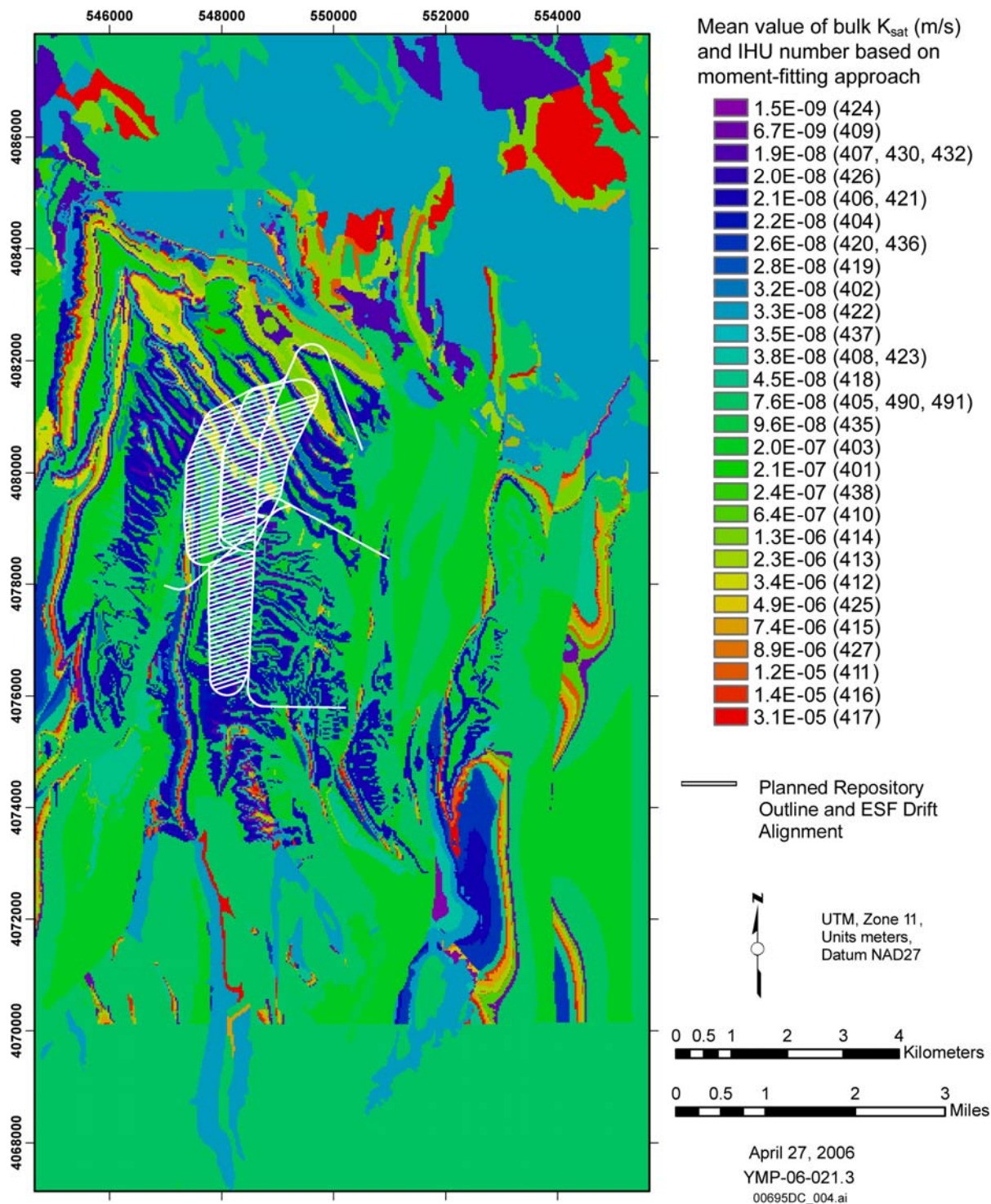
^a For three IHUs (402, 403, and 405), the number of observations is small (either one or two observations). For these IHUs, the uncertainty over the mean of bulk K_{sat} is represented as a uniform distribution and equal to one standard deviation. For all other IHUs, the uncertainty over the mean is represented as a normal distribution, with the minimum and maximum values represented by the 16th and 84th percentiles, respectively.

^b The mean values from the moment-fitting approach are displayed in Figure 6-11.

^c For calculation of the mean and variance of bedrock K_{sat} , the median of the natural log was set to -32.236 (equivalent to 10^{-14} m/s), and its standard deviation was set to zero.

NOTES: Where ln of bulk K_{sat} is reported, K_{sat} is in units of m/s. Spatial variability data were developed in output DTN: MO0605SPAFABRP.004, *Spatial Variability for Bedrock Permeability_v1.4_04_12_2006.xmcd*. Uncertainty data were developed in output DTN: MO0605SPAFABRP.004, *uncertainty_estimate_Bulk_Permability_v1.1_04_18_2006.xmcd*. The number of significant figures presented does not represent the degree of accuracy or precision in the estimate, but simply represents a choice made by the analyst as to how many figures to report.

IHU = infiltration hydrogeologic unit.



NOTES: Mean K_{sat} values are based on the consideration of filled fractures and are provided in Table 6-9, Approach #2: Moment Fitting. IHU numbers are provided in parentheses in the map legend.

ESF = Exploratory Studies Facility; IHU = infiltration hydrogeologic unit.

Figure 6-11. Distribution of Saturated Hydraulic Conductivity over the Infiltration Model Area Based on the Consideration of Filled Fractures

6.4.5.2 Uncertainty of Mean Bulk Bedrock K_{sat} Based on the Consideration of Filled Fractures

In addition to the spatial variability of K_{bulk} for each IHU, is also necessary to characterize the uncertainty of the mean value of K_{bulk} . That mean value, whether determined by the parameter-fitting or moment-fitting approach, is uncertain because it was calculated from few measurements of f_{vf} , K_{ff} , and K_m .

The mean values of K_{ff} and of K_m for each IHU, except for IHUs 402, 403, and 405, are known more or less precisely according to the Student's t -distribution based on the number of measurements. For units 402, 403, and 405, for which the number of measurements (one or two) was too small to use the Student's t -distribution, the uncertainty in the mean value of $\ln K_m$ is expressed as a uniform distribution with maximum and minimum values taken as the porosity-adjusted mean value (Section 6.4.4.2), plus or minus two standard deviations from output DTN: MO0605SPAFABRP.004, *Matrix and fracture-fill Ksat for each rock type.xls*, worksheet 'Matrix and fill summary', columns Q and R. The uncertainty of the mean value of f_{vf} is taken as a uniform distribution between the maximum and minimum values for each IHU recorded in output DTN: MO0605SPAFABRP.004, *Fracture Volume Fraction for Each Rock Type v7.xls*, worksheets 'Summary of Min. Fracture Data' and 'Summary of Max. Fracture Data', column C. These uncertainties must be propagated to the uncertainty of the mean value of either bulk K_{sat} or \ln bulk K_{sat} (both in Table 6-9) for each IHU.

The following approach was adopted to characterize the uncertainty of the mean without requiring excessive computation. Because the same measurements underlie both the parameter-fitting estimate and the moment-fitting estimate of the mean value of K_{bulk} for each IHU, the same uncertainty is applied to both estimates. Using Equation 6-4, K_{bulk} was calculated, using as input values the median $\ln K_{sat}$ (m/s) of fracture filling caliche and the median matrix $\ln K_{sat}$ (m/s) (output DTN: MO0605SPAFABRP.004, *Matrix and fracture-fill Ksat for each rock type.xls*, worksheet 'Matrix and fill summary', column Q) and the mean of \ln of f_{vf} (output DTN: MO0605SPAFABRP.004, *Fracture Volume Fraction for Each Rock Type v7.xls*, worksheet 'Summary of Avg. Fracture Data', column I). These result for each IHU in log space were compared to the mean of $\ln K_{bulk}$ determined from both the moment-fitting approach and the parameter-fitting approach of the Monte Carlo calculations. These comparisons are documented in output DTN: MO0605SPAFABRP.004, folder Regression approach, workbooks *regression_model_moments_fitting.xls* and *regression_model_parameters_fitting.xls*.

The uncertainty of the mean of either bulk K_{sat} or \ln bulk K_{sat} for each IHU was calculated using Mathcad® (output DTN: MO0605SPAFABRP.004, *uncertainty_estimate_Bulk_Permeability_v1.1_04_18_2006.xmcd*); executing a Monte Carlo calculation to calculate mean of bulk K_{sat} by Equation 6-4, with 2,000 samples of f_{vf} , K_m , and K_{ff} from their respective Student's t -distributions or uniform distributions. The standard deviation of 2,000 calculations of mean of bulk K_{sat} was determined, the uncertainty of mean of bulk K_{sat} (or mean of \ln bulk K_{sat}) is expressed as plus or minus one standard deviation in log space, and the corresponding 16th and 84th percentiles are shown in Table 6-9. The same standard deviation is used for both the parameter-fitting approach and the moment-fitting approach.

6.4.5.3 Comparison with Alcove 1 Infiltration Test

An infiltration test was conducted at Alcove 1 in the ESF during 1999 to 2000 (Liu et al. 2003 [DIRS 162470]); DTN: GS990108312242.006 [DIRS 162979]; DTN: GS000808312242.006 [DIRS 162980]).

Infiltration flux calculated from these data can be compared to the K_{bulk} calculated in Section 6.4.5.2 and summarized in Table 6-9. Infiltration flux was calculated, as shown in output DTN: MO0605SPAFABRP.004, *Alcove1_test.xls*, by converting irrigation data in DTNs: GS990108312242.006 [DIRS 162979] and GS000808312242.006 [DIRS 162980] from gallons to cubic meters and then dividing by the area of the test plot and the time interval between readings. Infiltration flux was plotted against time to identify when infiltration was steady; data during this period were averaged. During the longest period of steady infiltration, from March 17 to May 14, 2000, infiltration flux was 23.0 ± 1.2 mm/day.

Alcove 1 is 42.5 m from the north portal of the ESF (BSC 2004 [DIRS 170004], Figure 1-2) and the bedrock above it is identified as Tcr1 (Day et al. 1998 [DIRS 101557]), which is assigned to Tpcrl (IHU 404) (Table A-1). Because matrix K_{sat} data was not available for Tpcrl, Tptpul was used as a surrogate (Section 6.4.4.1; Section 5.2.6, Assumption 15). Fracture-volume-fraction data, however, are more important for the calculation of bulk K_{sat} , and these are available for Tpcrl (Table 6-4).

Table 6-9 gives a range of values that fall within the spatial variability of K_{bulk} for IHU 404 as well as the 16th and 84th percentiles of the distribution of values that describe the uncertainty of the mean value of K_{bulk} . These are determined for both the parameter-fitting approach and the moment-fitting approach. The greatest of these four upper limits is $7.1\text{E-}8$ m/s (from Table 6-9, IHU 404, Approach 2, mean of bulk K_{sat} plus one standard deviation), equal to 6.1 mm/day. This value is about one-fourth as great as the infiltration rate observed in the Alcove 1 test. Infiltration must pass through both soil and bedrock, so its rate is limited by the lesser of their two K_{sat} values. The soil at the Alcove 1 test site is classified as soil unit 5 or soil unit 9 (DTN: MO0512SPASURFD.000 [DIRS 175870]). The mean K_{sat} values for these soils are $8.14\text{E-}5$ and $4.08\text{E-}5$ cm/s respectively (DTN: MO0605SPASOILS.005 [DIRS 176922], *Rev5SummarySoilHydraulicParameters_5-1-06.xls*, worksheets ‘SoilUnit5Statistics’ [cell O72] and ‘SoilUnit9Statistics’ [cell M30]), equivalent to 70 and 35 mm/day. Therefore, the results of the Alcove 1 infiltration test suggest that the mean K_{bulk} calculated for Tpcrl (IHU 404) in Table 6-9 is an underestimate. The K_{bulk} may need to be increased by consideration of unfilled fractures; if this results in a K_{bulk} value greater than the observed infiltration rate, then the soil may actually limit the infiltration rate.

6.4.5.4 Assessment of Upper Bound Based on the Consideration of Partially Filled Fractures in Bedrock

The analyses in Sections 6.4.5.1 and 6.4.5.2 explicitly treat all fractures in bedrock, immediately below the soil-bedrock interface, as being completely filled with caliche. Caliche completely fills most of the steeply dipping fractures at pavement 2001, which exposes Tptpul and Tptpmn (Sweetkind et al. 1995 [DIRS 106959], p. 48, Figure 2, and Appendix 2). Most fractures observed at three exposures of the nonwelded paintbrush tuff in Solitario Canyon were unfilled,

but this lack of filling suggests that there has been little vertical fracture flow in the nonwelded paintbrush tuff (Sweetkind et al. 1995 [DIRS 106958], pp. 12 and 34).

6.4.5.4.1 Cubic-Law Calculation of Unfilled Aperture Fracture K_{sat}

For a bedrock unit with K_{sat} determined by its matrix K_{sat} , its fracture volume fraction, and the K_{sat} of fracture-filling material, the presence of a network of unfilled fractures would increase the K_{sat} value above the values listed in Table 6-9. This section examines the increase in bulk bedrock K_{sat} resulting from a network of unfilled fractures. Consistent with the conceptualization of bedrock as a “skin” at the bottom of the soil column, the fracture network is defined by (1) fracture trace length in meters per square meter of surface area, (2) the percentage of fractures that are not completely filled, and (3) unfilled aperture. This is equivalent to assuming that the caliche filling does not completely fill each fracture, but in some percentage of the fractures some aperture remains unfilled. The same fracture trace length data used in Section 6.3 to calculate fracture volume fraction are used with hydraulic apertures ranging from 50 μm to 1 mm (hydraulic aperture b). The percentage of fractures containing an unfilled aperture is also varied between 0% and 100%.

The saturated hydraulic conductivity of fracture networks, calculated based on the fracture length for each IHU, is shown in output DTN: MO0605SPABEDRK.005, *Fracture_lengths2 v2.xls*. The K_{sat} of these unfilled fractures would be added, as an example, to the K_{sat} values listed in Table 6-9; Table 6-10a presents the results for an additional 100 μm hydraulic aperture for all fractures, and compares these results to the K_{sat} values listed in Table 6-9 for all fractures completely filled.

The method of the calculation begins by determining the fracture length per unit area; the calculated data for the length of fracture traces measured in various mapped areas is provided in output DTN: MO0605SPAFABRP.004, *Fracture Volume Fraction for Each Rock Type v7.xls*, worksheets ‘Surface Calculation’, ‘Underground Calculation 1’, ‘Underground Calculation 2’, and ‘Underground Calculation 3’. For each mapped area, the total fracture length was divided by the mapped area to obtain the fracture density, N , in meters per square meter of bedrock. For IHUs represented by several mapped areas, the geometric mean of the several measurements was used.

The permeability due to this fracture network is (Freeze and Cherry 1979 [DIRS 101173], Equation 2.87):

$$k = (Nb^3)/12 \quad (\text{Eq. 6-5})$$

where N is the fracture density and b the hydraulic aperture.

This can also be expressed as:

$$k = (Nb)(b^2/12) \quad (\text{Eq. 6-6})$$

and this value was converted to K_{sat} using Equation 6-3. The first term in Equation 6-6 represents the fraction of area occupied by unfilled fractures and the second term represents the permeability of the unfilled fractures.

Table 6-10a. Comparison of Bedrock K_{sat} with all Fractures Filled to K_{sat} with 100 μm Unfilled Aperture in All Fractures

IHU		Bedrock Bulk K_{sat} (Mean Value, Moment Fitting) (m/s) With Considering Completely Filled Fractures (Table 6-9)	K_{sat} of Unfilled Fracture Network With 100 μm Hydraulic Aperture for All Fractures (m/s)	Ratio of Unfilled Fracture Network to Matrix and Filled Fractures
Number	Symbol			
401	hcr4	2.1E-07	7.9E-07	3.75E+00
402	hcr3	3.2E-08	7.9E-07	2.47E+01
403	hcr2	2.0E-07	7.9E-07	4.03E+00
404	hcr1	2.2E-08	5.1E-07	2.35E+01
405	hcul	7.6E-08	5.8E-07	7.65E+00
406	hcmn	2.1E-08	9.6E-07	4.49E+01
407	hcll	1.9E-08	7.7E-07	4.08E+01
408	hcln	3.8E-08	1.2E-06	3.15E+01
409	hcv2	6.7E-09	7.9E-07	1.17E+02
410	hcv1	6.4E-07	7.9E-07	1.22E+00
411	hbt4	1.2E-05	3.8E-07	3.18E-02
412	hym	3.4E-06	4.4E-07	1.29E-01
413	hbt3	2.3E-06	4.6E-07	2.02E-01
414	hpc	1.3E-06	5.8E-07	4.30E-01
415	hbt2	7.4E-06	5.2E-07	6.97E-02
416	htrv3	1.4E-05	8.9E-07	6.37E-02
417	htrv1	3.1E-05	6.2E-07	2.01E-02
418	htrn	4.5E-08	9.9E-07	2.21E+01
419	htrl	2.8E-08	7.9E-07	2.76E+01
420	htul	2.6E-08	5.8E-07	2.22E+01
421	htmn	2.1E-08	9.6E-07	4.49E+01
422	htll	3.3E-08	7.7E-07	2.29E+01
423	htln	3.8E-08	1.2E-06	3.14E+01
424	htpv3	1.5E-09	9.1E-07	6.05E+02
425	htv2v	4.9E-06	9.1E-07	1.85E-01
426	htv2z	2.0E-08	6.6E-07	3.30E+01
427	htv1v	8.9E-06	3.5E-07	3.94E-02
428	htv1z	1.9E-08	6.6E-07	3.42E+01
429	hacv	2.0E-04	3.1E-07	1.54E-03
430	hacz	1.9E-08	6.6E-07	3.41E+01
431	habtv	—	3.1E-07	—
432	habtz	1.9E-08	6.6E-07	1.61E+01
433	hpuvv	—	3.5E-07	—
434	hpuvz	7.0 E-06	6.6E-07	9.36E-02
435	hpuc	9.6E-08	7.9E-07	3.63E+00

Table 6-10a. Comparison of Bedrock K_{sat} with all Fractures Filled to K_{sat} with 100 μm Unfilled Aperture in All Fractures (Continued)

IHU		Bedrock Bulk K_{sat} (Mean Value, Moment Fitting) (m/s) With Considering Completely Filled Fractures (Table 6-9)	K_{sat} of Unfilled Fracture Network With 100 μm Hydraulic Aperture for All Fractures (m/s)	Ratio of Unfilled Fracture Network to Matrix and Filled Fractures
Number	Symbol			
436	hpmic	2.6E-08	8.8E-07	2.58E+01
437	hpbvz	3.5E-08	3.5E-07	2.26E+01
438	hbucm	2.4E-07	8.8E-07	3.66E+00

NOTES: K_{sat} of unfilled fracture network with 100 μm hydraulic aperture is provided in output DTN: MO0605SPABEDRK.005, *Fracture_lengths2.xls*.

The number of significant figures presented does not represent the degree of accuracy or precision in the estimate, but simply a choice by the analyst as to how many figures to report.

IHU = infiltration hydrogeologic unit.

As an example, data for IHU hcmn (406) were analyzed as follows (output DTN: MO0605SPABEDRK.005):

- Data from eight mapped areas were used to determine the fracture volume fraction for that IHU (*Fracture Volume Fraction for Each Rock Type v7.xls*, worksheet ‘Summary of Fracture Data’)
- For each mapped area, the ratio, N , of total fracture length to mapped area was calculated (*Fracture_lengths2 v2.xls*); the geometric mean of the eight values was calculated as 1.18 m/m^2 (*Fracture_lengths2 v2.xls*, worksheet ‘fracture length X 100 microns’ [cell N61])
- Nb , $b^2/12$, k , and K_{sat} were calculated (*Fracture_lengths2 v2.xls*) for percentages of unfilled fractures ranging from 0% to 100% (a correction factor applied to N) and for hydraulic apertures ranging from 50 μm to 1 mm.

In Table 6-10a, the calculated K_{sat} values for each IHU, due to an unfilled fracture network, with 100% of fractures having a hydraulic aperture of 100 μm , are compared to the K_{sat} values previously determined with all fractures filled (Table 6-9). The ratio of the K_{sat} of this unfilled fracture network to the bedrock bulk K_{sat} calculated with considering completely filled fractures is also listed in Table 6-10a. This ratio is the K_{sat} enhancement that such a network of unfilled fractures would impart to the bedrock. K_{sat} values for fracture networks with less than 100% unfilled fractures, and for other hydraulic apertures ranging from 50 μm to 1 mm, are calculated in output DTN: MO0605SPABEDRK.005, *Fracture_lengths2 v2.xls*; the values shown in Table 6-10a are only shown as an example for one hydraulic aperture applied to all fractures.

Among the IHUs, N varies, as does f_{vf} , although f_{vf} varies more widely than N . As a result, when unfilled fractures are considered, the K_{sat} calculated for the fracture network varies less among IHUs than the K_{sat} calculated with completely filled fractures; the presence of fractures tends to equalize the bulk K_{sat} of the IHUs. Also, in IHUs 411 through 417, 425, 427, and 429, where K_m is almost as great as K_{ff} , the resulting bulk K_{sat} calculated with considering completely filled

fractures, using Equation 6-4, is greater than the additional contribution of a network of 100% unfilled fractures with hydraulic aperture 100 μm (Table 6-10a).

Figure 6-12 shows the effect of the additional K_{sat} of partially filled fracture networks with additional apertures of 100 μm and 200 μm , with varying percent of fractures containing the additional aperture. The numbering of IHUs is generally from top to bottom, except that the alternating large and small K_{sat} values in IHUs 425 through 429 reflect the difference between vitric and zeolitic rock matrix.

For IHUs 411 through 416, 425, 427, and 429, the matrix is so permeable without any unfilled fractures (Table 6-8) that the presence of unfilled fractures does not significantly increase the saturated hydraulic conductivity.

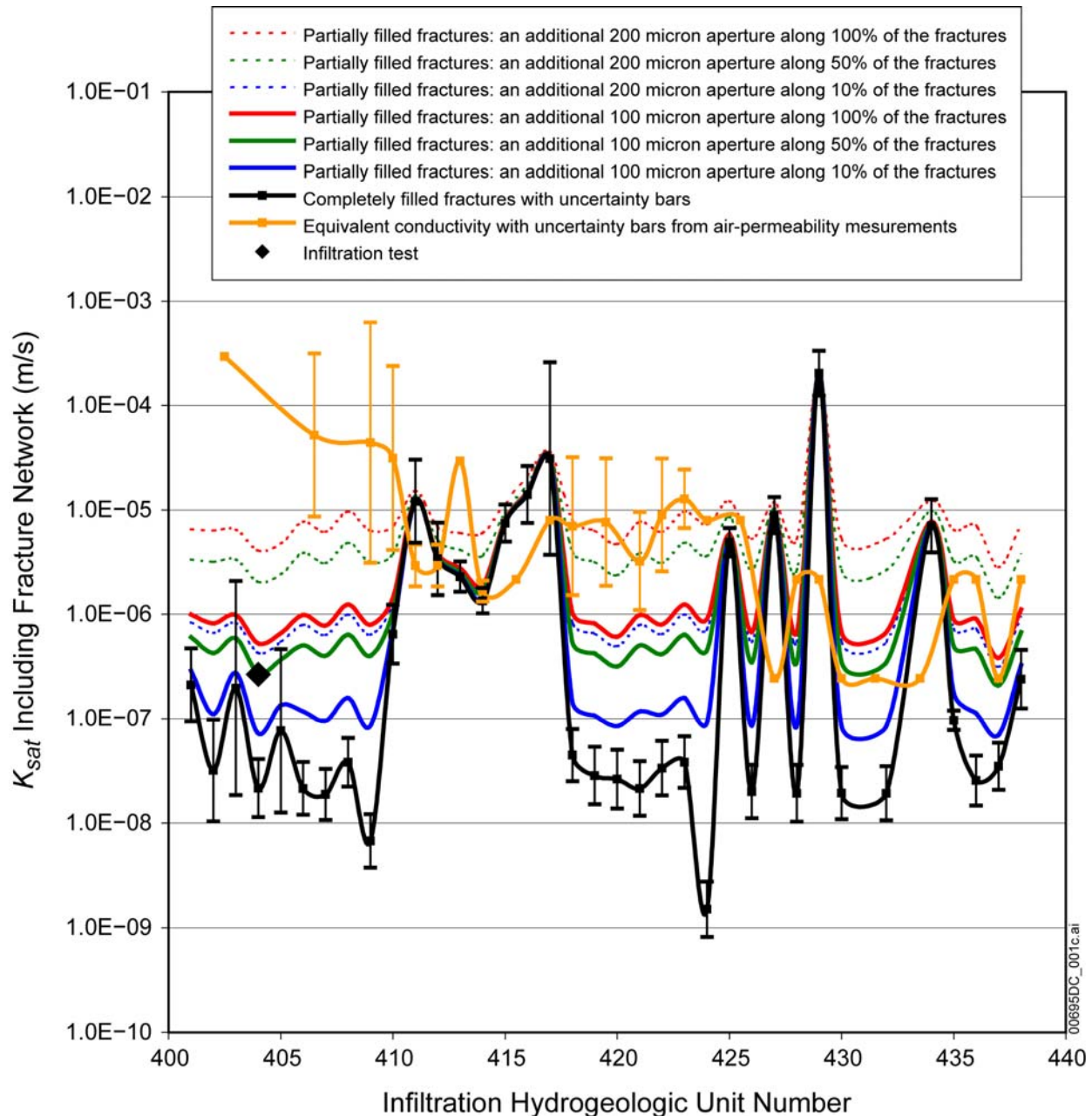
6.4.5.4.2 Estimates of Hydraulic Aperture of Partially Filled Fractures

This section examines plausible values for hydraulic apertures that might characterize a network of partially filled fractures. Examples are chosen from a field infiltration experiment, along with discrete-fracture simulations based on detailed-line-survey data and air-permeability data, and analysis of fracture spacing and air-permeability data. These examples, except for the infiltration experiment, exclude consideration of fracture infilling material, because they are based on data far below the soil-bedrock interface and, thus, represent maximum estimates of open-fracture K_{sat} ; that is for 100% open fractures.

An infiltration test was conducted in a pond excavated in the Tptpmn (IHU 421) (Glass et al. 2002 [DIRS 176044], Sections 2 and 3.4). From the length of observed fracture traces in the pond bottom and the infiltration rate, a hydraulic aperture of 200 μm was estimated. This test appears to have measured flow in open fractures. The infiltration surface, excavated 1 to 3 m below a pavement, may have been too distant from the pedogenic source of caliche for fracture infilling, thus allowing flow through open fractures.

Stochastically generated discrete-fracture networks, based on detailed line survey data and air-permeability testing, were simulated using FracMAN (Anna 1998 [DIRS 138501], Table 11; Anna 1998 [DIRS 144421], Tables 14 and 15). These simulations led to estimates of fracture permeability, k , which can be converted to equivalent K_{sat} and compared with the estimates in Table 6-10a. Anisotropic permeability was calculated; the vertical permeability is of interest here. Scale dependency was also noted. Ten simulations were performed for each of two models: one model measuring $150 \times 150 \times 60$ m and a second model measuring $200 \times 200 \times 60$ m (length \times width \times height) (Anna 1998 [DIRS 144421], p. 28).

For the 150 m model, the average vertical permeability was $2.66\text{E-}13 \pm 1.35\text{E-}13$ m² (Anna 1998 [DIRS 144421], Table 14), equivalent to a vertical hydraulic conductivity of $2.60\text{E-}6 \pm 1.32\text{E-}6$ m/s. Comparing this value with the values shown in Figure 6-12 for IHUs 401 through 410, which comprise the Tiva Canyon Tuff, shows that a network of 200 μm fractures, 50% unfilled, would account for this conductivity.



Source: Output DTN: MO0605SPABEDRK.005, *Fracture_lengths2 v2.xls*, worksheet 'Comparison to Filled Fractures'.

NOTES: While data are presented as continuous functions to improve visual depiction, the data are not continuous between IHUs. Filled-fracture data are the mean of bulk K_{sat} (Table 6-9, Approach 2: Moment Fitting). For some IHUs, for example IHUs 411 through 417, the bedrock matrix material is sufficiently permeable without any unfilled fractures so to not significantly increase saturated hydraulic conductivity. The orange curve for equivalent conductivity from air-permeability measurements is based on the hydrologic properties analysis (BSC 2004 [DIRS 170038], Table 6-5). The value plotted at IHUs 402 and 403 was calculated from data for UZ model layer tcw11. That value, however, is not an actual representation of the IHUs and, therefore, cannot be compared with K_{sat} for IHUs 401 to 404 (Section 6.4.5.4.2).

IHU = infiltration hydrogeologic unit; UZ = unsaturated zone.

Figure 6-12. Variation of Bulk Saturated Hydraulic Conductivity, K_{sat} , as a Function of Various Partially Filled Fracture Networks, with Comparison to the Alcove 1 Infiltration Test

For the 200 m model, the average vertical permeability was $5.37\text{E-}12 \pm 6.43\text{E-}13 \text{ m}^2$ (Anna 1998 [DIRS 144421], Table 15), equivalent to a vertical hydraulic conductivity of $5.26\text{E-}5 \pm 6.31\text{E-}6 \text{ m/s}$; which would require 100% unfilled fractures with apertures larger than 200 μm . The reason for the increase in fracture network permeability with the larger model was not clear (Anna 1998 [DIRS 144421], p. 29).

In a similar study for Topopah Spring Tuff, average vertical permeability values were calculated for blocks at 50, 100, 150, and 200 m scale as $2.65\text{E-}14$, $1.77\text{E-}14$, $1.58\text{E-}14$, and $5.01\text{E-}15 \text{ m}^2$ (Anna 1998 [DIRS 138501], Table 11); the respective equivalent K_{sat} values are $2.60\text{E-}07$, $1.73\text{E-}07$, $1.55\text{E-}07$, and $4.91\text{E-}08 \text{ m/s}$. This study found a decrease in fracture network permeability with increasing size of the model. The Topopah Spring Tuff comprises IHUs 416 through 428. For these IHUs, the results of the stochastic simulations are generally similar to K_{sat} values for partially filled fractures with an additional 100 μm hydraulic aperture along 10% of the fractures.

The additional hydraulic conductivity resulting from partially filled fractures can be compared to the permeability values shown in Table 6-10b (BSC 2004 [DIRS 170038], Table 6-5), which are based on air permeability (m^2) measurements in boreholes. These values were converted to saturated hydraulic conductivity (m/s) using Equation 6-3, and were plotted in Figure 6-12 (orange curve) for comparison. The air permeability tests that are the basis for these values were conducted in boreholes and, therefore, represent the permeability of deep fractures unaffected by pedogenic caliche. Table 6-10b and Figure 6-12 show that the hydraulic conductivity for the uppermost UZ model layers of tcw11 through ptn21, equivalent to IHUs 401 through 410, are greater than the corresponding values calculated for a network of partially filled fractures with an additional 200 μm hydraulic aperture along 100% of the fractures. The air permeability values for these shallow model layers could be affected by larger fracture apertures (that are typically filled at the surface) compared to the rock units at greater depth.

The hydrologic properties analysis (BSC 2004 [DIRS 170038], Table 6-5) also presents fracture frequency data. From these data, hydraulic apertures are calculated (Table 6-10b) using the approach described in the hydrologic properties analysis (BSC 2004 [DIRS 170038], Equation 6-7). Note that the air-permeability value reported for tcw11 yields a much larger hydraulic aperture, over 700 μm . That permeability value, however, is based on two measurements in the Pre-Rainier Mesa bedded tuff (Tmbt1), which is not part of UZ model layer tcw11 (DTN: GS970183122410.001 [DIRS 105580]; LeCain 1998 [DIRS 100052], pp. 17 to 20). The equivalent K_{sat} value, therefore, cannot be compared with values for IHUs 401 through 404. Excluding the tcw11 (IHUs 401 through 404), the average of the equivalent hydraulic apertures shown in Table 6-10b is approximately 206 μm .

Results of the Alcove 1 infiltration test show that bulk bedrock permeability must account for some contribution of unfilled fractures. Field observations indicate that a limited proportion of fractures is unfilled (Sanchez 2006 [DIRS 176569], pp. 26 to 61; Sweetkind et al. 1995 [DIRS 106959], p. 48, Figure 2, and Appendix 2; Sweetkind et al. 1995 [DIRS 106958], pp. 12 and 34).

Table 6-10b. Equivalent Fracture Apertures Calculated from Hydrologic Properties Analysis

UZ Model Layer ^a	Fracture Permeability, k_G^a (m^2)	Fracture Spacing, f^a (m^{-1})	Aperture, b^b (μm)	Equivalent IHU ^c
tcw11	3.00E-11 ^d	0.92	731 ^d	401-404
tcw12	5.30E-12	1.91	322	405-408
tcw13	4.50E-12	2.79	268	409
ptn21	3.20E-12	0.67	386	410
ptn22	3.00E-13	0.46	199	411
ptn23	3.00E-13	0.57	185	412
ptn24	3.00E-12	0.46	428	413
ptn25	1.70E-13	0.52	158	414
ptn26	2.20E-13	0.97	140	415-416
tsw31	8.10E-13	2.17	165	417
tsw32	7.10E-13	1.12	197	418
tsw33	7.80E-13	0.81	226	419-420
tsw34	3.30E-13	4.32	97	421
tsw35	9.10E-13	3.16	151	422
tsw36, 37	1.30E-12	4.02	157	423
tsw38	8.10E-13	4.36	131	424
tsw39	8.10E-13	0.96	216	425-426
ch1VI	2.20E-13	0.1	298	427
ch1Ze	2.50E-14	0.04	196	428
ch2v through ch5v	2.20E-13	0.14	266	429
ch2z through ch5z	2.50E-14	0.14	129	430
ch6	2.50E-14	0.04	196	431-432
pp4	2.50E-14	0.14	129	433-434
pp3	2.20E-13	0.2	236	435
pp2	2.20E-13	0.2	236	436
pp1	2.50E-14	0.14	129	437
bf3	2.20E-13	0.2	236	438
bf2	2.50E-14	0.14	129	—
tr3	2.20E-13	0.2	236	—
tr2	2.50E-14	0.14	129	—

^a BSC 2004 [DIRS 170038], Table 6-5^b BSC 2004 [DIRS 170038], Equation 6-7^c Table 6-3a.^d This value is reported for tcw11 (BSC 2004 [DIRS 170038], Table 6-5), but it is not representative of IHUs 401 through 404 (Section 6.4.5.4.2).

IHU = infiltration hydrogeologic unit; UZ = unsaturated zone.

Based upon the observations and the estimates of fracture aperture considered here, the recommended upper bound for bulk bedrock permeability is the value calculated for partially filled fractures with an additional 200 μm aperture along all fractures. The recommended lower bound for bulk bedrock permeability is the value for all fractures filled. Use of a log-uniform uncertainty distribution between the upper and lower bounds (Section 5.2.7, Assumption 16) allows for the contribution of unfilled fractures while still recognizing that most fractures are filled. A log-uniform distribution is appropriate to represent the uncertainty because bedrock K_{sat} , including the effect of partially filled fractures, may cover a large range (orders of magnitude) and little information is known about the shape of the distribution (Mishra 2002 [DIRS 163603], Section 2.3).

6.4.5.5 Summary of Bulk Bedrock K_{sat}

The analysis in Sections 6.4.5.1 and 6.4.5.2 calculates mean values for bulk bedrock K_{sat} for each IHU under the assumption that all fractures are completely filled with caliche. The analysis also provides estimates of spatial variability and of uncertainty of the mean value. These data are shown in Table 6-9 and Figure 6-11. Field observations (Sanchez 2006 [DIRS 176569], pp. 26 to 61) indicate that caliche infilling of fractures and other voids is pervasive in many areas, but in others, particularly where soil cover is thin (because soil is the source of the caliche), it is spotty, does not completely fill fractures, or is absent. Also, additional field observations (Sweetkind et al. 1995 [DIRS 106959], p. 48, Figure 2, and Appendix 2; Sweetkind et al. 1995 [DIRS 106958], pp. 12 and 34) show that in general at least some proportion of fractures are not completely filled (Section 6.4.5.4). Comparison of the infiltration rate measured in the Alcove 1 infiltration test with the mean bulk bedrock K_{sat} (Table 6-9) for IHU 404 (Section 6.4.5.3) (Figure 6-12) also suggests that the fractures at that location are not completely filled. In view of these observations, the bulk bedrock saturated hydraulic conductivity calculated for filled fractures must be regarded as a lower bound of bulk bedrock saturated hydraulic conductivity. The upper bound of bulk bedrock saturated hydraulic conductivity must be set by some estimate of the percent of fractures containing an additional hydraulic aperture.

The additional hydraulic conductivity that would result from unfilled fractures is calculated in output DTN: MO0605SPABEDRK.005, *Fracture_lengths2 v2.xls*, and some examples are shown in Figure 6-12. Few data are available to quantify either the proportion of fractures that are unfilled or the hydraulic aperture to characterize them. Reasonable values may be inferred from the sources identified in Section 6.4.5.4.2, including the Alcove 1 infiltration test, another infiltration test at Fran Ridge, and analysis of fracture air-permeability data and fracture frequency data. Based on these values, the upper bound of bulk bedrock K_{sat} has been calculated based on the consideration of an additional 200 μm hydraulic aperture with all fractures. For the purpose of stochastic simulation, the distribution of bulk bedrock K_{sat} between these bounds is taken as log-uniform. The mean and variance of bulk bedrock K_{sat} were calculated as follows (equations derived in Appendix C):

$$\mu = \frac{x_2 - x_1}{\ln(x_2) - \ln(x_1)} \quad (\text{Eq. 6-7})$$

$$\sigma^2 = \mu \left\{ \left(\frac{x_1 + x_2}{2} \right) - \mu \right\} \quad (\text{Eq. 6-8})$$

where μ and σ^2 are the mean and variance, respectively, of bulk bedrock K_{sat} and x_1 and x_2 are the lower and upper bounds of bedrock K_{sat} . These bounds, means, and variances are summarized in Table 6-11.

Table 6-11. Summary of Bulk Bedrock K_{sat}

IHU		Upper Bound ^a (m/s)	Lower Bound ^b (m/s)	Mean ^c (m/s)	Variance ^c (m ² /s ²)
Number	Symbol				
401	hcr4	6.5E-06	2.1E-07	1.8E-06	2.8E-12
402	hcr3	6.3E-06	3.2E-08	1.2E-06	2.4E-12
403	hcr2	6.5E-06	2.0E-07	1.8E-06	2.8E-12
404	hcr1	4.1E-06	2.2E-08	7.7E-07	9.9E-13
405	hcul	4.8E-06	7.6E-08	1.1E-06	1.5E-12
406	hcmn	7.7E-06	2.1E-08	1.3E-06	3.4E-12
407	hcll	6.1E-06	1.9E-08	1.1E-06	2.1E-12
408	hcln	9.6E-06	3.8E-08	1.7E-06	5.4E-12
409	hcv2	6.3E-06	6.7E-09	9.2E-07	2.1E-12
410	hcv1	7.0E-06	6.4E-07	2.7E-06	3.0E-12
411	hbt4	1.5E-05	1.2E-05	1.4E-05	7.9E-13
412	hym	6.9E-06	3.4E-06	4.9E-06	1.0E-12
413	hbt3	6.0E-06	2.3E-06	3.9E-06	1.1E-12
414	hpc	6.0E-06	1.3E-06	3.1E-06	1.7E-12
415	hbt2	1.2E-05	7.4E-06	9.4E-06	1.4E-12
416	htrv3	2.1E-05	1.4E-05	1.7E-05	4.2E-12
417	htrv1	3.6E-05	3.1E-05	3.3E-05	2.1E-12
418	htrn	7.9E-06	4.5E-08	1.5E-06	3.8E-12
419	htrl	6.3E-06	2.8E-08	1.2E-06	2.3E-12
420	htul	4.7E-06	2.6E-08	9.0E-07	1.3E-12
421	htmn	7.7E-06	2.1E-08	1.3E-06	3.4E-12
422	htll	6.2E-06	3.3E-08	1.2E-06	2.3E-12
423	htln	9.6E-06	3.8E-08	1.7E-06	5.4E-12
424	htpv3	7.3E-06	1.5E-09	8.5E-07	2.4E-12
425	htv2v	1.2E-05	4.9E-06	8.0E-06	4.3E-12
426	htv2z	5.3E-06	2.0E-08	9.4E-07	1.6E-12
427	htv1v	1.2E-05	8.9E-06	1.0E-05	6.5E-13
428	htv1z	5.3E-06	1.9E-08	9.4E-07	1.6E-12
429	hacv	2.0E-04	2.0E-04	2.0E-04	5.2E-13
430	hacz	5.3E-06	1.9E-08	9.4E-07	1.6E-12
431	habtv	—	—	—	—
432	habtz	5.3E-06	1.9E-08	9.4E-07	1.6E-12
433	hpuvv	—	—	—	—

Table 6-11. Summary of Bulk Bedrock K_{sat} (Continued)

IHU		Upper Bound ^a (m/s)	Lower Bound ^b (m/s)	Mean ^c (m/s)	Variance ^c (m ² /s ²)
Number	Symbol				
434	hpuvz	1.2E-05	7.0E-06	9.4E-06	2.3E-12
435	hpuc	6.4E-06	9.6E-08	1.5E-06	2.6E-12
436	hpmc	7.0E-06	2.6E-08	1.2E-06	2.8E-12
437	hpbvz	2.8E-06	3.5E-08	6.4E-07	5.1E-13
438	hbucm	7.2E-06	2.4E-07	2.1E-06	3.5E-12

Source: Output DTN: MO0605SPABEDRK.005, *Fracture_lengths2 v2.xls*, worksheet 'upper and lower bounds'.

^a Upper-bound K_{sat} is the sum of K_{sat} with all fractures filled (Table 6-9, moment-fitting mean value) and K_{sat} of 100% unfilled fractures with hydraulic aperture 200 μm (output DTN: MO0605SPABEDRK.005, *Fracture_lengths2 v2.xls*, worksheet 'upper and lower bounds')

^b Lower-bound K_{sat} is the K_{sat} with all fractures filled (Table 6-9, moment-fitting mean value)

^c Mean and variance are calculated using Equations 6-7 and 6-8

IHU = infiltration hydrogeologic unit.

6.5 UNCERTAINTIES AND LIMITATIONS

6.5.1 Conceptual Uncertainty

The conceptual approach for calculation of bedrock saturated hydraulic conductivity (K_{sat}) treats the bedrock as a “skin,” or a layer with zero thickness, at the bottom of the soil column. Because the thickness of the bedrock is not considered, the bulk K_{sat} is calculated based on fractions of the area occupied respectively by the fractures and by the matrix. This is equivalent to flow in parallel vertical paths. An alternative conceptualization that is not consistent with the treatment of bedrock as a skin is flow through horizontal layers of matrix and fractures in series. Such an approach would result in much lower K_{sat} values, with the effect of the fractures being nearly eliminated (Freeze and Cherry 1979 [DIRS 101173], Section 2.4).

For the purposes of calculation of a lower bound for bedrock K_{sat} , fractures are treated as being entirely filled with a permeable caliche, the K_{sat} of which determines their contribution to the bedrock K_{sat} . This treatment is based upon visual observations of fractures at the cleared pavements. The caliche is composed principally of pedogenic calcite. An upper bound for bedrock K_{sat} is determined by a calculation of the effective K_{sat} of unfilled fractures, in which the percentage of fractures containing an additional aperture is varied between 0% and 100%, and the additional hydraulic aperture is varied between 50 μm and 1 mm (output DTN: MO0605SPABEDRK.005, *Fracture_lengths2 v2.xls*).

The variation of bulk K_{sat} as a function of various partially filled fracture networks is shown in Section 6.4.5.4 (Figure 6-12) with a comparison to the Alcove 1 infiltration test. When 50% of the fractures are considered to have an additional 100 μm hydraulic aperture, then the resulting bulk K_{sat} more closely matches the results of the Alcove 1 infiltration test. Based on considerations (Section 6.4.5.4.2), including the Alcove 1 infiltration test, another infiltration test at Fran Ridge, and analysis of fracture air-permeability data and fracture frequency data, the upper bound for bedrock K_{sat} is calculated by attributing an additional 200 μm unfilled aperture to all fractures.

The conceptual approach for calculating fracture volume fraction (Section 6.3) is based in part on underground fracture mapping data that is not defined by a specified mapping area. Instead, mapping includes all fractures that are greater than 1 m and that cross the mapping trace line. This mapping approach is known as the detailed line survey. The approach for calculating fracture volume fraction uses the average fracture length to set the width of the mapped area in the assessment of underground fracture data. The mapped area is calculated as the average fracture length multiplied by the length of tunnel mapped. Because the majority of fractures are less than 4 m in length, a maximum fracture length of 4 m was used to avoid biasing the average fracture length toward long continuous fractures that would skew the width of the mapped area. Without a truncated fracture length, the calculated mapped area increases and there is an increased likelihood of potential fractures within the mapped area that do not cross the detailed line survey. Because fractures that do not cross the detailed line survey are not included in the source data, non-truncated fracture lengths could result in artificially low fracture volume fractions. With the fracture length limited to 4 m, both the fracture area and the mapped area are consequently limited, and the resulting effect to the fracture volume fraction (which is equal to the fracture area divided by the mapped area) is minimal.

The assessment of fractures in this analysis does not specifically address the effect of faulting. It is recognized that fracture density generally increases near faults. Therefore, the fracture volume fraction potentially increases near faults. Because fracture data from underground mapping have been collected near faults, an increase in fracture density resulting from faults has been included with the fracture-volume-fraction calculation. Additionally, the approach for assessing the upper-bound K_{sat} values by applying a 200 μm hydraulic aperture to all fractures accounts for additional unfilled fractures occurring near faults.

6.5.2 Data Uncertainty

Data uncertainty arises from sparse data for matrix K_{sat} for some IHUs (Section 6.4.4) and from a lack of data for unfilled fractures.

The mean values and standard uncertainties of the output data presented in Table 6-9 were determined based on the approach documented in output DTN: MO0605SPAFABRP.004, folder Uncertainty. This analysis considers uncertainty in the bulk bedrock permeability K_{bulk} with all fractures completely filled with caliche; this uncertainty is small compared with the uncertainty in the number and aperture of partially filled fractures, which is accounted for by establishing upper and lower bounds (Section 6.4.5.5).

An independent examination of the relative importance of sources of uncertainty in the calculation of K_{bulk} with completely filled fractures was carried out following the example of ANSI/NCSL Z540-2-1997 [DIRS 157394], Table H.1. Rearranging Equation 6-4 gives:

$$K_{bulk} = f_{vf} (K_{ff} - K_m) + K_m. \quad (\text{Eq. 6-9})$$

The inputs, f_{vf} , K_{ff} , and K_m , are independent of each other. Therefore ANSI/NCSL Z540-2-1997 [DIRS 157394], Section 5 and Equation (10), was used to estimate the uncertainty of K_{bulk} . In general, where y is the estimate of the measurand Y , the combined standard uncertainty of y is given by:

$$u_c^2(y) = \sum_{i=1}^n \left(\frac{\partial f}{\partial x_i} \right)^2 u^2(x_i) \quad (\text{Eq. 6-10})$$

where $u_c(y)$ is the combined standard uncertainty of y , f is the function that defines y in terms of the independent inputs x_i , and $u(x_i)$ is the uncertainty of each independent input x_i . In the present case, $y = K_{bulk}$, the x_i are f_{vf} , K_{ff} , and K_m , and f is the function in Equation 6-9. The three derivatives are developed from Equation 6-9:

$$\left(\frac{\partial K_{bulk}}{\partial f_{vf}} \right) = K_{ff} - K_m \quad (\text{Eq. 6-11})$$

$$\left(\frac{\partial K_{bulk}}{\partial K_{ff}} \right) = f_{vf} \quad (\text{Eq. 6-12})$$

$$\left(\frac{\partial K_{bulk}}{\partial K_m} \right) = (1 - f_{vf}) \quad (\text{Eq. 6-13})$$

Evaluation of Equation 6-10 requires, for each IHU, evaluation of these three derivatives and evaluation of the uncertainty $u(x_i)$ of the mean of each of the three inputs. This calculation is documented for IHU 405 in output DTN: MO0605SPAFABRP.004, *Uncertainty analysis.xls*. To evaluate the derivative in Equation 6-11, the arithmetic means of K_{ff} and K_m were calculated from the measured values, which respectively appear in output DTN: MO0605SPAFABRP.004, *Matrix and fracture fill Ksat for each rock type.xls*, worksheet ‘fill material 2,’ cells D3 through D6, and worksheet ‘Tpcpul(405) from porosity,’ cells R57 and R58. (For IHU 405 and for the fracture filling caliche, there were no “no flow” measurements; to calculate the arithmetic mean K_m for other IHUs, “no flow” measurements would be represented by zero values.) To evaluate the derivatives in Equations 6-12 and 6-13, the mean value of f_{vf} was taken from output DTN: MO0605SPAFABRP.004, *Fracture Volume Fraction for Each Rock Type v7.xls*, worksheet ‘Summary’, cell B7; this value also appears in Table 6-6.

Uncertainty of the means of the three inputs is calculated as follows. The uncertainty of K_{ff} is calculated as the standard deviation of measurements of K_{ff} (output DTN: MO0605SPAFABRP.004, *Matrix and fracture fill Ksat for each rock type.xls*, worksheet ‘fill material 2,’ cells D3 through D6) divided by the square root of the number of measurements. The uncertainty of f_{vf} is calculated by treating f_{vf} as uniformly distributed between maximum and minimum values shown in output DTN: MO0605SPAFABRP.004, *Fracture Volume Fraction for Each Rock Type v7.xls*, worksheet ‘Summary,’ cells D7 and C7. The uncertainty is then calculated as the square root of the variance, which is the difference between the maximum and minimum values divided by the square root of 12 (Hahn and Shapiro 1967 [DIRS 146529],

p. 128). Because only two measurements are available for K_m for IHU 405, it is also treated as uniformly distributed and its uncertainty is calculated the by the same formula, that is, the difference between the two measured values divided by the square root of 12. These measured values are shown in output DTN: MO0605SPAFABRP.004, *Matrix and fracture fill Ksat for each rock type.xls*, worksheet 'Tpcpul(405) from porosity,' cells R57 and R58. For IHUs with more K_m measurements, the standard deviation of measured values divided by the square root of the number of measurements would be used. IHU 405 was chosen to illustrate the calculation because it covers the largest area of any IHU, and the K_m value has a large uncertainty, being based on two measurements. The example is worked out in Table 6-12.

Table 6-12. Calculation of Combined Uncertainty of K_{bulk} for IHU 405

Mean Values		Uncertainties		Derivatives			Products	Squares of products
f_{vf}	0.013	$u(f_{vf})$	0.0046	$\partial K_{bulk} / \partial f_{vf}$	$K_{ff} - K_m$	1.7E-6 m/s	7.8E-9 m/s	6.1E-17 m ² /s ²
K_{ff}	1.7E-6 m/s	$u(K_{ff})$	5.7E-7 m/s	$\partial K_{bulk} / \partial K_{ff}$	f_{vf}	0.013	7.4E-9 m/s	5.4E-17 m ² /s ²
K_m	6.3E-9 m/s	$u(K_m)$	3.6E-9 m/s	$\partial K_{bulk} / \partial K_m$	$1 - f_{vf}$	0.99	3.5E-9 m/s	1.2E-17 m ² /s ²
Sum of squares								1.3E-16 m ² /s ²
Combined uncertainty (square root of sum)								1.1E-8 m/s

Source: Output DTN: MO0605SPAFABRP.004, *Uncertainty analysis.xls*.

The combined uncertainty of K_{bulk} is 1.1E-8 m/s. This example can be compared to a calculated value by inserting the mean values of the three inputs directly into Equation 6-4. In this case, the mean values of the three inputs f_{vf} , K_{ff} , and K_m are, respectively 0.013, 1.7E-6 m/s, and 6.3E-9 m/s (Table 6-12), leading to a calculated value for K_{bulk} of 2.8E-8 m/s (using Equation 6-4), which is about 2.5 times as great as the combined uncertainty. This analysis shows that the uncertainty in K_{bulk} stems mainly from uncertainty in f_{vf} and K_{ff} , even for an IHU with large uncertainty of K_m .

The uncertainty of bedrock saturated hydraulic conductivity, including a contribution from unfilled fractures, is expressed by the log-uniform distribution of values between the lower and upper bounds for each IHU, as summarized in Table 6-11. A log-uniform distribution is appropriate to represent the uncertainty because bedrock K_{sat} , including the effect of partially filled fractures, may cover a large range (orders of magnitude) and little information is known about the shape of the distribution (Mishra 2002 [DIRS 163603], Section 2.3). Partially filled fractures are considered to exist in all IHUs, based upon field observations (Sanchez 2006 [DIRS 176569], pp. 26 to 61; Sweetkind et al. 1995 [DIRS 106959], p. 48, Figure 2, and Appendix 2; Sweetkind et al. 1995 [DIRS 106958], pp. 12 and 34), but there are no data to suggest that the proportion of fractures that are partially filled is correlated among IHUs. Therefore, the uncertainty distribution among IHUs is treated as uncorrelated.

INTENTIONALLY LEFT BLANK

7. CONCLUSIONS

This analysis documents the development of site-specific bedrock saturated hydraulic conductivity for Yucca Mountain that is sufficient to provide input to an infiltration model. The bedrock saturated hydraulic conductivity data set compiled herein describes the upper and lower bound of the saturated hydraulic conductivity at the interface between the soil and bedrock and is only intended for use as input to the infiltration model. This analysis documents the mean of and the standard deviation of bedrock saturated hydraulic conductivity, which are log-uniformly distributed between the upper and lower bounds. This log-uniform distribution between the upper and lower bounds describes the uncertainty in the bedrock saturated hydraulic conductivity. The bedrock saturated hydraulic conductivity data set from this calculation has been entered into the Technical Data Management System as output DTNs:

- MO0603SPAGRIDD.003
- MO0605SPABEDRK.005
- MO0605SPAFABRP.004.

Calculation of bedrock saturated hydraulic conductivity consists of the following:

- Development of IHUs that group existing hydrologic and geologic units (Section 6.2 and Appendix A)
- Assignment of bedrock geology including IHUs for each element in the infiltration model base-grid geometry (Section 6.2 and output DTN: MO0603SPAGRIDD.003)
 - The geologic framework model was queried, and all cells within the geologic framework model range that were classified as alluvial type have been identified according to their underlying bedrock type
 - Areas on the north, east, and south edges of the model area are not covered by the geologic framework model and are still shown as alluvium (IHUs 490 and 491) in the final file (output DTN: MO0603SPAGRIDD.003)
 - For infiltration modeling, it is recommended that the saturated hydraulic conductivity value for IHU 405 be used as the bedrock saturated hydraulic conductivity value for those areas mapped as IHUs 490 and 491 (output DTN: MO0603SPAGRIDD.003)
- Calculation of fracture volume fraction within the rock mass for each IHU, based on fracture data from surface and underground mapping (Section 6.3)
 - The fracture volume fraction, which varies between zero and one, is represented as a beta distribution
- Assignment of matrix saturated hydraulic conductivity and fracture infill saturated hydraulic conductivity to each IHU, based on the matrix and fracture infill saturated hydraulic conductivity data from core specimens (Section 6.4)

- Both the matrix saturated hydraulic conductivities and the filled-fracture saturated hydraulic conductivities are lognormally distributed
- Each is characterized by a median value and a standard deviation in log units
- Calculation of bedrock saturated hydraulic conductivity for each IHU (Section 6.4 and output DTN: MO0605SPABEDRK.005)
 - The bedrock saturated hydraulic conductivity with the consideration of filled fractures is lognormally distributed and is calculated from the matrix saturated hydraulic conductivity, the fracture infill saturated hydraulic conductivity, and the fracture volume fraction
 - A Monte Carlo approach is used to estimate the bulk bedrock saturated hydraulic conductivity by sampling from the distributions of each input variable, those being matrix saturated hydraulic conductivity, fracture infill saturated hydraulic conductivity, and fracture volume fraction
 - The resulting Monte Carlo distribution of bulk bedrock saturated hydraulic conductivity values, representing the spatial variability, is fitted with two lognormal distributions: parameter fitting and moment fitting (Section 6.4.5.1)
 - The mean bedrock saturated hydraulic conductivity calculated with all fractures filled provides the lower bound for each IHU
 - Additional conductivity resulting from partially filled fractures is calculated for a range of apertures and percentages of partially filled fractures
 - The upper bound bedrock saturated hydraulic conductivity is provided by the consideration of a partially filled fracture network with an additional 200 μm hydraulic aperture with all fractures
 - The mean of and the standard deviation of bedrock saturated hydraulic conductivity, log-uniformly distributed between the upper and lower bounds, are reported and describe the uncertainty in the bedrock saturated hydraulic conductivity for each IHU
- Assessment of uncertainty to assess data sufficiency (Section 6.5).

The mean value for fracture infill K_{sat} , and the mean value of matrix K_{sat} for each IHU (except for IHUs 402, 403, and 405) is known more or less precisely according to the Student's t -distribution based on the number of measurements. For units 402, 403, and 405, for which the number of measurements (one or two) was too small to use the Student's t -distribution, the uncertainty in the mean value of matrix K_{sat} is expressed as a uniform distribution with the maximum and minimum equal to two standard deviations above and below the mean. These uncertainties must be propagated to the uncertainty of the mean value of bulk bedrock K_{sat} for

each IHU. A regression approach was adopted to characterize the uncertainty of the mean without requiring excessive computation (Section 6.4.5.2).

The uncertainty of the mean bulk bedrock K_{sat} for each IHU with the consideration of filled fractures was calculated using a Monte Carlo approach with 2,000 samples of fracture volume fraction, matrix K_{sat} , and fracture infill K_{sat} taken from their respective Student's t -distributions or uniform distributions. The standard deviation of 2,000 calculations of mean bulk bedrock K_{sat} was determined and the uncertainty of mean bulk bedrock K_{sat} is expressed as minimum and maximum values equal to one standard deviation above and below the mean (Section 6.4.5.2).

In this analysis, fractures are initially treated as being entirely filled with a permeable caliche, the K_{sat} of which determines their contribution to the bedrock K_{sat} . This treatment is based upon visual observations of fractures at the cleared pavements and provides the lower-bound K_{sat} values. The caliche is composed principally of pedogenic calcite. Consistent with the treatment of bedrock as a skin, this filling is only presumed to be present near the soil-bedrock interface. This approach is evaluated in Section 6.4.5.3 by comparison of the calculated K_{sat} with the results of the only long-term infiltration test that has been conducted at Yucca Mountain in Alcove 1 of the ESF. During the longest period of steady infiltration from the Alcove 1 test, infiltration flux was 23.0 ± 1.2 mm/day (Section 6.4.5.3). The bedrock unit above Alcove 1 is IHU number 404, which has an upper limit value of bulk bedrock K_{sat} of $7.1\text{E-}8$ m/s or approximately 6.1 mm/day (Section 6.4.5.3). Based on the infiltration test, the mean bulk K_{sat} calculated for IHU number 404 may be underestimated and the bulk K_{sat} may need to be increased by considering unfilled fractures.

The increase in bulk bedrock saturated hydraulic conductivity resulting from unfilled fractures was examined in Section 6.4.5.4 by calculating the K_{sat} of a network of partially filled fractures in each IHU, based upon the fracture length data (meters of fracture trace per square meter of area). For the partially filled fracture assessment, hydraulic apertures ranging from 50 μm to 1 mm were considered, with the proportion of fractures that are unfilled varied between 0% and 100%. The variation of bulk K_{sat} as a function of various partially filled fracture networks is shown on Figure 6-12 with a comparison to the Alcove 1 infiltration test. When 50% of the fractures is considered to have an additional 100 μm hydraulic aperture, then the resulting bulk K_{sat} more closely matches the results of the Alcove 1 infiltration test. Based upon observations summarized in Section 6.4.5.5, the upper bound of bedrock saturated hydraulic conductivity is set by including a network of partially filled fractures with an additional 200 μm hydraulic aperture along 100% of the fractures, while the lower bound is set by excluding unfilled fractures and by calculating saturated hydraulic conductivity based only on the matrix material and completely filled fractures.

The recommended values for bulk bedrock saturated hydraulic conductivity are listed in Table 6-11, including the mean and the standard deviation, which are log-uniformly distributed between the upper and lower bounds. The use of a log-uniform uncertainty distribution between the upper and lower bounds allows for the contribution of unfilled fractures while still recognizing that most fractures are filled. A log-uniform distribution is appropriate to represent the uncertainty because bedrock K_{sat} , including the effect of partially filled fractures, may cover a large range (orders of magnitude) and little information is known about the shape of the distribution (Section 6.5.2).

The assessment of bedrock saturated hydraulic conductivity addresses the criteria (Section 4.2) identified in Table 7-1. The bedrock saturated hydraulic conductivity data used in this analysis are sufficient to provide input to an infiltration model.

Table 7-1. Mapping of Yucca Mountain Review Plan Acceptance Criteria and Bedrock Saturated Hydraulic Conductivity Calculation

Acceptance Criteria	Subcriteria	Sections Where Addressed
Acceptance Criterion 2: Data are sufficient for model justification	The effects of fracture properties, fracture distributions, matrix properties, heterogeneities, time-varying boundary conditions, evapotranspiration, depth of soil cover, and surface-water runoff and runoff are considered, such that net infiltration is not underestimated.	6.3 – Consideration of fracture distributions 6.4 – Consideration of fracture distributions and matrix properties
Acceptance Criterion 3: Data uncertainty is characterized and propagated through the model abstraction	Models use parameter values, assumed ranges, probability distributions, and bounding assumptions that are technically defensible, reasonably account for uncertainties and variabilities, and do not result in an underrepresentation of the risk estimate.	6.4 – Basis for bedrock saturated hydraulic conductivity including uncertainty 6.5 – Uncertainty analyses
	The technical bases for the parameter values used in this abstraction are provided.	6.4 – Technical basis for bedrock saturated hydraulic conductivity
	Possible statistical correlations are established between parameters in this abstraction. An adequate technical basis or bounding argument is provided for neglected correlations.	6.5 – Discussion of parameter correlation in the calculation of bulk K_{sat}

NOTE: Acceptance Criteria 2 and 3 are from NUREG-1804 (NRC 2003 [DIRS 163274], Section 2.2.1.3.5.3).

8. INPUTS AND REFERENCES

8.1 DOCUMENTS CITED

- 138501 Anna, L.O. 1998. *Preliminary Three-Dimensional Discrete Fracture Model of the Topopah Spring Tuff in the Exploratory Studies Facility, Yucca Mountain Area, Nye County, Nevada*. Open-File Report 97-834. Denver, Colorado: U.S. Geological Survey. TIC: 236829.
- 144421 Anna, L.O. 1998. *Preliminary Three-Dimensional Discrete Fracture Model, Tiva Canyon Tuff, Yucca Mountain Area, Nye County, Nevada*. Open-File Report 97-833. Denver, Colorado: U.S. Geological Survey. TIC: 236723.
- 100029 Barr, D.L.; Moyer, T.C.; Singleton, W.L.; Albin, A.L.; Lung, R.C.; Lee, A.C.; Beason, S.C.; and Eatman, G.L.W. 1996. *Geology of the North Ramp — Stations 4+00 to 28+00, Exploratory Studies Facility, Yucca Mountain Project, Yucca Mountain, Nevada*. Denver, Colorado: U.S. Geological Survey. ACC: MOL.19970106.0496.
- 101191 Beason, S.C.; Turlington, G.A.; Lung, R.C.; Eatman, G.L.W.; Ryter, D.; and Barr, D.L. 1996. *Geology of the North Ramp - Station 0+60 to 4+00, Exploratory Studies Facility, Yucca Mountain Project, Yucca Mountain, Nevada*. Denver, Colorado: U.S. Geological Survey. ACC: MOL.19970106.0449.
- 107386 Broxton, D.E.; Chipera, S.J.; Byers, F.M., Jr.; and Rautman, C.A. 1993. *Geologic Evaluation of Six Nonwelded Tuff Sites in the Vicinity of Yucca Mountain, Nevada for a Surface-Based Test Facility for the Yucca Mountain Project*. LA-12542-MS. Los Alamos, New Mexico: Los Alamos National Laboratory. ACC: NNA.19940224.0128.
- 170038 BSC (Bechtel SAIC Company) 2004. *Analysis of Hydrologic Properties Data*. ANL-NBS-HS-000042 REV 00. Las Vegas, Nevada: Bechtel SAIC Company. ACC: DOC.20041005.0004.
- 169855 BSC 2004. *Development of Numerical Grids for UZ Flow and Transport Modeling*. ANL-NBS-HS-000015 REV 02. Las Vegas, Nevada: Bechtel SAIC Company. ACC: DOC.20040901.0001.
- 166107 BSC 2004. *Drift Degradation Analysis*. ANL-EBS-MD-000027 REV 03. Las Vegas, Nevada: Bechtel SAIC Company. ACC: DOC.20040915.0010; DOC.20050419.0001.
- 170029 BSC 2004. *Geologic Framework Model (GFM2000)*. MDL-NBS-GS-000002 REV 02. Las Vegas, Nevada: Bechtel SAIC Company. ACC: DOC.20040827.0008.

- 170004 BSC 2004. *In Situ Field Testing of Processes*. ANL-NBS-HS-000005 REV 03. Las Vegas, Nevada: Bechtel SAIC Company. ACC: DOC.20041109.0001; DOC.20051010.0001.
- 170007 BSC 2004. *Simulation of Net Infiltration for Present-Day and Potential Future Climates*. MDL-NBS-HS-000023 REV 00. Las Vegas, Nevada: Bechtel SAIC Company. ACC: DOC.20041109.0004.
- 173980 BSC 2005. *Particle Tracking Model and Abstraction of Transport Processes*. MDL-NBS-HS-000020 REV 02. Las Vegas, Nevada: Bechtel SAIC Company. ACC: DOC.20050808.0006.
- 175539 BSC 2005. *Q-List*. 000-30R-MGR0-00500-000-003. Las Vegas, Nevada: Bechtel SAIC Company. ACC: ENG.20050929.0008.
- 176107 BSC 2006. *Technical Work Plan for: Infiltration Model Assessment, Revision, and Analyses of Downstream Impacts*. TWP-NBS-HS-000012 REV 01. Las Vegas, Nevada: Bechtel SAIC Company. ACC: DOC.20060110.0002.
- 107905 Buesch, D.C. and Spengler, R.W. 1999. "Correlations of Lithostratigraphic Features with Hydrogeologic Properties, a Facies-Based Approach to Model Development in Volcanic Rocks at Yucca Mountain, Nevada." *Proceedings of Conference on Status of Geologic Research and Mapping in Death Valley National Park, Las Vegas, Nevada, April 9-11, 1999*. Slate, J.L., ed. Open-File Report 99-153. Pages 62-64. Denver, Colorado: U.S. Geological Survey. TIC: 245245.
- 100106 Buesch, D.C.; Spengler, R.W.; Moyer, T.C.; and Geslin, J.K. 1996. *Proposed Stratigraphic Nomenclature and Macroscopic Identification of Lithostratigraphic Units of the Paintbrush Group Exposed at Yucca Mountain, Nevada*. Open-File Report 94-469. Denver, Colorado: U.S. Geological Survey. ACC: MOL.19970205.0061.
- 104639 Byers, F.M., Jr.; Carr, W.J.; Orkild, P.P.; Quinlivan, W.D.; and Sargent, K.A. 1976. *Volcanic Suites and Related Cauldrons of Timber Mountain-Oasis Valley Caldera Complex, Southern Nevada*. Professional Paper 919. Washington, D.C.: U.S. Geological Survey. TIC: 201146.
- 157236 Christiansen, R.L.; Lipman, P.W.; Carr, W.J.; Byers, F.M., Jr.; Orkild, P.P.; and Sargent, K.A. 1977. "The Timber Mountain-Oasis Valley Caldera Complex of Southern Nevada." *Geological Society of America Bulletin*, 88, (7), 943-959. Boulder, Colorado: Geological Society of America. TIC: 201802.
- 153526 CRWMS M&O 2000. *EARTHVISION V5.1, Validation Test Report Rev 00*. STN: 10174-5.1-00. Las Vegas, Nevada: CRWMS M&O. ACC: MOL.20000927.0145.

- 100027 Day, W.C.; Dickerson, R.P.; Potter, C.J.; Sweetkind, D.S.; San Juan, C.A.; Drake, R.M., II; and Fridrich, C.J. 1998. *Bedrock Geologic Map of the Yucca Mountain Area, Nye County, Nevada*. Geologic Investigations Series I-2627. Denver, Colorado: U.S. Geological Survey. ACC: MOL.19981014.0301.
- 101557 Day, W.C.; Potter, C.J.; Sweetkind, D.S.; Dickerson, R.P.; and San Juan, C.A. 1998. *Bedrock Geologic Map of the Central Block Area, Yucca Mountain, Nye County, Nevada*. Miscellaneous Investigations Series Map I-2601. Washington, D.C.: U.S. Geological Survey. ACC: MOL.19980611.0339.
- 102929 Dickerson, R.P. and Drake, R.M., II 1998. *Geologic Map of the Paintbrush Canyon Area, Yucca Mountain, Nevada*. Open-File Report 97-783. Denver, Colorado: U.S. Geological Survey. ACC: MOL.19981014.0302.
- 101219 Eatman, G.L.W.; Singleton, W.L.; Moyer, T.C.; Barr, D.L.; Albin, A.L.; Lung, R.C.; and Beason, S.C. 1997. *Geology of the South Ramp - Station 55+00 to 78+77, Exploratory Studies Facility, Yucca Mountain Project, Yucca Mountain, Nevada*. Milestone SPG42CM3. Denver, Colorado: U.S. Geological Survey. ACC: MOL.19980216.0328.
- 101173 Freeze, R.A. and Cherry, J.A. 1979. *Groundwater*. Englewood Cliffs, New Jersey: Prentice-Hall. TIC: 217571.
- 101388 Gelhar, L.W. 1993. *Stochastic Subsurface Hydrology*. Englewood Cliffs, New Jersey: Prentice-Hall. TIC: 240652.
- 101226 Geslin, J.K. and Moyer, T.C. 1995. *Summary of Lithologic Logging of New and Existing Boreholes at Yucca Mountain, Nevada, March 1994 to June 1994*. Open-File Report 94-451. Denver, Colorado: U.S. Geological Survey. ACC: MOL.19941214.0057.
- 103330 Geslin, J.K.; Moyer, T.C.; and Buesch, D.C. 1995. *Summary of Lithologic Logging of New and Existing Boreholes at Yucca Mountain, Nevada, August 1993 to February 1994*. Open-File Report 94-342. Denver, Colorado: U.S. Geological Survey. ACC: MOL.19940810.0011.
- 157245 Gibson, J.D.; Shephard, L.E.; Swan, F.H.; Wesling, J.R.; and Kerl, F.A. 1990. "Synthesis of Studies for the Potential of Fault Rupture at the Proposed Surface Facilities, Yucca Mountain, Nevada." *High Level Radioactive Waste Management, Proceedings of the International Topical Meeting, Las Vegas, Nevada, April 8-12, 1990. 1*, 109-116. La Grange Park, Illinois: American Nuclear Society. TIC: 202058.
- 163705 Gilbert, R.O. 1987. *Statistical Methods for Environmental Pollution Monitoring*. New York, New York: John Wiley & Sons. TIC: 252619.

- 176044 Glass, R.J.; Nicholl, M.J.; Ramirez, A.L.; and Daily, W.D. 2002. "Liquid Phase Structure Within an Unsaturated Fracture Network Beneath a Surface Infiltration Event: Field Experiment." *Water Resources Research*, 38, (10), 17-1 - 17-16. Washington, D.C.: American Geophysical Union. TIC: 255850.
- 146529 Hahn, G.J. and Shapiro, S.S. 1967. *Statistical Models in Engineering*. New York, New York: John Wiley & Sons. TIC: 247729.
- 175683 Helsel, D.R. and Hirsch, R.M. 1995. *Statistical Methods in Water Resources*. Studies in Environmental Science 49. Amsterdam, The Netherlands: Elsevier. TIC: 237278.
- 101136 Istok, J.D.; Rautman, C.A.; Flint, L.E.; and Flint, A.L. 1994. "Spatial Variability in Hydrologic Properties of a Volcanic Tuff." *Ground Water*, 32, (5), 751-760. Worthington, Ohio: Water Well Journal Publishing Company. TIC: 224518.
- 100052 LeCain, G.D. 1998. *Results from Air-Injection and Tracer Testing in the Upper Tiva Canyon, Bow Ridge Fault, and Upper Paintbrush Contact Alcoves of the Exploratory Studies Facility, August 1994 through July 1996, Yucca Mountain, Nevada*. Water-Resources Investigations Report 98-4058. Denver, Colorado: U.S. Geological Survey. ACC: MOL.19980625.0344.
- 100773 Lipman, P.W.; Christiansen, R.L.; and O'Connor, J.T. 1966. *A Compositionally Zoned Ash-Flow Sheet in Southern Nevada*. Professional Paper 524-F. Washington, D.C.: U.S. Geological Survey. TIC: 219972.
- 162470 Liu, H-H.; Haukwa, C.B.; Ahlers, C.F.; Bodvarsson, G.S.; Flint, A.L.; and Guertal, W.B. 2003. "Modeling Flow and Transport in Unsaturated Fractured Rock: An Evaluation of the Continuum Approach." *Journal of Contaminant Hydrology*, 62-63, 173-188. New York, New York: Elsevier. TIC: 254205.
- 163603 Mishra, S. 2002. *Assigning Probability Distributions to Input Parameters of Performance Assessment Models*. SKB TR-02-11. Stockholm, Sweden: Svensk Kärnbränsleförsörjning A.B. TIC: 252794.
- 101269 Moyer, T.C. and Geslin, J.K. 1995. *Lithostratigraphy of the Calico Hills Formation and Prow Pass Tuff (Crater Flat Group) at Yucca Mountain, Nevada*. Open-File Report 94-460. Denver, Colorado: U.S. Geological Survey. ACC: MOL.19941208.0003.
- 103777 Moyer, T.C.; Geslin, J.K.; and Buesch, D.C. 1995. *Summary of Lithologic Logging of New and Existing Boreholes at Yucca Mountain, Nevada, July 1994 to November 1994*. Open-File Report 95-102. Denver, Colorado: U.S. Geological Survey. TIC: 224224.

- 139151 National Research Council. 1996. *Rock Fractures and Fluid Flow, Contemporary Understanding and Applications*. Washington, D.C.: National Academy Press. TIC: 235913.
- 163274 NRC (U.S. Nuclear Regulatory Commission) 2003. *Yucca Mountain Review Plan, Final Report*. NUREG-1804, Rev. 2. Washington, D.C.: U.S. Nuclear Regulatory Commission, Office of Nuclear Material Safety and Safeguards. TIC: 254568.
- 101280 Ortiz, T.S.; Williams, R.L.; Nimick, F.B.; Whittet, B.C.; and South, D.L. 1985. *A Three-Dimensional Model of Reference Thermal/Mechanical and Hydrological Stratigraphy at Yucca Mountain, Southern Nevada*. SAND84-1076. Albuquerque, New Mexico: Sandia National Laboratories. ACC: MOL.19980602.0331.
- 170727 Otto, S.J. and Buesch, D.C. 2003. "Porosity, Bulk Density, and Rock-Particle Density of Lithostratigraphic Components in Lithophysal Rocks of the Topopah Spring Tuff at Yucca Mountain, Nevada." *Abstracts with Programs - Geological Society of America*, 35, (6), 434-435. Boulder, Colorado: Geological Society of America. TIC: 254862.
- 100173 Price, R.H.; Connolly, J.R.; and Keil, K. 1987. *Petrologic and Mechanical Properties of Outcrop Samples of the Welded, Devitrified Topopah Spring Member of the Paintbrush Tuff*. SAND86-1131. Albuquerque, New Mexico: Sandia National Laboratories. ACC: NNA.19870601.0013.
- 176569 Sanchez, A. 2006. Conducting Confirmatory Field Observations for Special Infiltration Project [partial submittal]. Scientific Notebook SN-M&O-SCI-053-V1. Pages 1-83 ACC: MOL.20060306.0186.
- 100075 Sawyer, D.A.; Fleck, R.J.; Lanphere, M.A.; Warren, R.G.; Broxton, D.E.; and Hudson, M.R. 1994. "Episodic Caldera Volcanism in the Miocene Southwestern Nevada Volcanic Field: Revised Stratigraphic Framework, $^{40}\text{Ar}/^{39}\text{Ar}$ Geochronology, and Implications for Magmatism and Extension." *Geological Society of America Bulletin*, 106, (10), 1304-1318. Boulder, Colorado: Geological Society of America. TIC: 222523.
- 107248 Schuraytz, B.C.; Vogel, T.A.; and Younker, L.W. 1989. "Evidence for Dynamic Withdrawal from a Layered Magma Body: The Topopah Spring Tuff, Southwestern Nevada." *Journal of Geophysical Research*, 94, (B5), 5925-5942. Washington, D.C.: American Geophysical Union. TIC: 225936.
- 104181 Scott, R.B. and Bonk, J. 1984. *Preliminary Geologic Map of Yucca Mountain, Nye County, Nevada, with Geologic Sections*. Open-File Report 84-494. Denver, Colorado: U.S. Geological Survey. ACC: HQS.19880517.1443.

- 150228 Slate, J.L.; Berry, M.E.; Rowley, P.D.; Fridrich, C.J.; Morgan, K.S.; Workman, J.B.; Young, O.D.; Dixon, G.L.; Williams, V.S.; McKee, E.H.; Ponce, D.A.; Hildenbrand, T.G.; Swadley, W C; Lundstrom, S.C.; Ekren, E.B.; Warren, R.G.; Cole, J.C.; Fleck, R.J.; Lanphere, M.A.; Sawyer, D.A.; Minor, S.A.; Grunwald, D.J.; Lacznia, R.J.; Menges, C.M.; Yount, J.C.; Jayko, A.S.; Mankinen, E.A.; Davidson, J.G.; Morin, R.L.; and Blakely, R.J. 2000. *Digital Geologic Map of the Nevada Test Site and Vicinity, Nye, Lincoln and Clark Counties, Nevada, and Inyo County, California, Revision 4; Digital Aeromagnetic Map of the Nevada Test Site and Vicinity, Nye, Lincoln, and Clark Counties, Nevada, and Inyo County, California; and Digital Isostatic Gravity Map of the Nevada Test Site and Vicinity, Nye, Lincoln, and Clark Counties, Nevada, and Inyo County, California.* Open-File Report 99-554—A, —B, and —C. Denver, Colorado: U.S. Geological Survey. TIC: 248049; 251985; 251981.
- 100182 Sweetkind, D.S. and Williams-Stroud, S.C. 1996. *Characteristics of Fractures at Yucca Mountain, Nevada: Synthesis Report.* Administrative Report. Denver, Colorado: U.S. Geological Survey. ACC: MOL.19961213.0181.
- 177047 Sweetkind, D.S.; Barr, D.L.; Polacsek, D.K.; and Anna, L.O. 1997. *Administrative Report: Integrated Fracture Data in Support of Process Models, Yucca Mountain, Nevada.* Milestone SPG32M3. Denver, Colorado: U.S. Geological Survey. ACC: MOL.19990825.0109.
- 106958 Sweetkind, D.S.; Verbeek, E.R.; Geslin, J.K.; and Moyer, T.C. 1995. *Fracture Character of the Paintbrush Tuff Nonwelded Hydrologic Unit, Yucca Mountain, Nevada.* Administrative Report. Denver, Colorado: U.S. Geological Survey. ACC: MOL.19960311.0125.
- 106959 Sweetkind, D.S.; Verbeek, E.R.; Singer, F.R.; Byers, F.M., Jr.; and Martin, L.G. 1995. *Surface Fracture Network at Pavement P2001, Fran Ridge, Near Yucca Mountain, Nye County, Nevada.* Administrative Report. Denver, Colorado: U.S. Geological Survey. ACC: MOL.19960603.0119.

8.2 CODES, STANDARDS, REGULATIONS, AND PROCEDURES

- 157394 ANSI/NCSL Z540-2-1997. *American National Standard for Calibration — U.S. Guide to the Expression of Uncertainty in Measurement.* Boulder, Colorado: NCSL International. TIC: 251472.
- IT-PRO-0011. *Software Management.*
- LP-3.15Q-BSC. *Managing Technical Product Inputs.*
- LP-SIII.9Q-BSC. *Scientific Analyses.*
- LS-PRO-0203. *Q-List and Classification of Structures, Systems, and Components.*

8.3 SOURCE DATA, LISTED BY DATA TRACKING NUMBER

149461	GS000408312231.003. Relative Humidity Calculated Porosity Measurements on Samples from Borehole USW SD-9 Used for Saturated Hydraulic Conductivity. Submittal date: 04/10/2000.
162980	GS000808312242.006. Pulse Flow Meter Data for the Alcove 1 Infiltration Experiment from 02/19/99 to 06/20/00. Submittal date: 09/07/2000.
176825	GS060208314222.001. UE-25 NRG #1 Fracture Data for Core, September 4 & 14, 1992 and Fracture Data for Pavement, September 3, 16, 17, 18, and November 16-20, 1992. Submittal date: 03/09/2006.
107027	GS930283117461.001. Preliminary Geologic Map of Yucca Mountain, Nye County, Nevada, with Geologic Sections. Submittal date: 01/20/1993.
175720	GS940308314222.001. Fracture Data for Pavement ARP-1, 12/17-22/93, 2/8-12/94, 2/28/94, and 3/1/94. Submittal date: 03/24/1994.
157228	GS940408314224.004. Plan View Geologic Map of the Drainage Channel and North Portal. Submittal date: 04/20/1994.
175708	GS950108314222.001. Fracture Mapping at Fran Ridge, Pavement P2001. Submittal date: 01/03/1995.
175723	GS950508314222.003. Fracture Data from Three Natural Exposures of the PTN Section of Solitario Canyon. Submittal date: 05/09/1995.
175931	GS950608314211.026. Fracture Data Acquired from Television Logs, 1979-1985. Submittal date: 06/28/1995.
146873	GS950708312211.003. Fracture/Fault Properties for Fast Pathways Model. Submittal date: 07/24/1995.
108998	GS960808312231.001. Water Permeability and Relative Humidity Calculated Porosity for Boreholes UE-25 UZ-16 and USW UZ-N27. Submittal date: 08/28/1996.
108995	GS960808312231.005. Water Permeability and Relative Humidity Calculated Porosity for Samples from Boreholes USW SD-7, USW SD-9, USW SD-12 and USW UZ-14. Submittal date: 08/30/1996.
175721	GS960808314222.001. Fracture Study at the USW UZ-7A Drill Pad. Submittal date: 08/02/1996.

- 105580 GS970183122410.001. Results from Air-Injection and Tracer Testing in the Upper Tiva Canyon, Bow Ridge Fault, and Upper Paintbrush Contact Alcoves of the Exploratory Studies Facility, August 1994 through July 1996, Yucca Mountain, Nevada. Submittal date: 02/03/1997.
- 106048 GS970208314224.003. Geotechnical Data for Station 60+00 to Station 65+00, South Ramp of the ESF. Submittal date: 02/12/1997.
- 106049 GS970808314224.008. Provisional Results: Geotechnical Data for Station 65+00 to Station 70+00, South Ramp of the ESF. Submittal date: 08/18/1997.
- 106050 GS970808314224.010. Provisional Results: Geotechnical Data for Station 70+00 to Station 75+00, South Ramp of the ESF. Submittal date: 08/25/1997.
- 106057 GS970808314224.012. Provisional Results: Geotechnical Data for Station 75+00 to Station 78+77, South Ramp of the ESF. Submittal date: 08/25/1997.
- 107184 GS971008312231.006. Physical Properties and Saturated Hydraulic Conductivity of Cores from Surface Samples from the ESF Main Drift 29+00 M to 57+00 M. Submittal date: 10/06/1997.
- 105561 GS971108314224.020. Revision 1 of Detailed Line Survey Data, Station 0+60 to Station 4+00, North Ramp Starter Tunnel, Exploratory Studies Facility. Submittal date: 12/03/1997.
- 106007 GS971108314224.021. Revision 1 of Detailed Line Survey Data, Station 4+00 to Station 8+00, North Ramp, Exploratory Studies Facility. Submittal date: 12/03/1997.
- 106009 GS971108314224.022. Revision 1 of Detailed Line Survey Data, Station 8+00 to Station 10+00, North Ramp, Exploratory Studies Facility. Submittal date: 12/03/1997.
- 106010 GS971108314224.023. Revision 1 of Detailed Line Survey Data, Station 10 + 00 to Station 18 + 00, North Ramp, Exploratory Studies Facility. Submittal date: 12/03/1997.
- 107128 GS971208314221.003. Revised Bedrock Geologic Map of the Central Block Area, Yucca Mountain, Nevada. Submittal date: 12/30/1997.
- 175707 GS980608314224.004. Detailed Line Survey Data for Exploratory Studies Facility, North Ramp Starter Tunnel: Pilot Bore, Bench Cuts, Test Alcove #1, Slash Cuts, Drainage Cuts, and Portal Cut. Submittal date: 06/11/1998.
- 106752 GS980708312242.010. Physical Properties of Borehole Core Samples, and Water Potential Measurements Using the Filter Paper Technique, for Borehole Samples from USW WT-24. Submittal date: 07/27/1998.

107150	GS980708312242.011. Physical Properties and Hydraulic Conductivity Measurements of Lexan-Sealed Samples from USW WT-24. Submittal date: 07/30/1998.
106748	GS980808312242.014. Physical Properties of Borehole Core Samples and Water Potential Measurements Using the Filter Paper Technique for Borehole Samples from USW SD-6. Submittal date: 08/11/1998.
107154	GS980908312242.038. Physical Properties and Saturated Hydraulic Conductivity Measurements of Lexan-Sealed Samples from USW SD-6. Submittal date: 09/22/1998.
107158	GS980908312242.041. Physical Properties and Saturated Hydraulic Conductivity Measurements of Core Plugs from Boreholes USW SD-7, USW SD-9, USW SD-12, USW UZ-14, and UE-25 UZ#16. Submittal date: 09/24/1998.
109070	GS981108314224.005. Locations of Lithostratigraphic Contacts in the ECRB Cross Drift. Submittal date: 11/30/1998.
162979	GS990108312242.006. Pulse Flow Meter Data for the Alcove 1 Infiltration Experiment from 03/08/98 to 12/04/98. Submittal date: 01/29/1999.
107185	GS990308312242.007. Laboratory and Centrifuge Measurements of Physical and Hydraulic Properties of Core Samples from Busted Butte Boreholes UZTT-BB-INJ-1, UZTT-BB-INJ-3, UZTT-BB-INJ-4, UZTT-BB-INJ-6, UZTT-BB-COL-5 and UZTT-BB-COL-8. Submittal date: 03/22/1999.
148711	GS990408312231.001. Saturated Hydraulic Conductivity of Core from SD-9, 2/27 - 3/27/95. Submittal date: 04/27/1999.
108396	GS990408314224.001. Detailed Line Survey Data for Stations 00+00.89 to 14+95.18, ECRB Cross Drift. Submittal date: 09/09/1999.
105625	GS990408314224.002. Detailed Line Survey Data for Stations 15+00.85 to 26+63.85, ECRB Cross Drift. Submittal date: 09/09/1999.
109822	GS990708312242.008. Physical and Hydraulic Properties of Core Samples from Busted Butte Boreholes. Submittal date: 07/01/1999.
164604	GS990708314224.007. Detailed Line Survey Data for Busted Butte Access Drift and Busted Butte Cross Drift. Submittal date: 11/02/1999.
146848	MO0003COV00095.000. Coverage: Scotbons. Submittal date: 03/01/2000.
153777	MO0012MWDGFM02.002. Geologic Framework Model (GFM2000). Submittal date: 12/18/2000.

- 163795 MO0101XRDDRILC.002. XRD Analyses of Drill Core from Boreholes UE-25 A#1 and USW G-2. Submittal date: 01/26/2001.
- 155989 MO0109HYMXPROP.001. Matrix Hydrologic Properties Data. Submittal date: 09/17/2001.
- 175870 MO0512SPASURFD.000. Input File on Surficial Deposits Depth for Infiltration Modeling. Submittal date: 12/05/2005.
- 176585 MO0603GSCGEOMP.000. Digital Geologic Map of Nevada Test Site and Vicinity, Nye, Lincoln, and Clark Counties, Nevada, and Inyo County, California. Submittal date: 03/09/2006.
- 176922 MO0605SPASOILS.005. Soil Hydraulic Parameters and Associated Statistics for Infiltration Modeling at Yucca Mountain, NV. Submittal date: 05/02/2006.

8.4 OUTPUT DATA, LISTED BY DATA TRACKING NUMBER

MO0603SPAGRIDD.003. Gridded Infiltration Model Input File Showing Infiltration Hydrogeologic Units. Submittal date: 03/06/2006.

MO0605SPABEDRK.005. Bedrock Saturated Hydraulic Conductivity for Infiltration Hydrogeologic Units. Submittal date: 05/25/2006.

MO0605SPAFABRP.004. Supporting Calculation Files for the Assessment of Bedrock Saturated Hydraulic Conductivity. Submittal date: 05/25/2006.

8.5 SOFTWARE CODES

157019 2000. *Software Code: ARCINFO*. V.7.2.1. SGI, IRIX 6.5. STN: 10033-7.2.1-00.

167994 Dynamic Graphics 2000. *Software Code: EARTHVISION*. V. 5.1. IRIX 6.5. STN: 10174-5.1-00.

APPENDIX A

CORRELATION OF GEOLOGIC MAP UNITS AND INFILTRATION HYDROGEOLOGIC UNITS

A1. CORRELATION OF GEOLOGIC MAP UNITS AND INFILTRATION HYDROGEOLOGIC UNITS

The IHU stratigraphic system is primarily based on rock and hydrogeologic properties measured on rock samples. Most of these samples are core from surface-based and tunnel-based boreholes, although some samples were collected from exposures in the tunnel walls. The lithostratigraphic framework for rocks in the Paintbrush Group, the Calico Hills Formation, and Crater Flat Group is described in several reports (BSC 2004 [DIRS 170029]; Buesch et al. 1996 [DIRS 100106]; Buesch and Spengler 1999 [DIRS 107905]). Many of the IHUs are defined on the basis of the lithostratigraphic contacts used in the GFM2000 (BSC 2004 [DIRS 170029]); IHUs in the crystallized part of the Tiva Canyon Tuff, which was “undifferentiated” in the GFM2000, are based on lithostratigraphic contacts identified in various logging reports (Geslin et al. 1995 [DIRS 103330]; Geslin and Moyer 1995 [DIRS 101226]; Moyer et al. 1995 [DIRS 103777]).

Although core and measured properties, used to establish the properties for the IHUs, especially saturated conductivity (K_{sat}), are from various boreholes or locations, the compiled data for each IHU can be considered the “type section.” In detail, there are variations in the data within some IHUs that probably relate to the spatial position of the sample within the section or borehole relative to other data, and these variations typically relate to the geologic processes that formed the rocks. These vertical and lateral variations in properties within and between lithostratigraphic units, and by implication IHUs, are consistent with the overall stratiform characteristics and lateral continuity of the rocks at Yucca Mountain. This lateral continuity of the lithostratigraphic units and associated IHUs is fundamental to the correlation of the properties determined in boreholes to the exposures of the lithostratigraphic units at the ground surface.

Distributions of lithostratigraphic units at the ground surface are based on three geologic maps:

- DTN: GS971208314221.003 [DIRS 107128], *cb6k.ps* (Day et al. 1998 [DIRS 101557])
- DTN: MO0003COV00095.000 [DIRS 146848], *scothbons.e00* (Scott and Bonk 1984 [DIRS 104181])
- DTN: MO0603GSCGEOMP.000 [DIRS 176585], *ofr-99-0554-e00.tar* (Slate et al. 2000 [DIRS 150228], Open-File Report 99-554-A).

The map units and respective descriptions were compiled at various times, different map scales, and for different general purposes. Correlation of map units has been made to previous reports and maps (Day et al. 1998 [DIRS 101557]); however, map units are correlated to each other and to a standard lithostratigraphic system and the infiltration hydrogeologic units (Table A-1). The map unit symbols are from their respective published maps (Day et al. 1998 [DIRS 101557]; Scott and Bonk 1984 [DIRS 104181]; Slate et al. 2000 [DIRS 150228], Open-File Report 99-554-A), and the lithostratigraphic unit names and symbols are from one of three types of sources as listed for each unit:

1. Most lithostratigraphic unit names and symbols are from published reports (Buesch et al. 1996 [DIRS 100106]; Buesch and Spengler 1999 [DIRS 107905]) and are included as model units in the GFM2000 (BSC 2004 [DIRS 170029]).

2. Some lithostratigraphic unit names and symbols are from previously published maps, especially units exposed to the north of Yucca Wash. For example, a previously described informal lithostratigraphic unit name and symbol is “Rhyolite of Pinnacles Ridge” (Tm_p), which is used for the undivided map unit (Dickerson and Drake 1998 [DIRS 102929]). The term “informal” means that it is not an officially designated formation or lithostratigraphic unit, according to the U.S. Geological Survey Geologic Names Committee. These types of designations are indicated by phrases such as “rhyolite of...” The rhyolite of Pinnacles Ridge includes two main lithostratigraphic units: (1) lava flows referred to as the “lava flow of the rhyolite of Pinnacles Ridge” with the symbol Tm_{pl} where the “l” is for lava, and (2) pyroclastic deposits referred to as the “pyroclastic rocks of the rhyolite of Pinnacles Ridge” with the symbol Tm_{pt} where the “t” is for tuff.
3. Three formations, the Rainier Mesa, Yucca Mountain, and Pah Canyon Tuffs, have had various lithostratigraphic unit names and symbols in previously published reports. For example, Tm_{rw} refers to the welded Rainier Mesa Tuff (Day et al. 1998 [DIRS 101557]; Scott and Bonk 1984 [DIRS 104181]), but it does not indicate how welded are the rocks or whether the rocks are vitric or crystallized. Similarly, Tm_{rn} refers to the nonwelded Rainier Mesa Tuff (Scott and Bonk 1984 [DIRS 104181]), but it does not indicate whether the rocks are vitric or crystallized or whether they are near the top or base of the deposit. Some reports do not use the symbol Tm_{rn} (Day et al. 1998 [DIRS 101557]). These characteristics can be inferred from the descriptions in their respective reports (Day et al. 1998 [DIRS 101557]; Scott and Bonk 1984 [DIRS 104181]); the goal is to standardize the names and symbol nomenclature.

Wherever the Prow Pass, Bullfrog, and Tram Tuffs are divided, the names and symbols of the lithostratigraphic units have been updated to conform to relatively simple and descriptive nomenclature described by Buesch and Spengler (1999 [DIRS 107905]). In Table A-1, the updated symbols are indicated with footnote “f.” In the lithostratigraphic nomenclature described by Buesch and Spengler (1999 [DIRS 107905]), there are five lithostratigraphic facies that could be called zones, which are:

- Upper vitric (uv) that is nonwelded to partially welded and vitric
- Upper crystallized (uc) that is partially to moderately welded and crystallized
- Moderately welded (m) that is moderately to densely welded and crystallized
- Lower crystallized (lc) that is partially to moderately welded and crystallized
- Lower vitric (lv) that is nonwelded to partially welded and vitric.

In the application of this nomenclature system (Buesch and Spengler 1999 [DIRS 107905]) to the Rainier Mesa Tuff, by using the symbol “Tm_{rm},” the symbol is consistent with the descriptive nomenclature and indicates that the rocks in the Rainier Mesa Tuff are moderately welded and crystallized. Some partially welded and crystallized rocks are also included in descriptions of Tm_{rw} (Day et al. 1998 [DIRS 101557]; Scott and Bonk 1984 [DIRS 104181]).

There is no information, however, on the maps or in the descriptions to identify how much of the Tm_{rw} might be more appropriately identified as Tm_{rlc}, so, for simplicity, the symbol Tm_{rm} is used (Day et al. 1998 [DIRS 101557]; Scott and Bonk 1984 [DIRS 104181]). Similarly, by

using the symbol “Tmrlv,” the symbol is consistent with the nomenclature (Buesch and Spengler 1999 [DIRS 107905]) and indicates that the rocks in the lower part of the Rainier Mesa Tuff can range from nonwelded to partially welded and vitric.

There are three basic relations in the correlation of map units to lithostratigraphic units to IHUs that include “direct,” “equivalent,” and “surrogate” correlations:

1. Direct correlation. Many map units correlate directly with the lithostratigraphic and “type” infiltration hydrogeologic units (Table A-1, symbols highlighted in bold text). One example of a direct correlation is the crystal-poor, middle nonlithophysal zone of the Topopah Spring Tuff lithostratigraphic unit (Tptpmn) and the IHU (htmn).
2. Equivalent correlation. Some geologic map units and lithostratigraphic units do not have saturated hydraulic conductivity data, but there are other data not used in this analysis, such as density or porosity data measured on core or from geophysical logs, so a general equivalency in properties can be established and an equivalent IHU has been assigned to the geologic map unit. Also, some geologic map units are a combination of two or more lithostratigraphic units and IHUs, and on the basis of overall similarity with the specific lithostratigraphic units, an equivalent IHU has been assigned to the geologic map unit. Examples of equivalent correlations include:
 - a. The lower, vitric, nonwelded Rainier Mesa Tuff (Tmrlv) is equivalent to the IHU (hcv1).
 - b. The crystal-rich transition subzone of the Topopah Spring Tuff consists of two lithostratigraphic units (Tp trn1 and Tprl1) are equivalent to the IHU (htrl).
 - c. The crystal-poor vitric, nonwelded welded subzone of the Topopah Spring Tuff (Tptpv1) and the pre-Topopah Spring bedded tuff lithostratigraphic units (Tpbt1) are equivalent to the IHU (htv1v or htv1z depending on whether the rocks are vitric (v) or zeolitic (z)).
3. Surrogate correlation. Some geologic map units have no rock or hydrogeologic property data, so a surrogate IHU has been assigned. This is the case, for example, with the lava flows and pyroclastic rocks exposed north of Yucca Wash. Assignment of a surrogate is based on the similarity in lithostratigraphic features, including:
 - a. Rock type such as lava flows or pyroclastic deposits; pyroclastic flow or fallout tephra deposits
 - b. Type of material composing the rock; vitric, crystallized, or zeolitic
 - c. Occurrence of lithophysae, spots, or rims on fractures
 - d. General fracture characteristics.

These lithostratigraphic features are gleaned from descriptions in the three source maps and augmented from descriptions in the 1:6,000 scale geologic map (Dickerson and Drake 1998 [DIRS 102929]). No fieldwork or confirmation was done in support of determining the rock and hydrogeologic properties of these geologic map units. Many of the descriptions of map units are appropriate for a geologic map, but are too generic for establishing surrogate rock and hydrogeologic properties. At this junction in distributing lithostratigraphic and hydrogeologic properties to many of the geologic map units, the assignment of surrogate properties is not precise and to reflect this uncertainty, alternative surrogate IHUs are proposed for several geologic map units. Examples of surrogate correlations include:

- a. The lava flow of the rhyolite of Pinnacles Ridge (Tmpl) is mostly crystallized, crystal-rich rhyolite lava with flow banding and thick basal vitrophyre; therefore, the surrogate IHU is “htll,” which is correlative with the crystal-poor, crystallized, lower lithophysal zone of the Topopah Spring Tuff (Tptpl). Because of the thick basal vitrophyre, the map unit Tmpl was initially assigned the surrogate IHU “htrv1”; therefore, “htrv1” can be considered as an alternative IHU.
- b. The pyroclastic rocks of the rhyolite of Pinnacles Ridge (Tmpt) is locally crystallized (locally with spherulites) and altered at moderate-temperature and probably at low temperature; therefore, the surrogate IHU is “hacz,” which is correlative with the zeolitic pyroclastic rocks of the Calico Hills Formation. If the rocks are mostly vitric, however, then an alternative surrogate IHU is “hbt3,” which is correlative with the vitric, pyroclastic flow and fallout tephra deposits of the pre-Yucca Mountain bedded tuff (Tpbt3).

Table A-1 lists a detailed correlation of geologic map units to lithostratigraphic, infiltration hydrogeologic, and UZ flow model units. Table A-1 was condensed from output DTN: MO0605SPAFABRP.004, *Infiltrate Ap-A Bedrock Correlation 14Feb06.xls*, which includes the characteristics of the units and associated map numbers.

Table A-1. Detailed Correlation of Geologic Map Units to Lithostratigraphic, Infiltration Hydrogeologic, and Unsaturated Zone Flow Model Units

Map Units ^a	Map Units ^b	Map Units ^c	Map Units ^d	Lithostratigraphic Unit Name	Lithostratigraphic Unit Symbol	Source of Symbol	Equivalent IHU	IHU Number	Comments on IHU and Equivalent Unit	UZ Flow Model Layer ^e
QTac	QTc, Qay, Qai, QTa, Qeo, Qey	QTac, QTc	Qa, Qac, Qts	Alluvium/Colluvium	QTac	Day et al. 1998 [DIRS 101557]	—	—	This unit is included in the bedrock infiltration hydrogeologic units for display purposes on maps; values were not determined.	NA
—	Tgy, Tgc	—	—	Basin-fill sediments, undivided and Caldera moat-filling sediments	Tgy, Tgc	Slate et al. 2000 [DIRS 150228], Open File Report 99-544-A	—	—	This unit is included in the bedrock infiltration hydrogeologic units for display purposes on maps; values were not determined.	NA
Tbd	Tft	Td	NIMA	Basalt Dikes	Td	Day et al. 1998 [DIRS 101557]	htmn	421	The basalt dike has low porosity, is not wide, and has numerous cooling joints; therefore, the surrogate IHU is htmn.	NA
—	Tmr	—	NIMA	Rainier Mesa Tuff (undivided total formation)	Tmr	Slate et al. 2000 [DIRS 150228], Open File Report 99-544-A	htrv1	417	The total formation contains both nonwelded to partially welded vitric and partially to moderately welded crystallized ignimbrite; therefore, the average properties are probably similar to the IHU of htrv1. On the basis of general lithostratigraphic features, the map unit was initially assigned the surrogate IHU of hpuc (435); the calculated K_{sat} for this hpuc, however, is much larger than anticipated and is probably not as representative.	NA
Tmrw	Tmr	Tmrw	NIMA	Rainier Mesa - Moderately welded, crystallized	Tmrm ^f	Buesch and Spengler 1999 [DIRS 107905] ^f	htrn	418	This unit is partially to moderately welded, crystallized, crystal-rich ignimbrite; therefore, the surrogate IHU is htrn. Tmrm could also be represented by a surrogate IHU of hpmlc or hpuc, depending on the amount of welding and vapor-phase corrosion and mineralization.	NA
Tmrn	Tmr	Tmr	NIMA	Rainier Mesa - Lower nonwelded, vitric	Tmrlv ^f	Buesch and Spengler 1999 [DIRS 107905] ^f	hcv1	410	This unit is nonwelded to partially welded, vitric ignimbrite; therefore, its equivalent IHU is hcv1.	NA
—	Tmrf	NIMA	Tmp	Rhyolite of Pinnacles Ridge - undivided	Tmp	Dickerson and Drake 1998 [DIRS 102929]	htll	422	The map (precipitation) view is about 90% crystallized crystal-rich rhyolite lava with flow banding and thick basal vitrophyre, and about 5% is nonwelded to densely-fused vitric and altered at moderate-temperature, crystal-poor ignimbrite and fallout tephra; therefore, this mixture of properties are approximated with the surrogate IHU of htll.	NA
Tfpf	Tmrf	NIMA	Tmpl	Lava flow of the rhyolite of Pinnacles Ridge	Tmpl	Dickerson and Drake 1998 [DIRS 102929]	htll	422	The map (precipitation) view is about 90% crystallized, crystal-rich rhyolite lava with flow-banding and thick-basal vitrophyre; therefore, the surrogate IHU is htll. On the basis of general lithostratigraphic features, especially the thick-basal vitrophyre, the map unit was initially assigned the surrogate IHU of htrv1 (417).	NA
Tfpp	Tmrf	NIMA	Tmpt	Pyroclastic rocks of the rhyolite of Pinnacles Ridge	Tmpt	Dickerson and Drake 1998 [DIRS 102929]	hacz	430	This unit is nonwelded to densely-fused crystal-poor ignimbrite and fallout tephra that is crystallized locally with spherulites and altered at moderate temperature and probably low temperature; therefore, the surrogate IHU is hacz. If the rocks are mostly vitric, however, then the surrogate IHU is hbt3.	NA
—	Tpw	NIMA	Tmb	Rhyolite of Windy Wash - undivided	Tpw	Slate et al. 2000 [DIRS 150228], Open-File Report 99-554-A	htll	422	Using the analogy with Tmb for more detailed descriptions and map distribution of lava flows and pyroclastic rocks, the map (precipitation) view is about 70% crystallized, crystal-rich rhyolite lava with flow banding, and about 20% is nonwelded to partially welded zeolitic, or possibly vitric and locally altered at moderate-temperature to crystallized, crystal-poor ignimbrite. Because the K_{sat} values for htll span the values for the hcmn and hacz, the surrogate IHU is htll. On the basis of general lithostratigraphic features, these map units were initially assigned the surrogate IHU of hcll (407); the calculated K_{sat} for this hcll, however, is very small and probably not as representative as anticipated.	NA
Twf	Tpw	NIMA	Tmbl	Lava of the rhyolite of Windy Wash	Tpwl	Slate et al. 2000 [DIRS 150228], Open-File Report 99-554-A; modified from Dickerson and Drake 1998 [DIRS 102929]	hcmn	406	The map (precipitation) view is mostly crystallized, crystal-rich rhyolite lava with <u>flow banding</u> , and because the hcmn is mostly crystallized with fractures that include rims, the surrogate IHU is hcmn. On the basis of general lithostratigraphic features, these map units were initially assigned the surrogate IHU of hcll (407); the calculated K_{sat} for this hcll, however, is very small and probably not as representative as anticipated.	NA

INTENTIONALLY LEFT BLANK

Table A-1. Detailed Correlation of Geologic Map Units to Lithostratigraphic, Infiltration Hydrogeologic, and Unsaturated Zone Flow Model Units (Continued)

Map Units ^a	Map Units ^b	Map Units ^c	Map Units ^d	Lithostratigraphic Unit Name	Lithostratigraphic Unit Symbol	Source of Symbol	Equivalent IHU	IHU Number	Comments on IHU and Equivalent Unit	UZ Flow Model Layer ^e
Twp	Tpw	NIMA	Tmbt	Pyroclastic rocks of the rhyolite of Windy Wash	Tpwt	Symbol from Slate et al. 2000 [DIRS 150228], Open-File Report 99-554-A; modified from Dickerson and Drake 1998 [DIRS 102929]	hacz	430	This unit is nonwelded, altered ignimbrite and fallout tephra identified as “zeolitized” (Scott and Bonk 1984 [DIRS 104181]) and similar tuffaceous rocks in the rhyolite of Waterpipe Butte are described as “devitrified” (Dickerson and Drake 1998 [DIRS 102929]); therefore, the surrogate IHU is hacz. If the rocks are mostly vitric, however, then the surrogate IHU is hbt3.	NA
—	Tpr		Tpk	Rhyolite of Comb Peak - undivided	Tpk	Day et al. 1998 [DIRS 101557]	htll	422	The map (precipitation) view is about 65% crystallized, crystal-poor rhyolite lava with flow banding and basal vitrophyre, and about 35% is nonwelded, zeolitic (locally vitric or crystallized), crystal-poor ignimbrite and fallout tephra; therefore, this mixture of properties are approximated with the surrogate IHU of htll.	NA
Tfcf	Tpr	Tpkl	Tpkl, Tпки	Lava flow of the rhyolite of Comb Peak	Tpkl	Day et al. 1998 [DIRS 101557]	hcmn	406	The map (precipitation) view is mostly crystallized, crystal-poor rhyolite lava with <u>flow banding</u> , and because the hcmn is mostly crystallized with fractures that include rims, the surrogate IHU is hcmn. On the basis of general lithostratigraphic features, these map units were initially assigned the surrogate IHU of hcll (407); the calculated K_{sat} for this hcll, however, is very small and probably not as representative as anticipated.	NA
Tfcp	Tpr	Tpkt	Tpkt, Tpkr, Tpkw, Tpkh	Pyroclastic rocks of the rhyolite of Comb Peak (locally, the main ignimbrite is referred to as “tuff X”)	Tpkt	Day et al. 1998 [DIRS 101557]	Hacz	430	This unit is nonwelded to densely fused, crystal-poor ignimbrite and fallout tephra identified as “zeolitized” (Scott and Bonk 1984 [DIRS 104181]) and described as “devitrified” (Day et al. 1998 [DIRS 100027]; Dickerson and Drake 1998 [DIRS 102929]), which locally includes crystallized to moderate temperature altered; therefore, the surrogate IHU is hacz. If the rocks are mostly vitric, however, then the surrogate IHU is hbt3.	NA
—	Tpr	NIMA	Tpv	Rhyolite of Vent Pass - undivided	Tpv	Dickerson and Drake 1998 [DIRS 102929]	htll	422	The map (precipitation) view is about 80% crystallized, crystal-poor rhyolite lava with flow banding and thick basal vitrophyre, and about 20% is nonwelded, vitric and altered at moderate-temperature to crystallized crystal-poor ignimbrite and fallout tephra; therefore, this mixture of properties are approximated with the surrogate IHU of htll.	NA
Tfvf	Tpr	NIMA	Tpvl	Lava of the rhyolite of Vent Pass	Tpvl	Dickerson and Drake 1998 [DIRS 102929]	htll	422	The map (precipitation) view is mostly crystallized of crystal-poor rhyolite lava with spherulites and flow banding; therefore, the surrogate IHU is htll.	NA
Tfvp	Tpr	NIMA	Tpvt	Pyroclastic rocks of the rhyolite of Vent Pass	Tpvt	Dickerson and Drake 1998 [DIRS 102929]	hacz	430	This unit is nonwelded, crystallized locally with spherulites, and probably altered at moderate-temperature ignimbrite and fallout tephra; therefore, the surrogate IHU is hacz. If the rocks are mostly vitric, however, then the surrogate IHU is hbt3.	NA
bt	NM	Tpbt5	Tbt5	Post-Tiva bedded tuff	Tpbt5	Geslin et al. 1995 [DIRS 103330]	hbt3	413	The Tpbt5 has a variety of beds with various textures, and this variability is more similar to Tpbt3 than to Tpbt4; therefore, the equivalent IHU is hbt3.	NA
—	—	Tpu	—	Paintbrush Group, tectonic breccia	Tpu	Day et al. 1998 [DIRS 101557]	htrv	417	Compared to other IHUs, the IHU of htrv1 has moderate saturated hydraulic conductivity with a moderately large standard deviation, so it is probably appropriate as an “average” surrogate for the formation. The IHU of hcul can probably be used as an alternative surrogate.	NA
—	—	Tcu	—	Tiva Canyon Tuff, tectonic breccia	Tcu	Day et al. 1998 [DIRS 101557]	htrv	417	Compared to other IHUs, the IHU of htrv1 has moderate saturated hydraulic conductivity with a moderately large standard deviation, so it is probably appropriate as an “average” surrogate for the formation. The IHU of hcul can probably be used as an alternative surrogate.	NA
—	Tpcc	—	—	Caldera-collapse breccia of Claim Canyon caldera	Tpcc	Slate et al. 2000 [DIRS 150228], Open File Report 99-544-A	htll	422	This unit is soft to moderately resistant, breccia and megabreccia with a matrix of Tiva Canyon Tuff, so it is probably appropriate as an “average” surrogate.	NA
cu	Tpc	—	Tpc	Tiva Canyon Tuff (undivided, total formation)	Tpc	Buesch et al. 1996 [DIRS 100106]	htll	422	Compared to other IHUs, the IHU of htrv1 has moderate saturated hydraulic conductivity with a moderately large standard deviation, so it is probably appropriate as an “average” surrogate for the formation. As an alternative, the IHU of hcul might be used as a surrogate.	NA

INTENTIONALLY LEFT BLANK

Table A-1. Detailed Correlation of Geologic Map Units to Lithostratigraphic, Infiltration Hydrogeologic, and Unsaturated Zone Flow Model Units (Continued)

Map Units ^a	Map Units ^b	Map Units ^c	Map Units ^d	Lithostratigraphic Unit Name	Lithostratigraphic Unit Symbol	Source of Symbol	Equivalent IHU	IHU Number	Comments on IHU and Equivalent Unit	UZ Flow Model Layer ^e
ccr1, ccr2	Tpc	Tcrv	Tpc	Tiva Canyon Tuff - crystal-rich vitric zone	Tpcrv	Buesch et al. 1996 [DIRS 100106]	htrv1	417	There are no Q-status data for these rocks and, although this unit contains mostly vitric and nonwelded to moderately welded rocks, the hydrogeologic characteristics of this unit are probably dominated by densely welded rocks; therefore, the surrogate IHU is htrv1.	tcw11
ccr3	Tpc	Tcrn4	Tpc	Tiva Canyon Tuff - crystal-rich nonlithophysal zone, subvitrophyre transition subzone	Tpcrn4	Buesch et al. 1996 [DIRS 100106]	hcr4 ⁹	401 ⁹	Typically, the subvitric transition subzone of Tpcrn4 and map unit Tcrn4 is densely welded and crystallized, but locally this subzone is partially vitric, usually as pumice clasts, or corroded. Data from the core in Tpcrn4 form the type section ^h for the IHU of hcr4.	tcw11
ccr4	Tpc	Tcrn3	Tpc	Tiva Canyon Tuff - crystal-rich nonlithophysal zone, pumice-poor subzone	Tpcrn3	Buesch et al. 1996 [DIRS 100106]	hcr3 ⁹	402 ⁹	The pumice-poor subzone of Tpcrn3 and map unit Tcrn3 is densely welded and crystallized, but the porosity has been increased by vapor-phase corrosion. Data from the core in Tpcrn3 form the type section ^h for the IHU of hcr3.	tcw11
ccr5	Tpc	Tcr2	Tpc	Tiva Canyon Tuff - crystal-rich nonlithophysal zone, mixed pumice subzone	Tpcrn2	Buesch et al. 1996 [DIRS 100106]	hcr2 ⁹	403 ⁹	The mixed pumice subzone of Tpcrn2 and map unit Tcrn2 is densely welded and crystallized, but locally the porosity has been increased by vapor-phase corrosion. Data from the core in Tpcrn2 form the type section ^h for the IHU of hcr2.	tcw11
cuc	Tpc	Tcr2	Tpc	Tiva Canyon Tuff - crystal-rich nonlithophysal zone, mixed pumice subzone	Tpcrn2	Buesch et al. 1996 [DIRS 100106]	hcr2	403	The upper cliff zone (Scott and Bonk 1984 [DIRS 104181]) is equivalent to the lower part of the mixed pumice subzone (Buesch et al. 1996 [DIRS 100106]; Day et al. 1998 [DIRS 101557]); therefore, the equivalent IHU is hcr2.	tcw11
—	Tpc	Tcr1	Tpc	Tiva Canyon Tuff - crystal-rich lithophysal zone	Tpcrl	Buesch et al. 1996 [DIRS 100106]	hcr1 ⁹	404 ⁹	Typically, the crystal-rich lithophysal zone of Tpcrl and the nonlithophysal crystal-transition subzone of Tpcrn1 have a decrease in porosity of the matrix-groundmass compared to the Tpcrn. Data from the core in Tpcrn1 and Tpcrl form the type section ^h for the IHU of hcr1.	tcw11
cul	Tpc	Tcpul	Tpc	Tiva Canyon Tuff - crystal-poor upper lithophysal zone	Tpcpul	Buesch et al. 1996 [DIRS 100106]	hcul ⁹	405 ⁹	In lithophysal rocks, the porosity of the matrix-groundmass is small with a mean of 10.4% and the porosity of the rims and spots is large with a mean of 30.2%, so lithophysal rocks have a larger average porosity than nonlithophysal rocks (Otto and Buesch 2003 [DIRS 170727]). Data from the core in Tpcpul form the type section ^h for the IHU of hcul.	tcw12
cks, clc, cgks, crks, cuks, cml, clks, crs	Tpc	Tcpun, Tcpmn, Tcpum	Tpc	Tiva Canyon Tuff - crystal-poor middle nonlithophysal zone	Tpcpmn	Buesch et al. 1996 [DIRS 100106]	hcmn ⁹	406 ⁹	In nonlithophysal rocks such as the Tpcpmn, there can be spots or small amounts of lithophysae, and many of the fractures have rims, so porosity values tend to be smaller than lithophysal rocks, although locally there can be large porosity values because of the rims and spots. Data from the core in Tpcpmn form the type section ^h for the IHU of hcmn.	tcw12
cll	Tpc	Tcp1l	Tpc	Tiva Canyon Tuff - crystal-poor lower lithophysal zone	Tpcpl1	Buesch et al. 1996 [DIRS 100106]	Hcl1 ⁹	407 ⁹	Data from the core in Tpcpl1 form the type section ^h for the IHU of hcl1.	tcw12
chl, ch, (cc)	Tpc	Tcp1n, Tcp1nc	Tpc	Tiva Canyon Tuff - crystal-poor lower nonlithophysal zone	Tpcpln	Buesch et al. 1996 [DIRS 100106]	hcln ⁹	408 ⁹	The “vitric, densely welded” subzone of Tpcpv3 was included at the base of the superjacent “columnar” subzone of Tpcplnc for the purposes of hydrogeologic and thermal/mechanical properties (Buesch et al. 1996 [DIRS 100106]). There are no Q-status properties on samples from Tpcpv3, and it is only locally exposed along the southern part of Solitario Canyon. For this compilation of infiltration properties, the Tpcpv3 is also included in the IHU of hcln. Data from the core in Tpcpln form the type section ^h for the IHU of hcln.	tcw12
cc includes cc1, cc2, cc3	Tpc	Tcpv	Tpc	Tiva Canyon Tuff - crystal-poor vitric moderately welded subzone	Tpcpv2	Buesch et al. 1996 [DIRS 100106]	hcv2 ⁹	409 ⁹	Ideally, Tpcpv2 and Tpcpv1 would be depicted separately, but they were not mapped that way. The IHU of hcv1 of Tpcpv1 is probably more appropriate, because, typically, there is slightly more of it. This assignment, however, results in a larger change in properties with the superjacent units than when the IHU of hcv2 is used. Data from the core in Tpcpv2 form the type section ^h for the IHU of hcv2.	tcw13

INTENTIONALLY LEFT BLANK

Table A-1. Detailed Correlation of Geologic Map Units to Lithostratigraphic, Infiltration Hydrogeologic, and Unsaturated Zone Flow Model Units (Continued)

Map Units ^a	Map Units ^b	Map Units ^c	Map Units ^d	Lithostratigraphic Unit Name	Lithostratigraphic Unit Symbol	Source of Symbol	Equivalent IHU	IHU Number	Comments on IHU and Equivalent Unit	UZ Flow Model Layer ^e
—	Tpc	Tcpv	Tpc	Tiva Canyon Tuff - crystal-poor vitric nonwelded subzone	Tpcpv1	Buesch et al. 1996 [DIRS 100106]	hcv1 ^g	410 ^g	Source maps do not separately depict Tpcpv2 and Tpcpv1, so for the purpose of infiltration model units they are grouped into the IHU of hcv1. Data from the core in Tpcpv1 form the type section ^h for the IHU of hcv1.	ptn21
bt	NM	Tbt		pre-Tiva Canyon bedded tuff	Tpbt4	Buesch et al. 1996 [DIRS 100106]	hbt4 ^g	411 ^g	Because of the grouping of Tpbt4 with Tpcpv or Tpy, and the local inclusion of Tpbt4, Tpbt3, and Tpbt2 in “Tbt2” (Day et al. 1998 [DIRS 101557]), the Tpbt4 is not explicitly mapped at the ground surface. Data from the core in Tpbt4 form the type section ^h for the IHU of hbt4.	ptn22
ym	Tpy	Tpy	NIMA	Yucca Mountain Tuff (undivided, total formation)	Tpy	Buesch et al. 1996 [DIRS 100106]	hym	412	For most of the Tpy exposed at the ground surface and in boreholes in the southern part of Yucca Mountain, where the ignimbrite is nonwelded and vitric, the Q-status core data are appropriate for the IHU of hym. An IHU of hymm is appropriate for some of the rocks exposed at the surface and in boreholes in the north-central part of Yucca Mountain; this IHU, however, has not been developed. Where Tpy is not divided, the likely IHU equivalent is hym.	NA
ymu	Tpy	Tpy	NIMA	Yucca Mountain Tuff, upper vitric	Tpyuv ^f	Buesch and Spengler 1999 [DIRS 107905] ^f	hym ^g	412 ^g	This unit is nonwelded to partially welded ignimbrite that is typically vitric and locally crystallized, with some vapor-phase minerals or moderate-temperature alteration to smectite; therefore, the equivalent IHU is hym.	ptn22
ymm	Tpy	Tpy	NIMA	Yucca Mountain Tuff, moderately welded and crystallized	Tpym ^f	Buesch and Spengler 1999 [DIRS 107905] ^f	htll	422	This unit is moderately to densely welded, crystallized, ignimbrite, locally with sparse lithophysae of 3% to 5%; this middle part was described as being similar to the welded parts of the Tiva Canyon Tuff (Day et al. 1998 [DIRS 100027]). On the basis of general lithostratigraphic features, the map unit was initially assigned the IHU of hcll (407); the calculated K_{sat} for this htll, however, is very small and probably not as representative as anticipated; the best equivalent IHU is htll.	ptn23
yml	Tpy	Tpy	NIMA	Yucca Mountain Tuff, lower vitric	Tpylv ^f	Buesch and Spengler 1999 [DIRS 107905] ^f	hym	412	This unit is nonwelded to partially welded ignimbrite that is typically vitric and locally crystallized, with some vapor-phase minerals or moderate-temperature alteration to smectite; therefore, the equivalent IHU is hym.	ptn24
bt	NM	Tbt	NM	pre-Yucca Mountain bedded tuff	Tpbt3	Buesch et al. 1996 [DIRS 100106]	hbt3 ^g	413 ^g	Because of the grouping of Tpbt3 with Tpp and the local inclusion of Tpbt4, Tpbt3, and Tpbt2 in “Tbt2” (Day et al. 1998 [DIRS 101557]), the Tpbt3 is not explicitly mapped at the ground surface. Data from the core in Tpbt3 form the type section ^h for the IHU of hbt3.	ptn24
rz	Tpm	NIMA	NIMA	Rhyolite of Zig Zag Hill - undivided	Tpz	Day et al. 1998 [DIRS 101557]	htrv1	417	The lava flow is vitric, crystal-rich, flow-banded, and is less than 10 m thick (Day et al. 1998 [DIRS 100027]), and has very small amounts of porosity and variously spaced cooling joints; therefore, the surrogate IHU is htrv1.	NA
—	Tpm	NIMA	Tpg	Rhyolite of Black Glass Canyon - undivided	Tpg	Dickerson and Drake 1998 [DIRS 102929]	htll	422	The map (precipitation) view is about 80% crystallized, crystal-poor rhyolite lava with flow banding and basal autoclastic breccia, and nonwelded to partially welded vitric, and about 20% is altered at moderate-temperature to crystallized crystal-poor ignimbrite; therefore, these mixed properties are approximated with the surrogate IHU of htll.	NA
Tfbf	Tpm	NIMA	Tpgl	Lava of the rhyolite of Black Glass Canyon	Tpgl	Dickerson and Drake 1998 [DIRS 102929]	hcln	408	The map (precipitation) view is mostly crystallized, crystal-poor rhyolite lava with <u>flow banding</u> ; therefore, the surrogate IHU is hcln. On the basis of general lithostratigraphic features, these map units were initially assigned the surrogate IHU of hcll (407); the calculated K_{sat} for this hcll, however, is very small and is probably not as representative as anticipated.	NA
Tfbp	Tpm	NIMA	Tpgt	Pyroclastic rocks of the rhyolite of Black Glass Canyon	Tpgt	Dickerson and Drake 1998 [DIRS 102929]	hacz	430	This unit is nonwelded, crystallized locally with spherulites, altered at moderate-temperature, and altered ignimbrite and fallout tephra, locally silicified; therefore, the surrogate IHU is hacz. If the rocks are mostly vitric, however, then the surrogate IHU is hbt3.	NA
pc	Tpp	Tpp	Tpp	Pah Canyon Tuff (undivided, total formation)	Tpp	Buesch et al. 1996 [DIRS 100106]	hpc	414	Most of the Tpp exposed at Yucca Mountain, and in boreholes, are nonwelded to partially welded, except locally near the northern part; therefore, the equivalent IHU is hpc.	ptn25

INTENTIONALLY LEFT BLANK

Table A-1. Detailed Correlation of Geologic Map Units to Lithostratigraphic, Infiltration Hydrogeologic, and Unsaturated Zone Flow Model Units (Continued)

Map Units ^a	Map Units ^b	Map Units ^c	Map Units ^d	Lithostratigraphic Unit Name	Lithostratigraphic Unit Symbol	Source of Symbol	Equivalent IHU	IHU Number	Comments on IHU and Equivalent Unit	UZ Flow Model Layer ^e
pcu	Tpp	—	Tpp	Pah Canyon Tuff, upper vitric	Tppuv ^f	Buesch and Spengler 1999 [DIRS 107905] ^f	hpc ^g	414 ^g	Core samples from boreholes are nonwelded to partially welded and vitric; therefore, the IHU of hpc is very representative of the Tppuv. Data from the core in Tpp form the type section ^h for the IHU of hpc.	NA
pcm	Tpp	Tppw	Tpp	Pah Canyon Tuff, moderately welded and crystallized	Tppm ^f	Buesch and Spengler 1999 [DIRS 107905] ^f	hcv2	409	In the core from borehole G-2, the partially to moderately welded tuff is crystallized to argillically and is zeolitically altered (DTN: MO0101XRDDRILC.002 [DIRS 163795]). North of Yucca Wash, however, the rocks are moderately welded and crystallized (Broxton et al. 1993 [DIRS 107386]). Therefore, the surrogate IHUs are those of hcv2 and hcln for exposures along and north of Yucca Wash, respectively. If only one surrogate IHU is used for the Tppm, use hcv2. On the basis of general lithostratigraphic features, these map units were initially assigned the surrogate IHU of hcll (407); the calculated K_{sat} for this hcll, however, is very small and probably not as representative as anticipated.	NA
pcl	Tpp		Tpp	Pah Canyon Tuff, lower vitric	Tpplv ^f	Buesch and Spengler 1999 [DIRS 107905] ^f	hpc	414	Core samples from boreholes are nonwelded to partially welded and vitric; therefore, the equivalent IHU of hpc is very representative of the Tpplv.	NA
bt	NM	Tbt2	Tbt2	pre-Pah Canyon bedded tuff	Tpbt2	Buesch et al. 1996 [DIRS 100106]	hbt2 ^g	415 ^g	The Tpbt2 is nonwelded and vitric, although it is locally altered to clay minerals and reported as “smectite” (Day et al. 1998 [DIRS 101557]). Because of the grouping in many locations of the bedded tuffs Tpbt4, Tpbt3, and Tpbt2 (Day et al. 1998 [DIRS 101557]), the IHU of hbt2 probably applies to all “bt” units, including mapped units 32, 38, and 43 (Scott and Bonk 1984 [DIRS 104181]). Data from the core in Tpbt2 form the type section ^h for the IHU of hbt2.	ptn26
—	—	Ttu	—	Topopah Spring Tuff, tectonic breccia	Ttu	Day et al. 1998 [DIRS 101557]	htrv1	417	Because the “Thu” is highly brecciated, the IHU with a relatively large porosity of the matrix-groundmass and with a wide range of permeabilities is most appropriate; therefore, the surrogate IHU is htrv1. This map unit was initially represented by the surrogate IHU of htrn (418); htrn, however, has a smaller K_{sat} and standard deviation than htrv1 than what might be expected for a highly brecciated rock.	NA
tu	Tpt		Tpt	Topopah Spring Tuff (not divided, total formation)	Tpt	Buesch et al. 1996 [DIRS 100106]	htll	422	The Tptpll is, typically, the thickest unit and has properties that are intermediate to all other Tpt units; therefore, if only one representative unit is used, then the surrogate IHU is htll.	NA
	Tpt	Ttr	Tpt	Topopah Spring Tuff, crystal-rich member (undivided)	Tptr	Buesch et al. 1996 [DIRS 100106]	htrn	418	The exposure of the “Ttr” map unit is small, and north of Yucca Wash, and consists of the uppermost part of the crystal-rich member of Tptr; therefore, the surrogate IHU is htrn.	NA
NM	Tpt	—	Tpt	Topopah Spring Tuff, crystal-rich vitric nonwelded to moderately welded subzones	Tptrv3-2	Buesch et al. 1996 [DIRS 100106]	htrv3 ^g	416 ^g	The crystal-rich, vitric, nonwelded to moderately welded rocks are not mapped as a separate unit and are, typically, included in the overlying pre-Pah Canyon bedded tuff of Tpbt2. Data from the core in Tptrv3 and Tptrv2 form the type section ^h for the IHU of htrv3.	ptn26
tc	Tpt	Ttrv	Tpt	Topopah Spring Tuff, crystal-rich vitric densely welded subzone	Tptrv1	Buesch et al. 1996 [DIRS 100106]	htrv1 ^g	417 ^g	The crystal-rich, densely welded, vitric subzone of Tptrv1 and, locally, the crystallized, nonlithophysal, dense subzone of Tptrn3 are combined into the IHU of htrv1. Data from the core in Tptrv1 form the type section ^h for the IHU of htrv1.	tsw31
—	Tpt	Ttrn3	Tpt	Topopah Spring Tuff, crystal-rich nonlithophysal, dense subzone	Tptrn3	Buesch et al. 1996 [DIRS 100106]	Htrn	418	The crystallized, nonlithophysal, dense subzone of Tptrn3 is locally mapped as a separate unit in Solitario Canyon (Day et al. 1998 [DIRS 101557]); it was not identified, however, as a separate IHU. For the purposes of infiltration hydrogeologic units, the Tptrn3 is included with Tptrn2 to form the IHU of htrn. Initially, the Tptrn3 was represented by the equivalent htrv1 (417), because it is locally included in the Tptrv1 map unit; while data from the Tptrn3 was not included in the IHU of htrv1, it was, nonetheless, included in the IHU of htrn2.	tsw31
tr	Tpt	Ttrn2	Tpt	Topopah Spring Tuff, crystal-rich nonlithophysal, vapor-phase corroded subzone	Tptrn2	Buesch et al. 1996 [DIRS 100106]	htrn ^g	418 ^g	The crystal-rich, densely welded, crystallized, nonlithophysal, vapor-phase corroded subzone of Tptrn2 locally has abundant corroded pumice clasts. Data from the core in Tptrn form the type section ^h for the IHU of htrn.	tsw32

INTENTIONALLY LEFT BLANK

Table A-1. Detailed Correlation of Geologic Map Units to Lithostratigraphic, Infiltration Hydrogeologic, and Unsaturated Zone Flow Model Units (Continued)

Map Units ^a	Map Units ^b	Map Units ^c	Map Units ^d	Lithostratigraphic Unit Name	Lithostratigraphic Unit Symbol	Source of Symbol	Equivalent IHU	IHU Number	Comments on IHU and Equivalent Unit	UZ Flow Model Layer ^e
—	Tpt	Ttr1	Tpt	Topopah Spring Tuff, crystal-rich transition subzone	Tptrn1, Tptrl1	Buesch et al. 1996 [DIRS 100106]	htrl	419	The crystal-transition subzone can be in either the crystal-rich lithophysal or nonlithophysal zone of Tptrl1 or Tptrn1; the lower parts of the two zones were previously grouped (Day et al. 1998 [DIRS 100027]). Additionally, from relations of the core, the porosity in the Tptrl1 and Tptrn1 is, typically, more similar to that of the lithophysal zone of Tptprl and Tptpul than the crystal-rich nonlithophysal zone of Tptrn. Therefore, the equivalent IHU is htrl.	tsw33
ttl	Tpt	—	Tpt	Topopah Spring Tuff - crystal-rich lithophysal	Tptrl	Buesch et al. 1996 [DIRS 100106]	htrl ^g	419 ^g	The Tptrl consists of crystal-rich, densely welded, crystallized, lithophysal ignimbrite. Data from the core in Tptrl form the type section ^h for the IHU of htrl.	tsw33
NM	Tpt	NIMA	Tpt	Topopah Spring Tuff, lithic-rich zone	Tptf	Buesch et al. 1996 [DIRS 100106]	htll	422	The lithic-rich zone of Tptf is not represented on any of the source maps, but it is mostly nonlithophysal ignimbrite with local accumulations of lithophysae; therefore, the equivalent IHU is htll.	NA
trl, tul, tll, tl	Tpt	Ttpul	Tpt	Topopah Spring Tuff, crystal-poor upper lithophysal zone	Ttpul	Buesch et al. 1996 [DIRS 100106]	htul ^g	420 ^g	The Ttpul consists of crystal-poor, densely welded, crystallized, lithophysal ignimbrite. Data from the core in Ttpul form the type section ^h for the IHU of htul.	tsw33
tnl, tgnl, to, tb, tob(1 and 2), tbob	Tpt	Ttpmn	Tpt	Topopah Spring Tuff, crystal-poor middle nonlithophysal zone	Ttpmn	Buesch et al. 1996 [DIRS 100106]	htmn ^g	421 ^g	The Ttpmn consists of crystal-poor, densely welded, crystallized, nonlithophysal ignimbrite, although near the top is a “transition” subzone with minor amounts of lithophysae and, locally, there is a lithophysal-bearing subzone. Data from the core in Ttpmn form the type section ^h for the IHU of htpmn.	tsw34
tobl	Tpt	Ttpmnl	Tpt	Topopah Spring Tuff, crystal-poor middle nonlithophysal zone, lithophysal-bearing subzone	Ttpmn2	Buesch et al. 1996 [DIRS 100106]	htll	422	Although map unit 133 of Ttpmnl and map unit 256 of tobl are within a nonlithophysal zone, the rocks represented by these units are lithophysal and, typically, there are additional features, such as spots and fracture patterns that are associated with lithophysal units; therefore, the equivalent IHU is htll.	tsw34
tgrl, torl, tml, tpbl, trbb, tbol	Tpt	Ttpll	Tpt	Topopah Spring Tuff, crystal-poor lower lithophysal zone	Ttpll	Buesch et al. 1996 [DIRS 100106]	htll ^g	422 ^g	The Ttpll consists of crystal-poor, densely welded, crystallized, lithophysal ignimbrite. Data from the core in Ttpll form the type section ^h for the IHU of htll.	tsw35
tm	Tpt	base of section	Tpt	Topopah Spring Tuff, crystal-poor lower nonlithophysal zone	Ttpln	Buesch et al. 1996 [DIRS 100106]	htln ^g	423 ^g	The Ttpln consists of crystal-poor, densely welded, crystallized, nonlithophysal ignimbrite. Data from the core in Ttpln form the type section ^h for the IHU of htln. The Ttpln was divided (Buesch et al. 1996 [DIRS 100106]) into the hackly and columnar subzones of Ttplnh and Ttplnc, respectively, and a similar division was included in the UZ Flow Model units. For this compilation, however, the Ttpln was treated without division.	tsw36, tsw37
tv	Tpt	—	Tpt	Topopah Spring Tuff, crystal-poor, vitric, densely welded subzone	Ttpv3	Buesch et al. 1996 [DIRS 100106]	htpv3 ^g	424 ^g	The Ttpv3 consists of crystal-poor, densely welded, vitric ignimbrite. Data from the core in Ttpv3 form the type section ^h for the IHU of htpv3.	tsw38
—	Tpt	—	Tpt	Topopah Spring Tuff, crystal-poor, vitric, moderately welded subzone	Ttpv2	Buesch et al. 1996 [DIRS 100106]	htv2v and htv2z ^g	425 and 426 ^g	The Ttpv2 can be vitric or zeolitic, so the IHU can be htv2v or htv2z. On most geologic maps, however, the Ttpv2, Ttpv1, and Tpb1 are grouped together. For the Ttpv2, Ttpv1, and Tpb1 exposed near the north end of Yucca Mountain, the rocks are zeolitic, so an htv2z or htv1z can be used. For similar lithostratigraphic units exposed near Busted Butte, the rocks are vitric, so an htv2v or htv1v can be used. Regardless of how the properties are grouped to form an infiltration map unit, the properties, such as saturated hydraulic conductivity, will probably be an underrepresentation of the actual properties because of the mixing of moderately welded to nonwelded rocks. Data from the core in Ttpv2 form the type sections ^h for the IHUs of htv2v and htv2z.	tsw39 (V or Z)
tpw	Tpt	—	Tpt	Topopah Spring Tuff, crystal-poor, vitric, nonwelded subzone	Ttpv1	Buesch et al. 1996 [DIRS 100106]	htv1v and htv1z ^g	427 and 428 ^g	The Ttpv1 and Tpb1 were grouped into the IHUs of htv1v or htv1z; these units, however, are neither depicted separately on geologic maps nor are they separately mapped from Ttpv2. So, if Ttpv1 and Tpb1 are used for infiltration map units, then these IHUs will probably overestimate the porosity and K_{sat} values. Data from the core in Ttpv1 form the type sections ^h for the IHUs of htv1v and htv1z.	ch1 (V or Z)

INTENTIONALLY LEFT BLANK

Table A-1. Detailed Correlation of Geologic Map Units to Lithostratigraphic, Infiltration Hydrogeologic, and Unsaturated Zone Flow Model Units (Continued)

Map Units ^a	Map Units ^b	Map Units ^c	Map Units ^d	Lithostratigraphic Unit Name	Lithostratigraphic Unit Symbol	Source of Symbol	Equivalent IHU	IHU Number	Comments on IHU and Equivalent Unit	UZ Flow Model Layer ^e
NM	NM	—		pre-Topopah Spring bedded tuff	Tpbt1	Buesch et al. 1996 [DIRS 100106]	—	—	—	ch1 (V or Z)
—	Tac	—	Tac	Calico Hills Formation (undivided, total formation)	Tac	Moyer and Geslin 1995 [DIRS 101269]	htll	422	Aerial distributions of zeolitic pyroclastic rocks from maps are about 40% of the area and the lava flows are about 60% (Day et al. 1998 [DIRS 100027]; Dickerson and Drake 1998 [DIRS 102929]); therefore, the equivalent IHU is htll.	NA
Tht	Tac	—	Tacm-Tact	Calico Hills Formation, pyroclastic rocks flow	Tac5, Tac4, Tac3, Tac2, Tac1; or Tacm and Tact	Moyer and Geslin 1995 [DIRS 101269]; or Dickerson and Drake 1998 [DIRS 102929]	hacv and hacz ^g	429 and 430 ^g	The pyroclastic rocks of the Calico Hills formation exposed near the north end of Yucca Mountain are zeolitic, so the IHU of hacz can be used. For similar lithostratigraphic units exposed near Busted Butte, the rocks are vitric, so hacv can be used. Data from the core in Tac form the type sections ^h for the IHUs of hacv and hacz.	ch2, ch3, ch4, ch5 (V or Z)
Thf	Tac	—	Tacl	Calico Hills Formation, lava flows	Tacl	Dickerson and Drake 1998 [DIRS 102929]	htll	422	The map (precipitation) view is mostly crystallized, locally spherulitic, crystal-poor rhyolite lava with flow banding; therefore, the surrogate IHU is htll.	NA
Tha	Tac	—	—	Calico Hills Formation, brecciated lavas and tuffs	no symbol	—	hacz	430	Typically, most of the “tuff breccia” and the autobrecciated lavas, which form the carapace of the lava flows, were vitric, but have been zeolitized; therefore, the surrogate IHU is hacz.	NA
NM	NM	—	base of section	pre-Calico Hills bedded tuff	Tacbt	Moyer and Geslin 1995 [DIRS 101269]	habtv and habtz ^g	431 and 432 ^g	The Tacbt can be vitric or zeolitic, so the IHUs can be of habtv and habtz. On surface geologic maps, the Tacbt was typically mapped as part of the Tac. Where these rocks are exposed north of Yucca Mountain they are zeolitic and near Busted Butte they are vitric. Original sorting and bedding textures of Tacbt differ from overlying and underlying ignimbrites and, especially with zeolitic alteration, the Tacbt is an important hydrogeologic unit that can also be used for the Tact (Dickerson and Drake 1998 [DIRS 102929]). Data from the core in Tacbt form the type sections ^h for the IHUs of habtv and habtz.	ch6
—	Tw	—	—	Wahmonie Formation (not divided, total formation)	Tw	Slate et al. 2000 [DIRS 150228], Open-File Report 99-554-A	hacv	429	The Wahmonie Formation occurs in small exposures around Busted Butte and in several boreholes south and southeast of Busted Butte. These rocks consist of nonwelded vitric fallout tephra, ignimbrites, or debris-flow deposits and possibly fluvial stream deposits; therefore, the equivalent IHU is hacv.	NA
Tcpu	Tcp	—	—	Prow Pass Tuff (undivided, total formation)	Tcp	Moyer and Geslin 1995 [DIRS 101269]	hpuc	435	From the borehole samples, 43% of Tcp is crystallized, while only 16% is moderately welded (Tcpm); therefore, the equivalent IHU is hpuc. Initially, this map unit was identified as hpmlc, but the small proportion of the Tcpm indicates that this assignment was not appropriate.	NA
—	Tcp	—	—	Prow Pass Tuff, upper vitric	Tcpuv	Buesch and Spengler 1999 [DIRS 107905]	hpuvv and hpuvz ^g	433 and 434 ^g	Upper vitric lithofacies can be either vitric or zeolitic. Data from the core in Tcpuv form the type sections ^h for the IHUs of hpuv and hpuvz.	pp4
Tcpp	Tcp	—	—	Prow Pass Tuff, upper crystallized	Tcpuc	Buesch and Spengler 1999 [DIRS 107905]	hpuc ^g	435 ^g	This unit is partially welded, crystallized and partially vapor-phase corroded and mineralized ignimbrite. Data from the core in Tcpuc form the type section ^h for the IHU of hpuc.	pp3
Tcpm	Tcp	—	—	Prow Pass Tuff, moderately welded and crystallized	Tcpm	Buesch and Spengler 1999 [DIRS 107905]	hpmlc ^g	436 ^g	This unit is moderately to densely welded and crystallized, which includes the thin lower crystallized (partially welded and crystallized) lithostratigraphic unit. Data from the cores in Tcpm and Tcpic form the type section ^h for the IHU of hpmlc.	pp2
—	Tcp	—	—	Prow Pass Tuff, lower crystallized	Tcpic	Buesch and Spengler 1999 [DIRS 107905]	—	—	—	pp2
—	Tcp	—	—	Prow Pass Tuff, lower vitric	Tcplv	Buesch and Spengler 1999 [DIRS 107905]	hpbvz ^g	437 ^g	The Tcplv, Tcpbt, and Tcbuv are typically nonwelded to partially welded and mostly zeolitic, and can be vitric or zeolitic, so the IHUs can be of hpbvv or hpbvz. In boreholes G-3 and H-3, the upper part of Tcplv is vitric; only the zeolitic Tcplv, Tcpbt, and Tcbuv, however, are exposed near Yucca Mountain. Data from the core in Tcplv, Tcpbt, and Tcbuv form the type section ^h for the IHU of hpbvz.	pp1

INTENTIONALLY LEFT BLANK

Table A-1. Detailed Correlation of Geologic Map Units to Lithostratigraphic, Infiltration Hydrogeologic, and Unsaturated Zone Flow Model Units (Continued)

Map Units ^a	Map Units ^b	Map Units ^c	Map Units ^d	Lithostratigraphic Unit Name	Lithostratigraphic Unit Symbol	Source of Symbol	Equivalent IHU	IHU Number	Comments on IHU and Equivalent Unit	UZ Flow Model Layer ^e
Bt	Tcp	—	—	pre-Prow Pass bedded tuff	Tcpbt	Buesch and Spengler 1999 [DIRS 107905]	hpbvz	437	—	pp1
—	Tcb	—	—	Bullfrog Tuff (undivided, total formation)	Tcb	Slate et al. 2000 [DIRS 150228], Open-File Report 99-554-A	hbucm	438	From the borehole samples, 62% of Tcb is crystallized and 36% is moderately to densely welded; therefore, the equivalent IHU is hbucm.	NA
—	Tcb	—	—	Bullfrog Tuff, upper vitric	Tcbuv	Buesch and Spengler 1999 [DIRS 107905]	hpbvz	437	The Tcbuv is typically zeolitic; therefore, the equivalent IHU is hpbvz.	pp1
Tcb	Tcb	—	—	Bullfrog Tuff, welded (and crystallized)	Tcbuc, Tcbm, Tcblc	Buesch and Spengler 1999 [DIRS 107905]	hbucm^g	438^g	The upper and lower crystallized lithofacies of Tcbuc and Tcblc are partially to moderately welded and typically vapor-phase corroded and mineralized. The moderately to densely welded Tcbm is crystallized. In borehole G-2, which is closest to the exposures of the Tcb, the Tcbm comprises most of the crystallized rocks; therefore, they are grouped into the equivalent IHU of hbucm. Data from the core in Tcbuc, Tcbm, and Tcblc form the type section ^h for the IHU of hbucm.	bf3
base of section	base of section	—	—	Bullfrog Tuff, nonwelded (zeolitic)	Tcblv, Tcbbt	Buesch and Spengler 1999 [DIRS 107905]	—	—	This part of the section is not exposed at the surface near Yucca Mountain.	bf2

Sources: ^a Scott and Bonk 1984 [DIRS 104181] and DTN: MO0003COV00095.000 [DIRS 146848], *scotbons.e00*.
^b Slate et al. 2000 [DIR 150228], Open-File Report 99-554-A, and DTN: MO0603GSCGEOMP.000 [DIRS 176585], *ofr-99-0554-e00.tar*.
^c Day et al. 1998 [DIRS 101557] and DTN: GS971208314221.003 [DIRS 107128], *cb6k.ps*.
^d Dickerson and Drake 1998 [DIRS 102929].
^e BSC 2004 [DIRS 169855], Table 6-5.
^f The lithostratigraphic unit symbol follows the nomenclature convention that is defined, but not used in the source (Buesch and Spengler 1999 [DIRS 107905]).
^g This source data for the IHU, shown in **bold text**, are from core samples from the respective IHU; source data for other IHUs, shown in regular text without footnote “g” are from surrogate units.
^h Symbols for the IHUs are unique compared to other stratigraphic systems on the Yucca Mountain Project and they contain a nomenclature hierarchy based on the lithostratigraphic unit from which the saturated hydraulic conductivity data were used as the “type section” of the IHU. In the IHU symbol nomenclature, all symbols are lower case, begin with “h,” and contain the letters of the formation and subdivision (zone or unit). For example, the crystal-poor, middle nonlithophysal zone of the Topopah Spring Tuff with the lithostratigraphic symbol Ttptmn, has an IHU symbol of “htmn.”

NOTES: Descriptions of lithostratigraphic features have been translated into terms that are more consistent with present-day usage. For example:

- The use of “zone” in previous reports as a lithostratigraphic unit has several connotations and is not explicit in meaning (Buesch et al. 1996 [DIRS 100106]).
- The term “phenocrysts” has been retained for crystals in lava flows; in pyroclastic rocks, however, the originally used “phenocrysts” are referred to as “crystal fragments.”
- The originally used “devitrified” is referred to as “crystallized.” The term, however, was used for material that was, but is not now, glass (Dickerson and Drake 1998 [DIRS 102929]), so it can represent crystallized material in some deposits, material altered at moderate temperature in other deposits, and zeolitically altered material in other deposits.
- The originally used “ash-flow tuff” is referred to as “ignimbrite.”
- The originally used “airfall tuff” is referred to as “fallout tephra.”
- “Pyroclastic-fall” is retained because it describes specific types of material, but the name has been changed to “pyroclastic fallout tephra” or “pyroclastic fallout tuff.” Similarly, “ash-fall” has been changed to “ash-fall tephra” or “ash-fall tuff.”
- The originally used “reworked tuff” is referred to as “redeposited tuff.”
- “Vitrophyre” is retained for ignimbrites; this term, however, is equivalent to “vitric, densely welded tuff,” and “vitric, densely welded ignimbrite” or “vitric, densely welded fallout tephra” can be used if the mechanism of deposition is known.
- “Vitrophyric lava flow” is retained and is synonymous with “vitric” or “glassy” lava flow.
- The terms “nonwelded,” “partially (or partly) welded,” “moderately welded,” and “densely welded,” that are used in map descriptions, are based on qualitative descriptions and are not associated with quantitative values, such as density and porosity. Especially in some of the crystallized tuffs, rocks described as moderately welded on the basis of estimated porosity are actually densely welded and vapor-phase corroded.
- The original “ccr” (Scott and Bonk 1984 [DIRS 104181]) was not divided. For the present infiltration project, however, ccr has been divided into 216 for exposures south of borehole NRG-7a and 276 for exposures north of NRG-7a. This division is based on the relative abundance of detailed map units Tcrn4 and Tcrn2 (Day et al. 1998 [DIRS 100027]) with an attempt to represent the most abundant rocks exposed at the ground surface. The latitude of borehole NRG-7a was chosen on the basis of visual estimates of the abundance and distribution of map units (Day et al. 1998 [DIRS 100027]).
- Amounts of crystal fragments (Scott and Bonk 1984 [DIRS 104181]) are greater than typically used in more recent descriptions; therefore, the identification of rhyolite (crystal-poor) and quartz-latite (crystal-rich) and the lithophysal or nonlithophysal zones are more indicative than the amounts of crystal fragments.

IHU = infiltration hydrogeologic unit; NA = not applicable; NIMA = not in mapped area; NM = not mapped as a specific unit; NOOM = not on output map; Q = quality (Quality Assurance Program classification); UZ = unsaturated zone.

INTENTIONALLY LEFT BLANK

APPENDIX B

PROPAGATION OF VARIABILITY OR UNCERTAINTY FOR MEASURANDS WITH LOGNORMAL DISTRIBUTIONS

B1. PURPOSE

This appendix includes the following information pertaining to measurands with lognormal distributions:

- Terminology for lognormal distributions
- The W test for goodness-of-fit
- Estimators for the median, the uncertainty in the logarithm of the median, and the variance of the logarithm
- Formulas for obtaining the mean and variance of the measurand from the parameters of the lognormal distribution
- Formulas for propagating variability or uncertainty through products or sums of measurands.

The equations presented herein are based on industry-standard statistical methods as documented in the following sections and are appropriate for the assessment of uncertainty.

B2. DEFINITIONS

This appendix uses the following terms, as defined in ANSI/NCSL Z540-2-1997 [DIRS 157394], pp. 3, 9, 32, and 33:

- A **measurand** is a particular quantity subject to measurement. The measurements may be of a uniform quantity or of a quantity varying in space or time.
- For a series of n measurements of the same measurand, the **experimental standard deviation** is the quantity $s(q_k)$ characterizing the dispersion of the results and given by the formula:

$$s(q_k) = \sqrt{\frac{\sum_{k=1}^n (q_k - \bar{q})^2}{n-1}} \quad (\text{Eq. B-1})^1$$

with $s(q_k)$ being the result of the k^{th} measurement and \bar{q} being the arithmetic mean of the measurements. This dispersion may represent physical variation in space or time, or, it may represent dispersion of measurements of the same quantity.

- The expression $s(q_k)/\sqrt{n}$ is an estimate of the standard deviation of the distribution of \bar{q} and is called the **experimental standard deviation of the mean**.²

¹ Equation B-1 corresponds to the STDEV function in Excel®. Some sources define the standard deviation with n instead of $n-1$ in the denominator.

- The **standard uncertainty** is the uncertainty of the result of multiple measurements of the same quantity expressed as a standard deviation.
- In many cases a measurand Y is not measured directly, but is determined from N other quantities X_1, X_2, \dots, X_N through a functional relationship f :

$$Y = f(X_1, X_2, \dots, X_N) \quad (\text{Eq. B-2})$$

The **combined standard uncertainty** is the standard uncertainty of the result of a measurement when that result is obtained from the values of a number of other quantities. If the distributions of the N other quantities represent spatial or temporal variability, then the variability is expressed as the combined standard deviation.

This appendix uses the following additional definitions:

- The **distribution** of a measurand is the probability density function for measurements as the number of measurements becomes very large.
- The **true mean**, μ , of a measurand is the mean of its distribution.
- The **true variance**, σ^2 , of a measurand is the variance of its distribution.

B3. LOGNORMAL DISTRIBUTIONS

In many cases, a measurand has significant variability or uncertainty but is known to be non-negative so that the symmetric normal distribution is not a suitable model. In that case, a lognormal distribution may adequately fit the data set. The lognormal density function is (Gilbert 1987 [DIRS 163705], p. 152, Equation 12.1):

$$p(x) = \frac{1}{xS\sqrt{2\pi}} \exp\left[-\frac{1}{2S^2}(\ln x - M)^2\right] \quad (\text{Eq. B-3})$$

where M and S^2 are the true mean and variance² of the random variable $\ln X$. $\text{Exp}(M)$ is the median value of the random variable X and M is the median value of the random variable $\ln X$.

The W test is an effective method for testing whether a data set x_1, x_2, \dots, x_n , $n \leq 50$, has been drawn from an underlying lognormal distribution. The null hypothesis to be tested is:

H_0 : The population has a lognormal distribution.

² Some sources define the standard error in this way, using a standard deviation that has n in the denominator.

³ S^2 is a parameter of the distribution of $\ln X$. It should not be confused with s of Equation B-1, which is a function of the set of measurements.

The W test of this H_0 is conducted as follows (Gilbert 1987 [DIRS 163705], p. 159):

1. Compute

$$d = \sum_{i=1}^n (\ln x_i)^2 - \frac{1}{n} \left(\sum_{i=1}^n \ln x_i \right)^2 \quad (\text{Eq. B-4})$$

2. Order the n data from smallest to largest to obtain the sample order statistics $x_{[1]} \leq x_{[2]} \leq \dots \leq x_{[n]}$
3. If n is even, then set k to $n/2$. If n is odd, set k to $(n-1)/2$
4. For the observed n , find the coefficients a_1, a_2, \dots, a_k (Gilbert 1987 [DIRS 163705], pp. 259 to 260, Table A6)
5. Compute

$$W = \frac{1}{d} \left[\sum_{i=1}^k a_i (\ln x_{[n-i+1]} - \ln x_{[i]}) \right]^2 \quad (\text{Eq. B-5})$$

6. Reject H_0 at the 0.05 significance level, if W is less than the quantile $W_{0.05}$ given for sample size n (Gilbert 1987 [DIRS 163705], p. 261, Table A7).

If the hypothesis is not rejected, then

- The experimental mean of $\ln x$ is an unbiased estimator of M (Gilbert 1987 [DIRS 163705], p. 27, Equation 4.3).
- The experimental standard deviation of the mean of $\ln x$ is an estimate of the standard uncertainty in M (Gilbert 1987 [DIRS 163705], p. 28).
- The experimental standard deviation of $\ln x$ (Equation B-1 for $s(\ln x_k)$) is an unbiased estimator of S (ANSI/NCSL Z540-2-1997 [DIRS 157394], pp. 33, Section B.2.17, Note 1). If the measurements are taken at various locations and the measurand is known to vary in space, then S represents the actual spatial variation.

The true mean and the true variance of X , μ and σ^2 respectively, are (Gilbert 1987 [DIRS 163705], p. 156, Table 12.1)⁴:

$$\mu = \exp\left[M + S^2/2\right] \quad (\text{Eq. B-6})$$

$$\sigma^2 = \exp(2M + S^2) [\exp(S^2) - 1]. \quad (\text{Eq. B-7})$$

⁴ One can estimate μ and σ^2 by replacing M and S in Equations B-6 and B-7 with the experimental mean and standard deviation of $\ln x$. The results, however, are biased estimators of μ and σ^2 . The estimate of μ is biased upward (Gilbert 1987 [DIRS 163705], Section 13.1.2, pp. 167 and 168).

Equations B-6 and B-7 may be solved for M and S^2 to yield:

$$M = \ln\left(\mu^2 / \sqrt{\mu^2 + \sigma^2}\right) \quad (\text{Eq. B-8})$$

$$S^2 = \ln\left(1 + \sigma^2 / \mu^2\right) \quad (\text{Eq. B-9})$$

B4. PROPAGATION OF UNCERTAINTY

The standard uncertainty of y , where y is the estimate of the measurand Y and thus the result of the measurement, is obtained by appropriately combining the standard uncertainties of the input estimates x_1, x_2, \dots, x_N . This combined standard uncertainty of the estimate y is the positive square root of the combined variance $u_c^2(y)$, according to ANSI/NCSL Z540-2-1997 [DIRS 157394], p. 19, Equation (10), is:

$$u_c^2(y) = \sum_{i=1}^N \left(\frac{\partial f}{\partial x_i} \right)^2 u^2(x_i) \quad (\text{Eq. B-10})$$

where f is the function given in Equation B-2 and each $u(x_i)$ is a standard uncertainty. Equation B-10 is based on the approximation that all the input quantities are stochastically independent and on a first-order Taylor series approximation of $Y = f(X_1, X_2, \dots, X_N)$.

If the measurand Y is the product of two input estimates x_1 and x_2 , each with a lognormal distribution, then:

$$u_c^2(\ln y) = u^2(\ln x_1) + u^2(\ln x_2) \quad (\text{Eq. B-11})$$

Therefore, the distribution of Y may be approximated as a lognormal distribution with:

$$M(\ln x_1 x_2) = M(\ln x_1) + M(\ln x_2) \quad (\text{Eq. B-12})$$

$$S^2(\ln x_1 x_2) = S^2(\ln x_1) + S^2(\ln x_2) \quad (\text{Eq. B-13})$$

If, on the other hand, the measurand Y is the sum of two input estimates x_1 and x_2 , each with a lognormal distribution, then:

$$u_c^2(y) = u^2(x_1) + u^2(x_2) \quad (\text{Eq. B-14})$$

Therefore, Y has a distribution with mean and variance:

$$\mu(y) = \mu(x_1) + \mu(x_2) \quad (\text{Eq. B-15})$$

$$\sigma^2(y) = \sigma^2(x_1) + \sigma^2(x_2) \quad (\text{Eq. B-16})$$

If the distribution of Y is approximated as lognormal, then the mean of and the variance of the resulting distribution may be obtained by using Equations B-6 and B-7 to replace the right-hand sides of Equations B-15 and B-16. The results are:

$$\mu(y) = \exp\left[M(x_1) + S^2(x_1)/2\right] + \exp\left[M(x_2) + S^2(x_2)/2\right] \quad (\text{Eq. B-17})$$

$$\sigma^2(y) = \left\{ \exp\left[2M(x_1) + S^2(x_1)\right] \left\{ \exp\left[S^2(x_1)\right] - 1 \right\} \right. \\ \left. + \exp\left[2M(x_2) + S^2(x_2)\right] \left\{ \exp\left[S^2(x_2)\right] - 1 \right\} \right\} \quad (\text{Eq. B-18})$$

$M(x_1 + x_2)$ and $S^2(x_1 + x_2)$ is obtained by:

$$\mu^2(y) = \left\{ \exp\left[2M(x_1) + S^2(x_1)\right] + \exp\left[2M(x_2) + S^2(x_2)\right] \right. \\ \left. + 2 \exp\left[M(x_1) + S^2(x_1)/2\right] \exp\left[M(x_2) + S^2(x_2)/2\right] \right\} \quad (\text{Eq. B-19})$$

Then Equation B-8 may be used to obtain:

$$M(x_1 + x_2) = M(y) = 2 \ln[\mu(y)] - \frac{1}{2} \ln[\mu^2(y) + \sigma^2(y)] \quad (\text{Eq. B-20})$$

$$M(x_1 + x_2) = \left\{ \begin{aligned} & 2 \ln \left\{ \exp\left[M(x_1) + S^2(x_1)/2\right] + \exp\left[M(x_2) + S^2(x_2)/2\right] \right\} \\ & - \frac{1}{2} \ln \left\{ \begin{aligned} & \left\{ \exp\left[M(x_1) + S^2(x_1)/2\right] + \exp\left[M(x_2) + S^2(x_2)/2\right] \right\}^2 \\ & + \exp\left[2M(x_1) + S^2(x_1)\right] \left\{ \exp\left[S^2(x_1)\right] - 1 \right\} \\ & + \exp\left[2M(x_2) + S^2(x_2)\right] \left\{ \exp\left[S^2(x_2)\right] - 1 \right\} \end{aligned} \right\} \end{aligned} \right\} \quad (\text{Eq. B-21})$$

$$M(x_1 + x_2) = \left\{ \begin{aligned} & 2 \ln \left\{ \exp\left[M(x_1) + S^2(x_1)/2\right] + \exp\left[M(x_2) + S^2(x_2)/2\right] \right\} \\ & - \frac{1}{2} \ln \left\{ \begin{aligned} & 2 \exp\left[M(x_1) + S^2(x_1)/2\right] \exp\left[M(x_2) + S^2(x_2)/2\right] \\ & + \exp\left[2M(x_1) + 2S^2(x_1)\right] \\ & + \exp\left[2M(x_2) + 2S^2(x_2)\right] \end{aligned} \right\} \end{aligned} \right\} \quad (\text{Eq. B-22})$$

and Equation B-9 may be used to obtain:

$$S^2(x_1 + x_2) = S^2(y) = \ln[\mu^2(y) + \sigma^2(y)] - 2 \ln[\mu(y)] \quad (\text{Eq. B-23})$$

$$S^2(x_1 + x_2) = \begin{cases} \ln \left(\frac{2 \exp[M(x_1) + S^2(x_1)/2] \exp[M(x_2) + S^2(x_2)/2]}{+ \exp[2M(x_1) + 2S^2(x_1)]} \right. \\ \left. + \exp[2M(x_2) + 2S^2(x_2)] \right) \\ - 2 \ln \{ \exp[M(x_1) + S^2(x_1)/2] + \exp[M(x_2) + S^2(x_2)/2] \} \end{cases} \quad (\text{Eq. B-24})$$

or

$$S^2(x_1 + x_2) = \begin{cases} 2 \ln \{ \exp[M(x_1) + S^2(x_1)/2] + \exp[M(x_2) + S^2(x_2)/2] \} \\ - 2M(x_1 + x_2) \end{cases}. \quad (\text{Eq. B-25})$$

APPENDIX C

MEAN OF AND STANDARD DEVIATION OF LOG-UNIFORM DISTRIBUTIONS

C1. MEAN AND STANDARD DEVIATION OF LOG-UNIFORM DISTRIBUTIONS

Let a random variable, X , have a log-uniform distribution from X_1 to X_2 , which means that the logarithm of X has a uniform distribution. That is, defining a random variable Y that is equal to $\ln(X)$, Y has a uniform distribution from $Y_1 = \ln(X_1)$ to $Y_2 = \ln(X_2)$.

Therefore, the cumulative probability distribution for Y is

$$P_Y(Y) = \frac{Y - Y_1}{Y_2 - Y_1}, \quad Y_1 \leq Y \leq Y_2 \quad (\text{Eq. C-1})$$

and the cumulative probability distribution for X is

$$P_X(X) = \frac{\ln(X) - \ln(X_1)}{\ln(X_2) - \ln(X_1)}, \quad X_1 \leq X \leq X_2. \quad (\text{Eq. C-2})$$

The probability density function for X is

$$p_X(X) = \frac{\partial P_X(X)}{\partial X} = \frac{1}{X[\ln(X_2) - \ln(X_1)]}, \quad X_1 \leq X \leq X_2, \quad (\text{Eq. C-3})$$

which satisfies the requirement that

$$\int_{X_1}^{X_2} p_X(X) dX = 1. \quad (\text{Eq. C-4})$$

The mean value of the log-uniform distribution is

$$\mu_X = \int_{X_1}^{X_2} p_X(X) X dX = \int_{X_1}^{X_2} \frac{1}{[\ln(X_2) - \ln(X_1)]} dX = \frac{X_2 - X_1}{[\ln(X_2) - \ln(X_1)]}. \quad (\text{Eq. C-5})$$

The variance of the log-uniform distribution is

$$\sigma_X^2 = \int_{X_1}^{X_2} p_X(X) (X - \mu_X)^2 dX = \int_{X_1}^{X_2} p_X(X) (X^2 - 2\mu_X X + \mu_X^2) dX \quad (\text{Eq. C-6})$$

so that

$$\sigma_X^2 = \int_{X_1}^{X_2} p_X(X) X^2 dX - 2\mu_X \int_{X_1}^{X_2} p_X(X) X dX + \mu_X^2 \int_{X_1}^{X_2} p_X(X) dX = \int_{X_1}^{X_2} p_X(X) X^2 dX - \mu_X^2, \quad (\text{Eq. C-7})$$

which is a well-known relationship.

However,

$$\int_{X_1}^{X_2} p_X(X) X^2 dX = \int_{X_1}^{X_2} \frac{1}{X [\ln(X_2) - \ln(X_1)]} X^2 dX = \frac{X_2^2 - X_1^2}{2 [\ln(X_2) - \ln(X_1)]} = \mu_X (X_2 + X_1)/2$$

(Eq. C-8)

so that

$$\sigma_X^2 = \mu_X \left[\frac{(X_2 + X_1)}{2} - \mu_X \right].$$

(Eq. C-9)